4-17-2015 12:00 AM

Experimental and Numerical Study on Full-Scale Precast Steel Fibre-Reinforced Concrete Pipes

Nedal Mohamed, *The University of Western Ontario*

Supervisor: Prof. Moncef Nehdi, *The University of Western Ontario*

A thesis submitted in partial fulfillment of the requirements for the Doctor of Philosophy degree in Civil and Environmental Engineering

EXPERIMENTAL AND NUMERICAL STUDY ON FULL-SCALE PRECAST STEEL FIBRE-REINFORCED CONCRETE PIPES

(Thesis format: Integrated Article)

by

Nedal **Mohamed**

Graduate Program in Engineering Science
Department of Civil and Environmental Engineering

A thesis submitted in partial fulfillment
of the requirements for the degree of
Doctor of Philosophy

The School of Graduate and Postdoctoral Studies
The University of Western Ontario
London, Ontario, Canada

ABSTRACT

Reinforced concrete (RC) pipes are widely used as open channels (non-pressurized pipes) for sewage and storm water conveyance. RC pipes have generally achieved a reliable long-term performance. Depending on multiple parameters (e.g. pipe diameter, pipe wall thickness, required strength, etc.) the pipe may have up to three welded reinforcement cages in order to resist anticipated loads. Each cage is an assembled unit of steel reinforcement consisting of circumferential and longitudinal bars or wires. The fabrication process of steel cage reinforcement is time- and labour-consuming. Thus, eliminating the steel cage reinforcement will yield an overall reduction in the production cost of precast concrete pipes. Dispersed steel fibres can be an effective alternative for the reinforcement of concrete pipes.

The aim of this study is to explore the use of steel fibres as reinforcement in dry-cast concrete pipes. Mechanical properties of dry-cast steel-fibre reinforced concrete (DCSFRC) fabricated using multiple steel fibre types at various dosages were characterized. Consequently, precast pipes reinforced with Dramix RC-65/35-CN and Dramix RC-80/60-CN fibres at various dosages were fabricated. An extensive experimental program was carried out in order to evaluate the structural performance of the full-scale steel fibre-reinforced concrete (SFRC) pipes that were produced in comparison to plain concrete (PC) and RC pipes. Precast pipes had internal diameters of 300, 450, and 600 mm as well as a Type C wall thickness. The structural performance of pipes was characterized using both the continuous and cyclic three-edge-bearing tests (TEBT). Furthermore, the soil-pipe interaction of buried full-scale SFRC pipes was investigated. Finally, a three dimensional non-linear finite element model of the TEBT of SFRC pipes was developed. Subsequently, a parametric study covering multiple pipe configuration and reinforcement parameters was conducted.

Results showed that hooked-end fibres with the largest fibre aspect ratio (Dramix RC-80/60-CN) induced the best flexural performance of DCSFRC specimens. While crimped fibres (Novocon XR) were the least effective at enhancing the flexural strength and post-peak behaviour of DCSFRC. The load carrying capacity of SFRC pipes increased with increased fibre dosage. Results of the TEBT for 300 mm diameter pipes showed that the reinforcement specified for Class V pipes in ASTM C76 “Standard Specification For Reinforced Concrete

Culvert, Storm Drain, And Sewer Pipe" could be achieved using a steel fibre dosage of 20 kg/m³, while a fibre dosage of 30 kg/m³ was sufficient for 450 and 600 mm diameter pipes to satisfy the same strength class (Class V). Furthermore, provided using a sufficient fibre dosage, SFRC pipes exhibited higher residual strengths and less deformations than that of RC pipes when subjected to small to moderate loading levels. In addition, results showed that using a hybrid system of short (Dramix RC-65/35-CN) and long (Dramix RC-80/60-CN) fibres did not result in synergetic effects.

Full-scale testing results of buried SFRC pipes indicated that the pipes could sustain live loads consisting of a fully loaded 625CL Standard Ontario Truck without exhibiting any cracks or significant deformations, even when the pipe was installed in the least quality installation type (Type IV). This indicated that the current design recommendations for the pipe wall thickness in ASTM C76 (Type C wall) are overly conservative. Furthermore, it was found that the post-cracking behaviour of buried SFRC pipes was more sensitive to the installation type than to the type of steel fibre reinforcement.

Finally, the developed FE model was able to predict the ultimate D-loads of SFRC pipes with an average error of 6.50% when compared to D-loads obtained from testing SFRC pipes using the TEBT. The findings of the FE parametric study were presented in a tabular form that can be used as a design aid supplementary to the newly released ASTM C1765 "Standard Specification for Steel Fiber Reinforced Concrete Culvert, Storm Drain, and Sewer Pipe".

The experimental findings of this study should assist the precast concrete industry in producing more economical SFRC pipes without the need for costly and time consuming welded steel cage reinforcement. The numerical and analytical study findings can provide a simple and rational tool for the design of such SFRC pipes.

Keywords: Steel, fibre, reinforced concrete, precast, pipe, hybrid fibres, three-edge-bearing, full-scale, testing, structural performance, ultimate load, diametrical deformation, buried concrete pipe, soil-pipe interaction, standard installation, finite element, modelling.

CO-AUTHORSHIP STATEMENT

This thesis was prepared according to the integrated-article layout designated by the Faculty of Graduate Studies at Western University, London, Ontario, Canada. All the work stated in this thesis including experimental testing, data analysis, numerical modeling, and writing draft manuscripts for publication was carried out by the candidate under the supervision and guidance of Dr. M.L. Nehdi. Any other co-author (if applicable) assisted in conducting the experimental program and/ or revision of the initial draft of the manuscript. The following publications have been either accepted or submitted to peer-reviewed technical journals and international conferences:

1) **Mohamed**, **N.**, Soliman, A.M. and Nehdi, M.L., "Full-scale pipes using dry-cast steel fibre-reinforced concrete" *Construction and Building Materials*, 72, 2014, p.p. 411-422.
2) **Mohamed**, **N.**, Soliman, A.M. and Nehdi, M.L., "Mechanical performance of full-scale precast steel fibre-reinforced concrete pipes" *Engineering Structures*, 84, 2015, pp. 287-299.
3) **Mohamed**, **N.**, Soliman, A.M. and Nehdi, M.L., "Field performance of buried full-scale steel fibre reinforced concrete pipes" *Construction and Building Materials*, Submitted.
4) **Mohamed**, **N.** and Nehdi, M.L., "Rational finite element assisted design of precast steel fibre reinforced concrete pipes." *Engineering Structures,* Submitted.
5) **Mohamed**, **N.**, Soliman, A.M., and Nehdi, M.L., "Utilization of steel fibres in precast concrete pipes." *Tunnels and Underground Spaces: Sustainability and Innovations: Proceedings of Tunnelling Association of Canada Annual Meeting*, Montreal, QC, Canada, 18-20 Oct, 2012, 8 p.
6) **Mohamed**, **N.**, Soliman, A.M. and Nehdi, M.L., "Optimum fibre content for precast steel fibre-reinforced concrete pipes." *Fibre Reinforced Concrete: from Design to Structural Applications: Proceedings of 2nd FRC International Workshop (1st ACI–fib Joint Workshop)*, Polytechnique de Montreal, Montreal, QC, Canada, 24-25 July 2014. Ed. Charron, J.P., Massicotte, B., Mobasher, B., and Plizzari, G., 2014, pp. 500-510.

DEDICATION

To: *My Father: Abdelaziem Abdelraziek Mohamed*

My Mother: Hana Ali

My Brothers: Nader and Omar

My beloved Wife: Doria

ACKNOWLEDGMENTS

First of all, thanks to God for providing me such opportunities and capabilities that led me towards the completion of this dissertation.

I would like to state my sincere appreciation and humble thankfulness to my worthy research advisor and mentor Prof. Moncef Nehdi, for his invaluable guidance, supervision, encouragement, and support throughout this study.

I would like to acknowledge the support of ConCast Pipe (Guelph, ON) and the Ontario Concrete Product Plant (Oakville, ON) to this research through the fabrication and delivery of the full-scale SFRC pipe specimens. Bekaert and Propex are also appreciated for their material donations. Special thanks are due to the work-study undergraduate students and my graduate student colleagues who helped during specimens' preparation for various tests. The role of the University Machine Shop in fabricating the load and reaction frames is appreciated.

I would also like to thank Mr. Wilbert Logan, supervisor of the Concrete and Structures Laboratory at Western University, for his help and suggestions during the various stages of the experimental work.

Special thanks are due to my friend and fellow researcher Dr. Ahmed Soliman for his valuable guidance, suggestions, and editorial corrections. In addition, special thanks are due to Mr. Sammy Wong for facilitating communications with ConCast Pipe.

Finally, I would like to thank my father and my mother whose sacrifices and prayers paved the way to my success. I owe all of my achievements to them. I would like to express my deep gratitude and appreciation to my brothers. Furthermore, I would like to acknowledge my wife's support, encouragement, and patience, which played a vital role towards the completion of this study.

TABLE OF CONTENTS

LIST OF TABLES

LIST OF FIGURES

LIST OF SYMBOLS

b	width of SFRC specimen (mm)
$D_{0.3}$	D- load that induces a crack of 0.3 mm width and a length of 300 mm according to ASTM C76 (N/m/mm)
D_{ult}	D- load at failure according to ASTM C76 (N/m/mm)
d_f	steel fibre cross-section diameter (mm)
E_f	modulus of elasticity of steel fibres (GPa)
E_{pre}	fracture energy of SFRC specimen up to peak load (N.mm)
E_{post}	post-peak fracture energy at certain deflection δ (N.mm) = E_{total} - E_{pre}
$E_{total,}$	total fracture energy of SFRC specimen up to certain deflection δ (N.mm)
$F_{0.3}$	load that induces a crack of 0.3 mm width and a length of 300 mm according to ASTM C76 (kN/m)
F_c	specified pipe proof (design) load according to EN 1916 and NBR 8890 (kN/m)
F_{cr}	First cracking load of concrete pipe (kN/m)
F_f	tensile strength of steel fibres (N/mm²)
$F_{post,\ max}$	maximum load reached in the second load cycle of TEBT according to NBR 8890 (kN/m)
F_n	specified ultimate crushing load of concrete pipe according to EN 1916 and NBR 8890 (kN/m)

F_{ult}	ultimate crushing load of concrete pipe (kN/m)
f_1	flexural strength of SFRC (N/mm²)
f_c'	compressive strength of SFRC (N/mm²)
f_t	splitting tensile strength of SFRC (N/mm²)
h	depth of SFRC specimen (mm)
L	span of SFRC specimen (mm)
L_f	steel fibre length (mm)
P_{ult}	Pipe ultimate (failure) load (kN)
$P_{0.3}$	load that induces a crack of 0.3 mm width and a length of 300 mm according to ASTM C76 (kN)
PCS_m	post-crack strength of SFRC specimen at certain deflection L/m (N/mm²)
V_f	fibre content in SFRC mixture
φ	fibre aspect ratio
δ_{peak}	specimen vertical deflection at spigot at $F_{post,\,max}$ (mm)
δ	specimen vertical deflection (mm)

CHAPTER ONE

1 INTRODUCTION

1.1 GENERAL

Reinforced concrete pipes have been in wide-spread use for many decades in North America. They have often been used as open channels (non-pressurized pipes), particularly for the conveyance of sewage and storm water. They have generally shown reliable long-term performance. In the late 1890's, the manufacturing of precast concrete pipes became a recognizable industry in Ontario. The Ontario Concrete Pipe Association (OCPA) was founded in 1957. OCPA has joined several industrial and governmental agencies to establish standards for the manufacture of high quality concrete pipe products. The Canadian Concrete Pipe Association (CCPA) was founded in 1992 (OCPA, 2010).

Due to the advent of new pipe materials such as corrugated steel, PVC and HDPE, which have been gradually introduced into the market over the last half a century, reinforced concrete pipes have lost some of their market share. Pipes made from these materials are structurally classified as flexible, while concrete pipes are rigid pipes. A rigid pipe is stiffer than the surrounding soil. It relies on its own resistance as a ring to support external loads. Conversely, a flexible pipe relies on the horizontal thrust from the soil at its sides to resist vertical loads without excessive deformation. A flexible pipe has to sustain at least 10% decrease in its vertical diameter without any risk of damage to the material (Young, 1984). Thus, concrete pipes have the advantage of handling low quality bedding soils without affecting the hydraulics of the flow.

New pipe materials are relatively lighter in weight than concrete, which enables the manufacturing of longer pipe segments; leading to an easier installation process. The length of one concrete pipe segment is 2.44m, while that of an HDPE pipe can be as long as 13m. From a durability perspective, concrete pipes are more susceptible to chemical and biological attacks than plastic pipes. On the other hand, concrete pipes have superior impact and fire resistance. The final pipe selection is usually a compromise between the initial installation cost and the long-term performance.

1.2 RESEARCH NEEDS AND MOTIVATION

The structural applications of steel fibre-reinforced concrete (SFRC) have recently been increasing due to improvements it imparts, such as increased toughness, impact and fatigue resistance, and enhanced durability. However, detailed and commonly accepted guidelines for the design of SFRC structures have not been included in main building codes. The motivation behind this research project is to develop a more competitive concrete pipe by using steel fibres to eliminate the pipe's steel reinforcement cage. Manufacturing of the steel cage from conventional steel reinforcement requires special bending, welding, and placement machinery, and is thus time-consuming. Pre-manufactured steel fibres, on the other hand, can be added in the mixer of any concrete batch plant similar to other mixture ingredients without significant process modification. Steel fibre-reinforced concrete can be produced and cast in pipe moulds similar to ordinary plain concrete. Therefore, SFRC pipes can be an economical alternative to conventionally reinforced concrete pipes.

1.3 SPECIFIC RESEARCH OBJECTIVES

This research program aims at exploring the adequacy of using steel fibres to replace conventional steel reinforcement in precast concrete pipes. Savings in the cost of materials and in the work hours spent in building steel cages for pipe reinforcement will yield less costly and more competitive precast concrete pipes. The specific research goals are to:

1) Conduct an exploratory study on the engineering properties of dry-cast steel fibre-reinforced concrete fabricated using different types and dosages of steel fibres, in order to recommend steel fibre types suitable for the manufacturing of full-scale SFRC pipe specimens.

2) Produce full-scale 300, 450, and 600 mm diameter precast pipes fabricated with various dosages of steel fibres as the sole reinforcement and evaluate the mechanical performance of the produced SFRC pipes using the three-edge-bearing test compared to that of plain concrete (PC) and regularly reinforced concrete (RC) pipes.

3) Determine steel fibres dosages that are sufficient for 300, 450 and 600 mm diameter SFRC pipes to satisfy the strength requirements of Class V pipes according to the ASTM C497 standard.

4) Study the behaviour of buried full-scale SFRC pipes and the soil-pipe interaction for pipes installed in Type III and Type IV standard installations.

5) Develop a three-dimensional finite element model that can simulate the three-edge-bearing test of SFRC pipes. Utilize the developed model to conduct a parametric study to predict the load-deformation curves for different combinations of pipe strength/pipe diameter/ wall thickness/ steel fibres type/ steel fibres dosage.

6) Develop a simplified design tool that can be used in conjunction with the ASTM C1765 standard for the design SFRC pipes.

1.4 THESIS OUTLINE

This dissertation has been prepared according to the integrated-article format predefined by the Faculty of Graduate Studies at Western University, London, Ontario, Canada. It consists of seven chapters covering the scope of this study: performance and modelling of precast steel fibre-reinforced concrete pipes. Substantial parts of this thesis have been published, accepted, or submitted for possible publication in peer-reviewed technical journals and

international conferences. Chapter 1 provides a brief introduction along with the research motivation, objectives, and original contributions to research.

Chapter 2 provides a brief overview of precast concrete pipes, standards and specifications regulating the industry, testing methods and design procedures. In addition, a brief review of current structural applications of SFRC, focusing on precast concrete pipes, is also provided.

Chapter 3 presents an experimental program covering the mechanical characterization of multiple dry-cast SFRC (DCSFRC) mixtures fabricated using four different types of steel fibres at different dosages. Consequently, full-scale 300 mm diameter precast SFRC pipe specimens were fabricated using two different types of steel fibres that were recommended based on the findings of the previous step. SFRC pipes were tested using the continuous procedure of the three-edge-bearing test specified in ASTM C470.

Chapter 4 presents an experimental program covering the fabrication and analysis of the mechanical performance of full-scale 450 and 600 mm diameter precast SFRC pipe specimens. SFRC pipes were fabricated using the recommended steel fibre types at three different dosages. SFRC pipes were tested using the cyclic procedure of the three-edge-bearing test specified in the European standard EN 1916:2002.

Chapter 5 evaluates the structural behaviour and soil-pipe interaction of buried full-scale SFRC pipes compared to that of plain and regularly reinforced concrete pipes. Sound (un-cracked) and cracked SFRC pipes were tested under realistic live loads.

Chapter 6 presents the development, calibration, and further verification of a non-linear three-dimensional finite element model of SFRC pipes under the three-edge-bearing test. Furthermore, a parametric study, covering multiple parameters, was conducted and its results were presented. In addition, design tables for SFRC pipes with diameters ranging between 300 mm and 1200 mm are also introduced.

Chapter 7 summarizes the research conclusions and future recommendations.

1.5 ORIGINAL CONTRIBUTIONS

This research fills a knowledge gap concerning precast SFRC pipes. Previous studies reported using several types and dosages of steel fibres in the fabrication of SFRC pipes, however, the selection of the used steel fibre types and dosages was not based on a systematic rational approach. Although, the problem of SFRC pipe design encompasses multiple variables, these studies only dealt with specific design scenarios (i.e. ultimate loads achieved by pipes with a specific combination of pipe diameter, wall thickness, fibre type, and fibre dosage), and thus lacked a comprehensive approach to the problem. Furthermore, the structural performance of buried SFRC pipes and the soil-pipe interaction are yet to be explored.

This study is divided into four main phases, each aiming at addressing part of the problem. The specific original contributions of this research include:

1) Providing a detailed study of the mechanical properties of DCSFRC. Findings and recommendations of this stage justified the selection of the steel fibre type and dosage used in the full-scale production of SFRC pipes.

2) Providing the technical support that facilitated, for the first time in Canada, the production of industry full-scale SFRC pipes with steel fibres as the sole reinforcement. Several adjustments were applied to the automated production system employed in the sponsoring precast concrete plant to accommodate the new product.

3) Conducting a detailed study of and comparison between the mechanical behaviour of PC, RC, and SFRC pipes tested under both of the continuous and cyclic three-edge-bearing test. Findings of this study demonstrated the superiority of SFRC pipes over RC pipes. Therefore, the precast concrete pipe industry can promote the new product with scientifically substantiated data.

4) Providing, for the first time in the literature, a detailed study on the soil-structure interaction of SFRC pipes. Both cases of sound (un-cracked) and cracked pipe were considered.

5) Finally, developing design tables for SFRC pipes of internal diameter ranging between 300 and 1200 mm.

1.6 REFERENCES

Ontario Concrete Pipe Association (OCPA), "*Concrete Pipe Design Manual,"* Ontario Concrete Pipe Association, Kitchener, Ontario, 2010, 145 p. http://www.ocpa.com/

Young, O.C., Trott, J.J., "*Buried rigid pipes structural design of pipelines,"* Elsevier Applied Science Publishers, Essex, 1984, 234 p.

CHAPTER TWO

2 LITERATURE REVIEW

2.1 PRECAST CONCRETE PIPES

As mentioned earlier; the precast concrete pipe industry has been well established in Ontario and Canada for a long time. Nowadays, this industry is governed by provincial, national, and international standards. These standards (outlined in **Table 2-1**) cover the manufacturing, materials and product specifications, testing and construction processes. Recently, the ASTM standard C1765 "Specification for Steel Fibre Reinforced Concrete Culvert, Strom Drain, and Sewer Pipe" for SFRC pipes was published to regulate the production of SFRC pipes in the US. However, currently there is no Canadian standard for SFRC pipes.

2.1.1 Manufacture of Precast Concrete Pipes

The process of manufacturing concrete pipes starts with the assembly of the reinforcement cage, if any. Cage machines, mandrels, and wire rollers are the three most common means of fabricating reinforcing cages in a concrete pipe plant. A concrete pipe can have up to three steel cages depending on its diameter, wall thickness and the required pipe strength. Globally, five common methods are used in concrete pipe manufacturing. Four of these methods use mechanical means to place and compact a dry concrete mixture into the pipe form. These are centrifugal, dry cast/vibration, packerhead, tamp, and wet cast. The fifth method (wet cast method) uses a more conventional wet mix and casting procedure. In the dry cast/vibration method, the mould consists of an inside core mould and an outside mould.

Table 2-1 Standards regulating the precast concrete pipe industry and other related precast products in North America

American Society for Testing and Materials, ASTM	Canadian Standards Association, CSA	Ontario Provincial Standard Specifications, OPSS
C14 "Specification for Concrete Sewer, Storm Drain, and Culvert Pipe"	A257.0 "Methods for Determining Physical Properties of Concrete Pipe"	407 "The Construction of Manholes, Catch Basins, Ditch Inlets and Valve Chambers"
C76 "Specification for Reinforced Concrete Culvert, Storm Drain, and Sewer Pipe"	A257.1 "Concrete Culvert, Storm Drain and Sewer Pipe"	408 "Adjusting or Rebuilding Manholes, Catch Basins, Ditch Inlets and Valve Chambers"
C118 "Specification for Concrete Pipe for Irrigation or Drainage"	A257.2 "Reinforced Concrete Culvert, Storm Drain and Sewer Pipe"	422 "Precast Reinforced Concrete Box Culverts and Box Sewers"
C443 "Specification for Joints for Circular Concrete Sewer and Culvert Pipe Using Rubber Gaskets"	A257.3 "Joints for Circular Concrete Sewer and Culvert Pipe Using Rubber Gaskets"	1351 "Components for Precast Reinforced Concrete Catch Basins, Manholes, Ditch Inlets and Valve Chambers"
C665 "Specification for Reinforced Concrete D-Load Culvert, Storm Drain, and Sewer Pipe"	A257.4 "Precast Circular Concrete Manhole Sections, Catch Basins & Fittings"	1820 "Circular Concrete Pipe"
C497 "Test Methods for Concrete Pipe, Manhole Sections, or Tile"		1821 "Precast Reinforced Concrete Box Culverts and Box Sewers"
C497 "Standard Specification for Steel Fiber Reinforced Concrete Culvert, Storm Drain, and Sewer Pipe"		

That assembly is placed vertically on a supporting plate and the reinforcement cage with its spacers is placed within the mold space. Concrete is fed in under mechanical vibration. When the mould is filled, a ring descends onto the top of the concrete and applies pressure (Levitt, 2007). An electronic management system regulates the supply of concrete and the application

of the pressure head. The form is removed immediately, as the newly formed pipe can support its self-weight. The pipe is then transferred to the curing room. The most common curing method in the concrete pipe industry is the low pressure steam curing. For instance, Haktanir *et al.* (2007) reported a concrete pipe-curing regime as follows: after the removal of the steel mould, the pipe rests at room temperature in the plant for 6 hours. The first phase of curing is increasing the ambient temperature at a rate of 12 ^{o}C per hour. The second stage is the application of steam curing at a constant temperature of 60 ^{o}C for a period of 12 hours. The third stage is cooling back to room temperature at the rate of 12 ^{o}C per hour.

2.1.2 Concrete Mixture

The nature of the precast concrete pipe manufacturing mandates the use of especially designed concrete mixtures. Minimizing the time of production requires immediate removal of the concrete pipe from its mould. Thus, the fresh concrete should be sufficiently cohesive to maintain its shape after consolidation. Hence, dry cast concrete or zero-slump concrete is widely used in precast concrete manufacturing. The general rule is to use as much water as the pipe can tolerate without cracking or slumping when the mould is stripped off. The term zero-slump concrete refers to concrete having a slump from zero to 25 mm (ACI 211.3, 2009). Generally, such concrete has poor workability when compacted by hand rodding; however, acceptable workability can be achieved when using vigorous mechanical vibration and other consolidation techniques as described earlier. The most commonly used technique for measuring the consistency of mixtures having a slump of less than 25 mm is the Vebe apparatus. **Table 2-2** shows a comparison between results obtained using the Vebe test and the conventional slump test (ACI 211.3, 2009).

The cohesiveness of the mixture can be improved by increasing the amount of fines in the concrete mixture. This can be achieved by using well-graded aggregates and reducing the volume of the coarse aggregate. The maximum nominal size recommended for aggregates used in the production of precast concrete pipes is 19 mm (ACI 211.3, 2009). Supplementary cementitious materials such as fly ash, silica fume and ground granulated blast furnace slag can be added to increase the cohesiveness and decrease segregation. Such admixtures

increase the mechanical strength of concrete at early and/or late ages, decrease cracking, and permeability, thus leading to higher resistance to chemical attack (Li, 2011).

Table 2-2 Comparison of consistency measurements for slump and Vebe apparatus

Consistency description	Slump, mm	Vebe, sec
Extremely dry	-	32 to 18
Very stiff	-	18 to 10
Stiff	0 to 25	10 to 5
Stiff plastic	25 to 75	5 to 3
Plastic	75 to 125	3 to 0
Very plastic	125 to 190	-

2.1.3 Three Edge Bearing Test and D-Load

The recognized standard test for the mechanical strength of a reinforced concrete pipe is the Three-Edge-Bearing test (TEBT). In this test, the load is applied by a hydraulic jack as a line load along the crown of the pipe, while the pipe is supported on a two closely spaced bearing strips along the invert as sketched in **Fig. 2-1**.

The pipe performance is evaluated based on two criteria; these are the ultimate crushing load of the pipe P_{ult} (or the ultimate strength) and the load that produces a crack with a width of 0.3 mm and a length of 300 mm $P_{0.3}$ (or the design strength). Both values are expressed in kN. Current CSA and ASTM standards define the ultimate and design strength of reinforced concrete pipes in terms of D-loads. A D-load is the total load per meter of pipe length divided by the inside diameter of the pipe in millimeter N/m/mm. Thus, a group of pipes that have the same strength will support the same D-load regardless of the pipe diameter. Pipe classification based on D-load requirements according to CSA A257.2 and ASTM C76 standards are shown in **Table 2-3**. These standards provide guidelines for the circumferential reinforcement (inner and outer cages and elliptical cage, if any) and wall thickness required for pipes that have diameters ranging between 300 mm and up to 3600 mm to achieve the designated D-load for their classes.

ASTM C655 “Standard Specification for Reinforced Concrete D-Load Culvert, Storm Drain, and Sewer Pipe” allows a reinforced concrete pipe to be designed, using the direct design method (**Section 2.1.4**), to support a specific D-load (i.e. D-Load that does not fall under strength classes specified in ASTM C76). In such case, the pipe designation shall be the $D_{0.3}$ load. The relationship between the ultimate strength D_{ult} and $D_{0.3}$ shall be 1.5 for design strength designations up to 100 N/m/mm, and of 1.25 for design strength designations greater than 150 N/m/mm. The factor can be prorated for design strength designations between 100 and 150 N/m/mm.

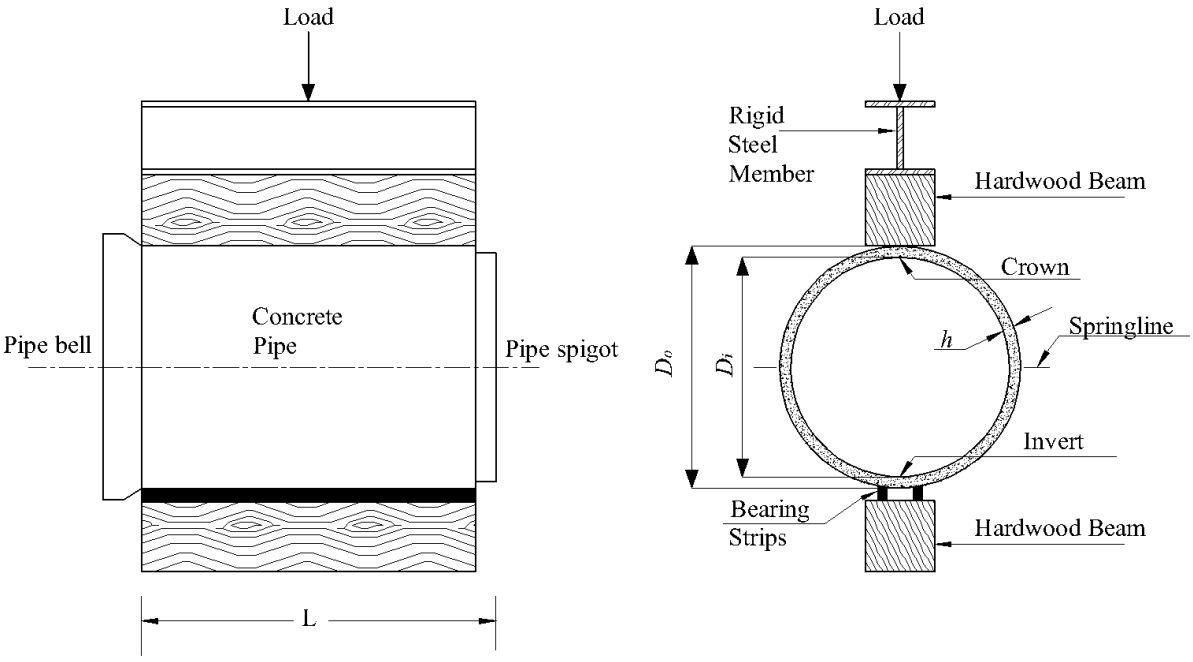

Figure 2-1: Three-edge-bearing test setup.

The European standards EN 1916:2002 “Concrete Pipes and Fittings, Unreinforced, Steel Fibre and Reinforced” describe a different procedure for conducting TEBT for SFRC pipes (**Fig. 2-2-a**):

Table 2-3 Classification of reinforced concrete pipes based on required design and ultimate D-Load

ASTM Class	CSA Class	Design Strength $D_{0.3}$ (N/m/mm)	Ultimate Strength D_{ult} (N/m/mm)
I	-	40	60
II	50D	50	75
III	65D	65	100
IV	100D	100	150
V	140D	140	175

- Stage 1-2: The pipe should withstand a load of 0.67 F_n, where F_n is the minimum crushing load required, appropriate to its nominal size and strength class for one minute without showing any crack.
- Stage 2-3: If no crack is found, the load is taken to the ultimate (collapse) load F_u that is greater than F_n.
- Stage 4-5: After the sustained load has fallen to 95% or less of the ultimate (collapse) load, it is released, then reapplied to 0.67 F_n and sustained for one minute.

This procedure is more rigorous than the procedure specified for conventionally reinforced pipes since SFRC pipes have to show no sign of cracks at a load of 0.67 F_n, while conventionally reinforced pipes are allowed to exhibit a surface crack of 0.3 mm width and a length of 300 mm. In addition, conventionally reinforced pipes do not have to conform to the requirements of stages 4 and 5 of the test. The cyclic loading procedure is specified to ensure adequate fibre-bond in the post-cracking stage of SFRC pipes.

Figure 2-2-b summarizes the TEBT procedure specified in ASTM C1765 for SFRC pipes testing. The pipe ultimate D-load (D_u) shall exceed the required D-load specified for the targeted pipe class (D_{Test}). When D_u is reached, the pipe is de-loaded immediately and then reloaded up to $D_{Service}$. Similar to EN 1916:2002, $D_{Service}$ equals to 0.67 D_u. **Table 2-4** shows SFRC pipes classification according to ASTM C1765.

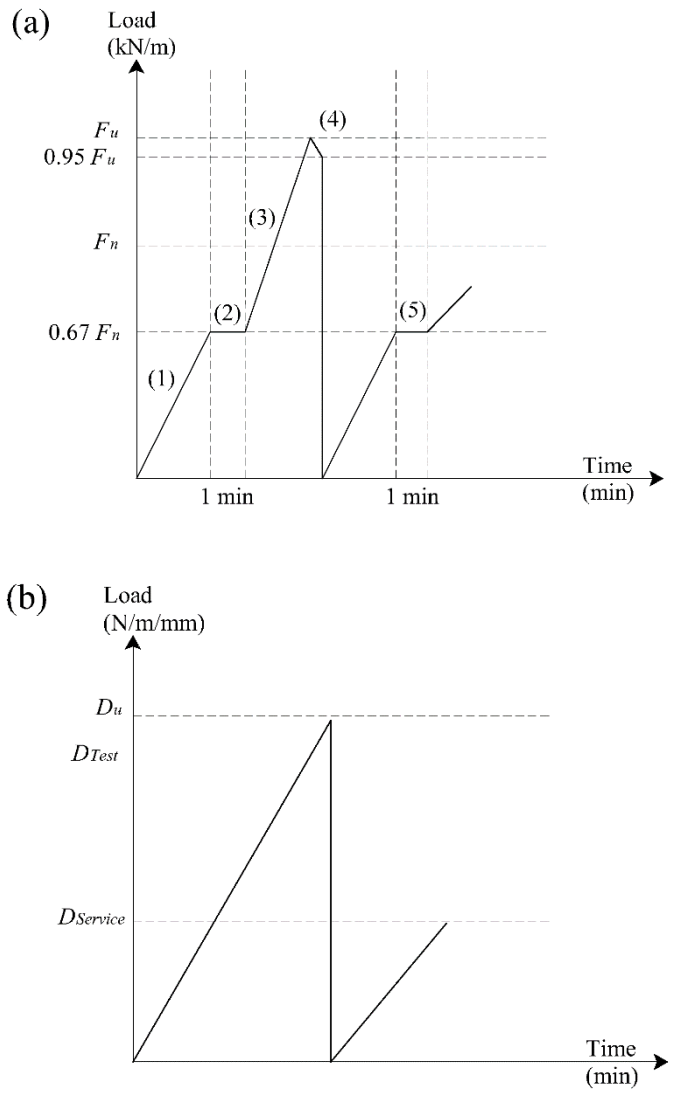

Figure 2-2 TEBT for SFRC pipes according to a) EN 1916:2002, and b) ASTM C1765.

Table 2-4 SFRC pipes strength requirements according to ASTM C1765

Pipe Class	$D_{service}$ (N/m/mm)	D_{Test} (N/m/mm)
I	40	60
II	50	75
III	67.5	100
IV	100	150
V	150	225

2.1.4 Design Methods

The structural design of reinforced concrete pipes is a relatively complex problem due to the curved nature of the pipe itself and the soil-pipe interaction involved in both supporting the pipe and the load transfer to the pipe barrel. The straining actions occurring in the pipe section due to the applied loads depend greatly on the way the pipe was installed.

2.1.4.1 Soil-Pipe Construction

The soil-pipe construction consists of the precast reinforced concrete pipe, in-situ soil in the foundation below the pipe and between the vertical or slopping trench walls, and the placed soils (constructed bedding and backfill) below, around and above the pipe up to the surface (ACPA, 1993).

There are three main types of soil-pipe construction methods; namely trench type constructions, embankment type constructions, and jacking type constructions. Trench type is when the pipeline is located completely below the natural ground surface in narrow excavations, and then the backfill of in-situ soil is placed on top and around the pipe up to the surface. Embankment type construction is divided into two groups: positive and negative projection. In positive projection construction, the pipe is installed with the top of the pipe projecting above the surface of the natural ground or compacted fill, and then covered with earth fill. In negative projection construction, the pipe is installed in relatively shallow trenches of such depth that the top of the pipe is below the level of the natural ground surface, and then covered with earth fill to a height appreciably greater than the distance from the natural ground surface to the top of the pipe.

Figure 2-3 shows pipe terminology and the standard trench/ embankment construction. D_o and D_i are the outside and inside diameter of the pipe, respectively. Overfill soil categories are summarized in **Tables 2-5** and **2-6**. In jacking-tunneling type construction, the pipe is installed simultaneously with the excavation process. In this construction type, the pipe will be subjected to extra axial load due to the jacking pressure.

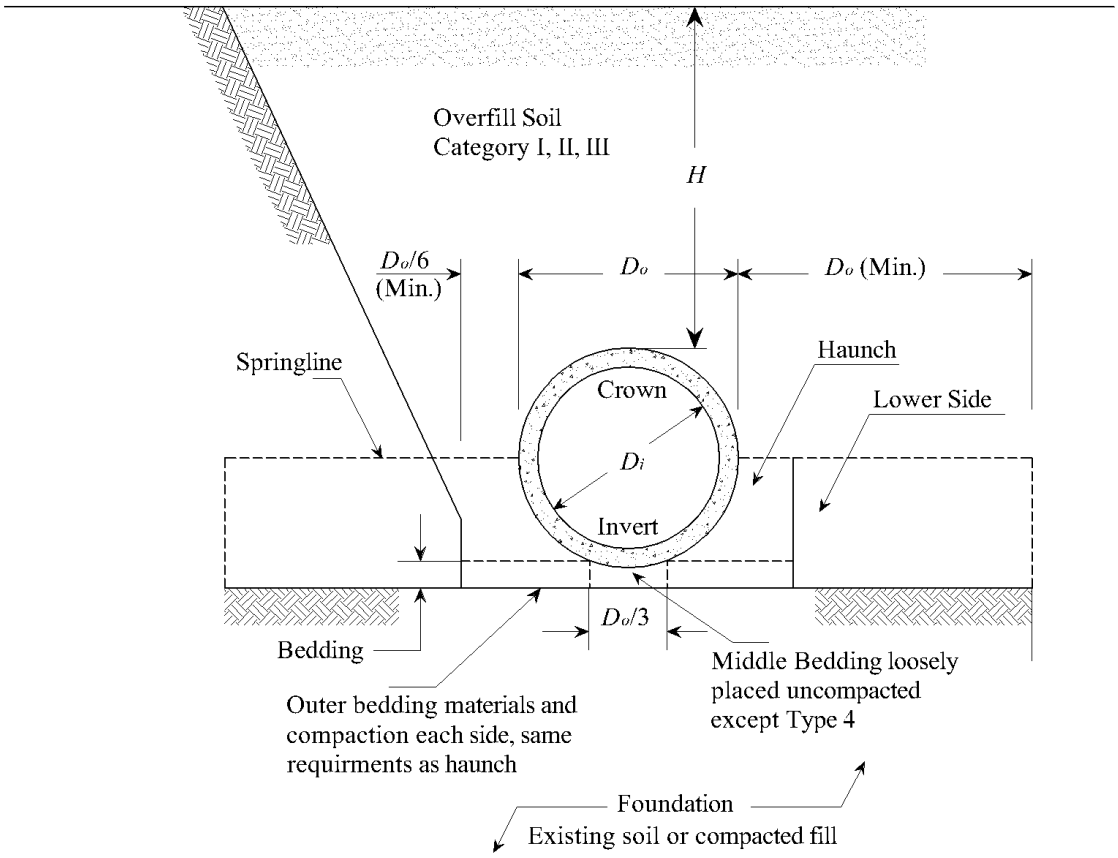

Figure 2-3 Standard Trench/ Embankment Construction.

2.1.4.2 Standard Installations and Bedding Factors

Bedding is the placed or natural soil immediately below or adjacent to the bottom of the pipe that is in place before the pipe is positioned in the construction (ACPA, 1993). The bedding factor is a factor that relates the behavior of the pipe under the field condition of loading to that under the more severe three-edge–bearing test. The bedding factor for a particular pipeline, and consequently the supporting strength of the buried pipe, depends upon two characteristics of the installation: width and quality of bedding and magnitude of the lateral pressure against the sides of the pipe.

Table 2-5 Standard installations soil and minimum compaction requirements

Installation Type	Bedding Thickness	Haunch and Outer Bedding	Lower Side
Type 1	D_o/ 24 minimum, not less than 75 mm. If rock foundation, use D_o/ 12 minimum, not less than 150 mm.	95% Category I*	90% Category I, 95% Category II, or 100% Category III
Type 2	D_o/ 24 minimum, not less than 75 mm. If rock foundation, use D_o/ 12 minimum, not less than 150 mm.	90% Category I, or 95% Category II	85% Category I, 90% Category II, or 95% Category III
Type 3	D_o/ 24 minimum, not less than 75 mm. If rock foundation, use D_o/ 12 minimum, not less than 150 mm.	85% Category I, 90% Category II, or 95% Category III	85% Category I, 90% Category II, or 95% Category III
Type 4	No bedding required, except if rock foundation, use D_o/ 12 minimum, not less than 150 mm.	No compaction required, except if Category III, use 85% Category III	No compaction required, except if Category III, use 85% Category III

* "95% Category I" refers to Category I soil material, as indicated in **Table 2-6**, with minimum standard Proctor compaction of 95%.

There are two general approaches for the design of reinforced concrete pipes; the indirect design method and the direct design method. Both methods are valid and widely accepted. The indirect design method follows an empirical procedure that was first introduced by (Spangler, 1933). The required pipe strength is determined as a ratio between the total applied field loads to the bedding factor. Based on the required D-load, the strength, reinforcement requirement and pipe wall thickness are given in the previously mentioned standards (CSA A-257, ASTM C76).

Table 2-6 Equivalent USCS and AASHTO soil classifications for soil designations

SIDD Soil	Soil Types		Percent Compaction	
	USCS	AASHTO	Standard Proctor	Modified Proctor
Gravely Sand (Category I)	SW, SP, GW, GP	A1, A3	100	95
			95	90
			90	85
			85	80
			80	75
			61	59
Sandy Silt (Category II)	GM, SM, ML, Also GC, SC with less than 20% passing #200 sieve	A2, A4	100	95
			95	90
			90	85
			85	80
			80	75
			49	46
Silty Clay (Category III)	CL, MH, GC, SC	A5, A6	100	90
			95	85
			90	80
			85	75
			80	70
			45	40

The direct design method follows a more rational procedure in terms of moment, thrust, and shear to determine the required pipe strength. It was first introduced by the ACPA in 1993 and it is incorporated in the American Society of Civil Engineers Standards as "ASCE Standard Practice for Direct Design of Buried Precast Concrete Pipe in Standard Installation (SIDD)". The method allows for the design of reinforcing for concrete pipe based on five limit states: 1) reinforcement tension, 2) concrete compression, 3) radial tension, 4) diagonal tension, and 5) crack control.

Moreover, there are four standard installations introduced by the American Concrete Pipe Association (ACPA) as a result of a long range research program that started in 1970. Although these standard installations (beddings) were introduced along with the Direct Design method, they have been incorporated in the indirect design method to replace the historical A, B, C and D beddings that were introduced by Marston (1930) and Spangler (1933). These four standard installations provide a wide range of soil-pipe interaction scenarios due to variation in the quality of the backfill soil or quality of the compaction. Type 1 installation requires a lower strength pipe, while Type 4 installation requires a higher

strength pipe, because it was developed for conditions of little or no control over materials or compaction. These four installations are well explained in (ACPA, 2011). **Tables 2-5** and **2-6** illustrate the soil categories associated with the four installation types.

It is worth mentioning that both design methods generally use similar approaches in calculating the loads applied on the pipeline. Sections 2.1.4.3 and 2.1.4.4 will explain both methods in further detail.

2.1.4.3 Indirect Design Method

The indirect design method requires the following procedure:

1. Establishing the pipe diameter, wall thickness, and type of standard installation
2. Determination of the vertical earth load and live load forces acting on the pipe
3. Determination of the bedding factors
4. Applying factor of safety
5. Determination of required pipe D-Load strength

The diameter of the pipe is usually determined by the hydraulic design of the pipeline. The wall thickness is given in the ASTM C76 standard. The wall thickness, h in mm is determined as follows:

$$\text{Wall A: } h = \frac{D_i}{12} \qquad \textbf{Eq. 2-1}$$

$$\text{Wall B: } h = \frac{D_i}{12} + 25 \qquad \textbf{Eq. 2-2}$$

$$\text{Wall C: } h = \frac{D_i}{12} + 44 \qquad \textbf{Eq. 2-3}$$

where D_i is the internal pipe diameter in mm. The selection of a standard installation is based on the anticipated quality of the construction process. A Type 1 standard installation requires the highest construction quality and degree of inspection. Conversely, a Type 4 standard installation requires virtually no construction or quality inspection. Thus, for the same depth

of installation, Type 4 installation will require a higher strength pipe with larger wall thickness than Type 1 installation.

2.1.4.3.1 Calculation of earth load, W_e

The type of installation has a significant effect on the loads carried by the rigid pipe. As indicated earlier; a concrete pipe can be installed in either an embankment or trench condition. In the embankment condition, the soil alongside the pipe will settle more than the soil above the rigid pipe structure, thereby imposing an additional load to the prism of soil directly above the pipe. This phenomenon is known as soil arching and is accounted for using a "Vertical Arching Factor". Thus, the total earth load is calculated using the following equation:

$$W_e = VAF \text{ x } PL \qquad \textbf{Eq. 2-4}$$

where *PL* "Prism Load" is the weight of the prism of earth directly above the outside diameter of the pipe in N/m. *PL* can be calculated from **Eq. 2-5.**

$$PL = \frac{wD_o}{1000}\left[H + \frac{0.107D_o}{1000}\right] \qquad \textbf{Eq. 2-5}$$

where: w is the soil unit weight (N/m^3)

D_o is the outside diameter of the pipe (mm)

H is height of fill from the crown to the ground surface (m)

Figure 2-4 shows the vertical arching factors and Heger earth pressure distribution for the standard installations. The load from the weight of the earth over and around the pipe is applied to the pipe as a non-uniformly distributed external pressure whose magnitude and distribution is a function of the relative deformation of the pipe and soil (ACPA, 1993).

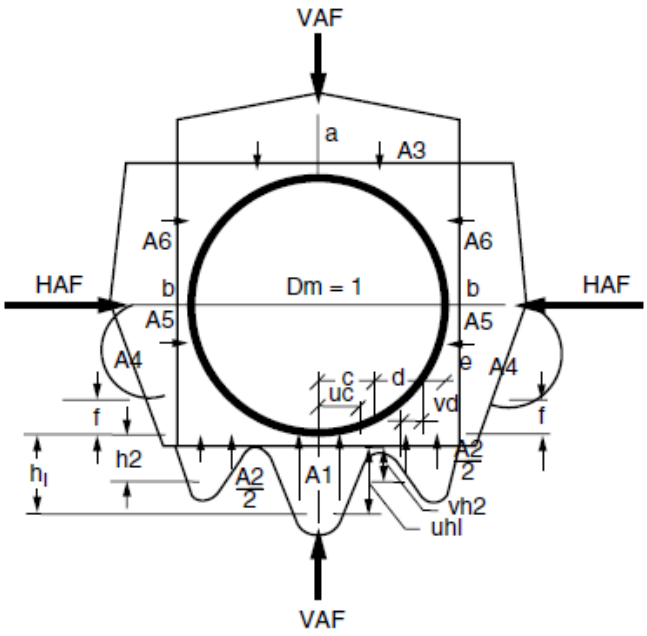

Installation Type	VAF	HAF	A1	A2	A3	A4	A5	A6	a	b	c	e	f	u	v
1	1.35	0.45	0.62	0.73	1.35	0.19	0.08	0.18	1.40	0.40	0.18	0.08	0.05	0.80	0.80
2	1.40	0.40	0.85	0.55	1.40	0.15	0.08	0.17	1.45	0.40	0.19	0.10	0.05	0.82	0.70
3	1.40	0.37	1.05	0.35	1.40	0.10	0.10	0.17	1.45	0.36	0.20	0.12	0.05	0.85	0.60
4	1.45	0.30	1.45	0.00	1.45	0.00	0.11	0.19	1.45	0.30	0.25	0.00	-	0.90	-

Notes:

1. VAF and HAF are vertical and horizontal arching factors. These coefficients represent no dimensional total vertical and horizontal loads on the pipe, respectively. The actual total vertical and horizontal loads are (VAF) x (*PL*) and (HAF) x (*PL*), respectively, where *PL* is the prism load.
2. Coefficients A1 through A6 represent the integration of non-dimensional vertical and horizontal components of soil pressure under the indicated portions of the component pressure diagrams (i.e. the area under the component pressure diagrams). The pressures are assumed to vary either parabolically or linearly, as shown, with the non-dimensional magnitudes at governing points represented by h1, h2, uh1, vh2, a and b. Non-dimensional horizontal and vertical dimensions of component pressure regions are defined by c, d, e, uc, vd, and f coefficients.
3. d is calculated as (0.5-c-e).
   h_1 is calculated as (1.5A1) / (c) (1+u).
   h_2 is calculated as (1.5A2) / [(d) (1+v) + (2e)]

Figure 2-4 Arching coefficients and Heger Earth Pressure Distribution.

In the trench construction condition, the earth load on the pipe can be computed using **Eq. 2-6:**

$$W_e = \frac{C_d w B_d^2}{1000} + \frac{0.107 D_o^2}{1000} w \qquad \textbf{Eq. 2-6}$$

where: B_d is the trench width (m)

C_d is the trench load coefficient, $C_d = \frac{1 - e^{-2K\mu \frac{H}{B_d}}}{2K\mu}$

Where: K = ratio of active lateral unit pressure to vertical unit pressure

μ = tan $\emptyset$, coefficient of friction between the fill material and sides of the trench, where $\emptyset$ is the angle of internal friction.

Typical values of K and μ range from 0.11 to 0.19 depending on the soil type (Moore, 2001).

2.1.4.3.2 Calculation of live load, W_L

In the design of a pipeline, it is necessary to evaluate the effect of live loads (W_L). The most encountered loads are wheel loads from trucks and heavy vehicles. However, buried pipelines may also pass under railroads or airport runways. These concentrated surface loads are distributed through the pavement and the earth cover over the pipeline. On any plane in the earth cover, the intensity of the load is greatest directly below the point of load application, and decreases in all directions outward from the center of application. In addition, the intensity of the load decreases when the distance between the plane and the surface increases.

A detailed procedure for calculating the effective live loads on pipeline is introduced in the ACPA (2011). The same procedure is also specified in article 3.6 of "AASHTO LRFD Bridge Design Specifications". It is worth mentioning that AASHTO Bridge Specifications allow the surface wheel loads to be neglected if the height of earth cover over the crown of the pipe is greater than 8 ft (2.44 m).

2.1.4.3.3 Pipe weight and fluid load, W_F

The pipe weight is usually neglected in the indirect design method since it is always active in the three-edge-bearing test. The fluid weight is typically about the same order of magnitude as the pipe weight. Generally, it represents a significant portion of the pipe design load only for large diameter pipes under relatively shallow fills. The AASHTO Standard Specifications for Highway Bridges recommend the fluid weight to be taken as 62.4 lbs/ft^3 (1000 kg/m^3), unless otherwise specified.

The subsequent step in the indirect design method is the determination of the Bedding Factor, B_f. **Table 2-7** shows the bedding factors in the embankment condition for the four standard installations at different pipe diameters. Bedding factors for pipe diameters other than listed in the Table can be interpolated. It has to be mentioned that these B_f values are calculated based on the direct design approach and the new standard installations introduced by the ACPA (1993). The older approach was based on the historical A, B, C and D beddings introduced by Spangler (1933) and Marston (1930).

The **Equation 2-7** below is used to calculate the bedding factor in the case of the trench construction condition:

$$B_f = \frac{(B_{fe} - B_{fo})(B_d - D_o)}{(B_{dt} - D_o)} + B_{fo} \qquad \textbf{Eq. 2-7}$$

where:

D_o = outside diameter of pipe

B_d = trench width at top of pipe

B_{dt} = transition width at top of pipe

B_{fe} = bedding factor in the case of embankment condition

B_{fo} = minimum bedding factor for the trench condition (**Table 2-8**)

The factor of safety (*FS*) employed in the indirect design method is the ratio between the ultimate D-load strength and the 0.3 mm crack D-load strength, which is between 1.25 and 1.50 depending on the targeted D-load, as specified in ASTM C655.

Table 2-7 Bedding factor values, B_f for the embankment condition

Pipe Diameter (in)	Standard Installation			
	Type 1	Type 2	Type 3	Type 4
300	4.4	3.2	2.5	1.7
600	4.2	3.0	2.4	1.7
900	4.0	2.9	2.3	1.7
1800	3.8	2.8	2.2	1.7
3600	3.6	2.8	2.2	1.7

Table 2-8 Minimum bedding factors, B_{fo} for the trench condition

Standard Installation	Minimum Bedding factor, B_{fo}
Type 1	2.3
Type 2	1.9
Type 3	1.7
Type 4	1.5

The final step in the indirect design method is to determine the required D-Load strength of the pipe as indicated in **Eq. 2-8**, where $B_{fL.L}$ is the live load bedding factor:

$$D-load=\left[\left(\frac{W_e+W_f}{B_f}\right)+\left(\frac{W_L}{B_{fL.L}}\right)\right]x\frac{FS}{D_i} \qquad \textbf{Eq. 2-8}$$

2.1.4.4 Direct Design Method

The direct design method specifically addresses the anticipated pipe loading conditions in the field. This method requires the following procedure:

1. Establishing the pipe diameter, wall thickness and type of standard installation
2. Determination of the vertical earth load and live load forces acting on the pipe
3. Determining the moments, thrusts and shears due to the applied loads at the critical sections (invert crown and spring line). **Equations 2-9** to **2-11** are used for the calculation of these straining actions at the critical sections:

$$M_i = C_{mi}\left(\frac{W_i D_m}{2}\right) \qquad \textbf{Eq. 2-9}$$

$$N_i = C_{ni} W_i \qquad \textbf{Eq. 2-10}$$

$$V_i = C_{vi} W_i \qquad \textbf{Eq. 2-11}$$

where M_i, N_i and V_i are the moment, thrust and shear forces, respectively. C_{mi}, C_{ni} and C_{vi} are non-dimensional coefficients used for determining the straining actions M_i, N_i and V_i, respectively. W_i represents any of the loads acting on the pipe. D_m is the intermediate diameter of the pipe. The values of the C_{mi}, C_{ni} and C_{vi} coefficients are given elsewhere (ACPA, 1993) for each of the four standard installations types.

4. The next step is the structural design of the pipe using established reinforced concrete design principles for the following limit and serviceability states:
    a. Reinforcement design for flexural strength limit
    b. Shear (diagonal tension) strength limit
    c. Stirrup reinforcement design (if any)
    d. Service limit for crack width control

Section 12 of the "AASHTO LRFD Bridge Design Specifications" provides the design equations for the above-mentioned limit and serviceability states.

2.2 APPLICATION OF SFRC IN PRECAST PIPES

Fibre-reinforced concrete (FRC) is defined, according to ACI 116R (2005), as concrete containing dispersed randomly oriented fibres. The most commonly used fibres in FRC are steel fibres. Steel fibre-reinforced concrete (SFRC) was first introduced by Romualdi and Mandel (1964). The role of fibres is to bridge micro- and macro-cracks that occur in a cementitious matrix due to various states of stress, leading to a great increase in the toughness of cementitious materials. Originally, steel fibres were used primarily for crack control, to replace the secondary reinforcement often used for that purpose in flat slabs, pavements and tunnel linings, as well as in various repair applications (Bentur and Mindess, 2007). Currently, there is an increased tendency to use steel fibres in structural applications to replace conventional steel reinforcing rebar or to act in a complementary fashion with it.

However, the improvements in strength due to steel fibre addition are modest, except for high fibre volumes.

Several studies investigated the use of steel fibres in precast concrete pipes (e.g. MacDonald and Trangsrud, 2004; Haktanir *et al.*, 2007; de la Fuente and de Figueiredo, 2011; de la Fuente *et al.*, 2012; and Abolmaali *et al.*, 2012). These studies and their main findings are summarized below:

2.2.1 MacDonald and Trangsrud (2004)

MacDonald and Trangsrud (2004) conducted an experimental study on concrete pipes having a diameter of 0.53 m, a C Type wall (thickness = 89 mm) designed as Class V pipes according to ASTM C76. Two mixture proportions were used as shown in **Table 2-9**. Mixture 1 was used for both of making pipes with welded wire fabrics without fibres, and for making pipes with welded wire fabric and fibres. Mixture 2 was used for making pipes with steel fibres alone. Pipes made using Mixture 1 having only fibres crumbled when moved. The employed steel fibre had a length of 40 mm, an aspect ratio of 40 with a rectangular cross-section, and its ends were enlarged and bent. The fibre dosages tested were 20, 39 and 59 kg/m^3. The TEBT was conducted according to the procedure described in ASTM C497. Pipes made with Mixture 1 were tested at ages of 1 and 7 days. Pipes made with Mixture 2 were tested at ages of 2 and 5 days.

Table 2-9 Mixture proportions used for pipe fabrication (MacDonald and Trangsrud, 2004)

Material (kg/m^3)	Mixture #1	Mixture #2
Cement	326	341
Fly ash	89	74
Superplasticizer	1	1
Coarse aggregate	681	984
Fine aggregate	1369	1067
Moisture content	199	158
w/c	0.48	0.38

The TEBT results for pipes made with steel fibres as sole reinforcement are shown in **Table 2-10.** From these results, it was concluded that SFRC pipes would gain strength with maturity in consistence with the strength gain of concrete. Pipes having a steel fibre content of 20 kg/m^3 did not fulfill the D-load requirements of Class V pipes specified in ASTM C76. Pipes having a steel fibre content of 39 kg/m^3 were successful when tested at the age of 5 days. It is worth noting that in all of the SFRC pipes tested, regardless of the fibre content, the first crack load, the 0.25 mm crack load, and the ultimate (failure) load had the same value. This is an indication of a brittle behaviour. This finding is in contrast with de la Fuente *et al*. (2011) who reported that pipes having a fibre content of 40 kg/m^3 exhibited a strain hardening behaviour after reaching the ultimate load. This discrepancy may be due in part to the testing method. Load control tests may not properly capture post-crack behaviour as opposed to displacement-controlled tests.

Table 2-10 TEBT results for SFRC pipes (MacDonald and Trangsrud, 2004)

Fibre content (kg/m^3)	Load (kN/m)			Age (days)
	First Crack	0.25 mm Crack	Ultimate Load	
20	82.4	82.4	82.4	2
	88.3	88.3	88.3	5
	8% average difference			
39	91.2	91.2	91.2	2
	94.14	94.14	94.14	5
	3% average difference			
59	108.85	108.85	108.85	2
	110.82	110.82	110.82	5
	3% average difference			

Note: Required $F_{0.25}$ and F_{ult} loads for Class V with a D_i = 525 mm are 73.5 and 91.9 kN/m, respectively according to ASTM C76.

2.2.2 Haktanir *et al.* (2007)

Haktanir *et al.* (2007) conducted an experimental study to compare the behaviour of plain concrete and conventionally reinforced concrete pipes with that of SFRC pipes. A total of 35 pipes having an internal diameter of 500 mm were cast. All pipes had a wall thickness of 65 mm. Conventionally reinforced pipes had only one elliptical steel cage with a total reinforcement area of 5.1 cm^2/m. This design was in accordance with the Turkish standards

TS-821-EN-191. Comparing the wall thickness, concrete strength, and reinforcement; this design falls somewhere between Class III and Class IV of the standard five classes specified in ASTM C76. Two types of steel fibres were used to manufacture the SFRC pipes. These are ZP 308 (length: 30 mm, aspect ratio: 40) and Dramix RC-80/60-BN (length: 60 mm, aspect ratio: 80). Details of the mixture design are shown in **Table 2-11.**

Table 2-11 Mixture proportions used for pipe fabrication (Haktanir *et al*., 2007)

Material	Dosage (kg/m^3)
Portland cement	350
Water	117
River sand (SSD)	710
Crushed sand (SSD)	604
Crushed medium aggregate (SSD)	301
Crushed coarse aggregate (SSD)	401
Steel fibres	25, 40

Note: SSD means in saturated surface dry condition

Table 2-12 shows a summary of the results of pipes tested under the TEBT. The TEBT was carried out in a similar manner to that specified in ASTM C497. In all cases, SFRC pipes fulfilled the requirements of the Turkish standard TS-821-EN-191. However, only SFRC pipes with Dramix RC-80/60-BN fulfilled the requirements of Class IV according to ASTM C76. It was concluded that longer fibres were more suitable for precast pipe application, with negligible strength increase when the fibre content was increased from 25 to 40 kg/m^3.

Table 2-12 TEBT results for plain concrete, reinforced concrete and SFRC pipes (Haktanir *et al.*, 2007)

Type of Pipe	Average Ultimate Load (kN/m)	Relative Difference with Respect to RCP (%)
Plain concrete pipe (CP)	43.0	-
Reinforced concrete pipe (RCP)	73.7	-
SFRC pipe (ZP-308 @ 25 kg/m^3)	70.2	-5
SFRC pipe (ZP-308 @ 40 kg/m^3)	74.9	+2
SFRC pipe (RC-80/60-BN @ 25 kg/m^3)	78.3	+6
SFRC pipe (RC-80/60-BN @ 40 kg/m^3)	80.5	+9

Note**:** Required ultimate load F_u = 67.5 kN/m according to TS-821-EN-1916. Required ultimate load F_u = 50 and 75 kN/m for Class III and IV, respectively according to ASTM C76.

2.2.3 de la Fuente *et al.* (2011)

Another experimental study was conducted by de la Fuente *et al*. (2011). In this study, a total of 18 pipes divided into two series having an internal diameter of 600 mm and a fibre dosage of 10, 20 and 40 kg/m^3 were tested. All pipes had a wall thickness of 72 mm. Three pipes were cast for each fibre dosage. The water/cement ratio (w/c) was increased in the second series to achieve better workability and surface finish. Dramix RC-80/60-BN steel fibres were used in this study. Pipes were tested according to the TEBT procedure described in EN 1916:2002. The study aimed to manufacture SFRC pipes that can satisfy the requirements of Class C-90 of EN 1916:2002. The required service crushing load, F_n and ultimate load, F_u for this class for a 600 mm internal diameter pipe are 36 and 54 kN/m, respectively. This class is comparable to Class III in ASTM C76 where the required $F_{0.3}$ and F_{ult} loads for a pipe of the same size are 39 and 60 kN/m, respectively.

Table 2-13 shows the mixture design that was used in fabricating the SFRC pipes. It was found that the observed first crack load (F_{cr}) was similar for all pipes tested, regardless of the fibre dosage. In addition, the first crack always appeared in the internal face of the invert at the male end of the pipe. However, the load displacement curve (F-v) for the tested pipes showed that pipes having a fibre dosage of 40 kg/m^3 behaved differently from pipes having lower amounts of fibres. Pipes having low amounts of fibres (10 and 20 kg/m^3) exhibited a displacement softening behaviour pattern (i.e. loss of load resistance capacity) with the increase of displacement once the ultimate failure load (F_u) was reached. On the other hand, pipes with a fibre dosage of 40 kg/m^3 showed a displacement hardening behavior when the yielding point was reached. Thus, it was deduced that in such pipes, fibres could perform a task similar to that of traditional reinforcing bars. **Table 2-14** shows the individual and average values of the reported F_{cr} and F_u loads.

Table 2-13 Mixture proportions used for SFRC pipes fabrication (de la Fuente *et al*., 2011)

Material	Dosage (kg/m^3)
River sand	679
Crushed sand	340
Granitic crushed coarse aggregate	1067
Cement	355
Water	152
Fibres	10, 20 and 40

Table 2-14 TEBT results for SFRC pipes (de la Fuente *et al*., 2011)

Series	Dosage (kg/m^3)	F_{cr} (kN/m)				F_u (kN/m)			
		T1	T2	T3	Avg.	T1	T2	T3	Avg.
1st	10	38.4	39.2	n/a	38.8	59.6	48.0	n/a	54.0
	20	38.4	40	n/a	39.2	56.0	49.6	n/a	52.8
	40	37.2	39.2	40.0	38.8	62.4	65.2	59.6	62.4
2nd	10	40.0	33.2	40.0	37.6	50.8	52.8	55.2	52.8
	20	39.2	38.0	34.0	37.2	60.4	58.0	51.6	56.8
	40	32.0	32.0	46.0	36.8	60.8	56.0	77.2	64.8

Note: F_{cr} is the first crack load. Required F_n and F_u loads are 36 and 54 kN/m, respectively.

2.2.4 Abolmaali *et al.* (2012)

Abolmaali *et al.* (2012) reported the production of 66 SFRC pipes. Pipes had internal diameters ranging between 400 and 1200 mm with B Type and C Type walls. Dramix RC-65/35-CN (length = 35 mm, aspect ratio = 65) steel fibres were used as sole reinforcement at dosages ranging between 13.1 and 65.5 kg/m³. They reported that a fibre dosage of 20 kg/m³ for 600 mm diameter pipe, 40 kg/m³ for 900 mm diameter pipe, and 65 kg/m³ for 1200 mm diameter pipe seem to be optimum for Class III pipe requirements according to ASTM C76 standard. It has to be mentioned that these SFRC pipe specimens were cast at four different precast concrete plants using different concrete mixtures.

2.3 SUMMARY

This chapter presented an overview of the manufacture and design of reinforced concrete pipes. RC pipes are facing a rapidly shrinking market share due to the advent of new pipe materials such as corrugated steel, PVC and HDPE. This is partly because these new pipes are relatively lighter and in some cases less costly. However, concrete pipes are generally more favourable when considering the long-term performance of pipelines.

An emerging solution to restore the competitiveness of concrete pipes is to replace the time- and labour-consuming steel cage reinforcement with dispersed easily mixed steel fibres. Only a few studies were accessible in the open literature regarding the application of steel fibres in precast concrete pipe manufacturing. All of these studies used a trial and error approach in order to specify an optimum steel fibre content that is sufficient for a specific pipe diameter/pipe wall configuration to reach specific pipe strength. However, a comprehensive and inclusive approach to the problem has not yet been reported. Furthermore, no information could be found in the literature on the soil-pipe interaction of SFRC pipes.

Thus, the present study aims at filling this knowledge gap. An experimental study on the mechanical properties of dry-cast steel fibre reinforced concrete fabricated using four different types of steel fibres at three dosages was carried out. Based on the findings of this initial phase, two types of steel fibres were selected for the fabrication of full-scale SFRC pipes having internal diameters of 300, 450, and 600 mm. The structural performance of SFRC pipes was characterized in terms of achieved crack and ultimate loads, vertical and horizontal deformations and concrete strain at critical sections compared to that of PC and RC pipes using the continuous and cyclic three-edge-bearing test. In addition, the performance of buried SFRC pipes was investigated. The resulting experimental data was used to calibrate and validate a finite element model simulating the three-edge-bearing test. The model was used to carry out a parametric study that explored the effects of pipe diameter, pipe wall thickness, steel fibres type, steel fibres dosage, and targeted pipe strength class. Finally, design tables for SFRC pipes have been as an alternative to the trial and error approach that has been used so far.

2.4 REFERENCES

Abolmaali, A., Mikhaylova, A., Wilson, A. and Lundy, J., "Performance of steel fibre-reinforced concrete pipes." *Journal of the Transportation Research Board*, 2313(1), 2012, pp. 168-177.

ACI Committee 211, "Guide for selecting proportions for no-slump concrete," ACI 211.3R-09, American Concrete Institute, Farmington Hills, MI, USA, 2009, 26 p.

ACI Committee 116, "Cement and concrete terminology," ACI 116R-05, American Concrete Institute, Farmington Hills, MI, USA, 2005, 50 p.

ASTM C76-13, "Standard specification for reinforced concrete culvert, storm drain, and sewer pipe." ASTM International, West Conshohocken, PA, 2013, 11 p.

ASTM C497-13, "Standard test methods for concrete pipe, manhole sections or tile." American Society for Testing and Materials, ASTM International, West Conshohocken, PA, 2013, 14 p.

ASTM C655-14, "Standard specification for reinforced concrete D-load culvert, storm drain, and sewer pipe." ASTM International, West Conshohocken, PA, 2014, 6 p.

ASTM C1765-13, "Standard specification for steel fibre reinforced concrete culvert, storm drain, and sewer pipe." ASTM International, West Conshohocken, PA, 2014, 6 p.

American Concrete Pipe Association, "*Concrete pipe design manual*," American Concrete Pipe Association, Irving, TX, 2011, 560 p.

American Concrete Pipe Association, "*Concrete pipe technology handbook: a presentation of historical and current state-of-the-art design and installation methodology*," American Concrete Pipe Association, Irving, TX, 1993, 350 p.

American Society of Civil Engineers Standards, "*Standard practice for direct design of buried precast concrete pipe using standard installations*," ASCE 15-98, American Society of Civil Engineers, Reston, VA, 2001, 50 p.

Bentur, A., and Mindess, S., "*Fibre-Reinforced Cementitious Composites."* 2nd edition; New York: Taylor & Francis, 2007, 660 p.

CSA A257 Series "Standards for concrete pipe and manhole sections," Canadian Standards Association, Mississauga, ON, 2014, 98 p.

EN 1916, "Concrete pipes and fittings, unreinforced, steel fibre and reinforced," European Committee for Standardization, Brussels, Belgium, 2002, 89 p.

de la Fuente, A., and de Figueiredo, D., "Experimentation and numerical simulation of steel fibre reinforced concrete pipes." *Materiales de Construcción,* 61(302), 2011, pp. 275-288.

de la Fuente, A., Escariz, R.C., de Figueiredo, A.D., Molins, C., and Aguado, A., "A new design method for steel fibre reinforced concrete pipes" *Construction and Building Materials,* 30, 2012, pp. 547-555.

Levitt, M., "*Precast concrete: materials, manufacture, properties and usage*," 2nd edition, Taylor & Francis, New York, NY, 2007, 224 p.

Li, Z., "*Advanced concrete technology*," John Wiley & Sons, Hoboken, NJ, 2011, 624 p.

Haktanir, T., Ari, K., Altun, F., and Karahan, O., "A comparative experimental investigation of concrete, reinforced-concrete and steel-fibre concrete pipes under three-edge-bearing test," *Construction and Building Materials,* 21(8), 2007, pp. 1702-1708.

MacDonald, C. and Trangsrud, J., "Steel fiber product introduction through pre-cast reinforced concrete pipe." *ACI Special Publication,* 222, 2004, pp. 185-199.

Marston, A., "The theory of external loads on closed conduits in the light of the latest experiments." *Iowa Engineering Experiment Station Bulletin,* 96, 1930.

Moore, I.D. "Buried pipes and culverts," in *Geotechnical and Geoenvironmental Engineering Handbook* edited by Rowe, R.K., Kluwer Academic, 2001, pp. 541-567.

Romualdi, J.P., and Mandel, J.A., "Tensile strength of concrete affected by uniformly distributed and closely spaced short lengths of wire reinforcement," in *ACI Journal Proceedings*, 61 (6), 1964, pp. 657-671.

Spangler, M.G., "The supporting strength of rigid pipe culverts," *Iowa State College Bulletin*, 112, 1933.

CHAPTER THREE

3 FULL-SCALE PIPES USING DRY-CAST STEEL FIBRE-REINFORCED CONCRETE[1]

3.1 INTRODUCTION

Steel fibres (SFs) enhance the post-cracking behaviour of hardened concrete through maintaining some of its load-carrying capacity after crack formation. Moreover, during fracture, energy is consumed in the de-bonding, pulling-out, and rupture of fibres leading to higher concrete toughness (Bentur and Mindess, 2007). The overall improvement in the engineering properties of concrete owing to SFs addition is a function of several variables, including the fibre shape, length, aspect ratio, volume fraction with respect to the total concrete volume, and the quality of the hosting matrix (Brandt, 2008).

Recently, structural applications of steel fibre-reinforced concrete (SFRC) have been increasing. For instance, SFRC has been used in tunnel linings (Cook *et al.*, 2007, Yan *et al.*, 2013, Abbas *et al.*, 2014 a, b), slabs on grade (Roesler *et al*., 2004), pavements on metal decks (Murakoshi *et al*., 2008), and seismic retrofitting and rehabilitation of various concrete structures (Morgan, 1984, Ramakrishnan, 1984; Ilki *et al*., 2004; Wang and Lee, 2007; di Tommaso *et al*., 2008). However, only about 5% of the total amount of FRC that is produced annually is used in precast members (Bentur and Mindess, 2007).

[1] A version of this chapter was published in the *Construction and Building Materials Journal* (2014). Part of this chapter was published in the Tunneling Association of Canada Conference, Montreal, Canada (2012).

This chapter investigates the mechanical properties of dry-cast concrete incorporating different types of commercially available steel fibres at different addition rates. Adequate type and dosage of steel fibres for manufacturing full-scale dry-cast steel fibre-reinforced concrete (DCSFRC) precast pipes were identified. Moreover, the flexural behaviour of full-scale 300 mm diameter DCSFRC pipes was explored in comparison to that of plain concrete (PC) and regularly reinforced concrete (RC) pipes with similar diameter.

3.2 EXPERIMENTAL PROGRAM

3.2.1 Materials and Mixture Proportions

A commercial precast pipe dry-cast concrete mixture was adapted for the fabrication of laboratory specimens. A total of 15 mixtures including a control mixture were cast. High early-strength portland cement and ground granulated blast furnace slag (GGBFS) were used in the binder formulation. Gravel with a maximum nominal size of 13 mm was used as the coarse aggregate. Natural sand with a fineness modulus of 2.82 was used as the fine aggregate. The water-to-cementitious materials ratio (w/cm) for all mixtures was 0.38. A polycarboxylate super-plasticizer was added at a rate of 0.16% by mass of the cementitious materials. A non-ionic surfactant-dispersing admixture was added at a rate of 0.20% by mass of the cementitious materials. Four commercially available steel fibres were used. Steel fibres were either collated (Type A and B) or dispersed (Type C and D). The steel fibre dosage in the tested concrete mixtures (W_f) was 20, 40, and 60 kg/m^3 (V_f = 0.25, 0.50, and 0.75 % by volume fraction). The effect of synergistic hybridization between fibres A (short) and B (long) was also investigated. The composition of the tested DCSFRC mixtures and different properties of the used steel fibres are shown in **Tables 3-1** and **3-2**, respectively.

3.2.2 Specimens Preparation and Testing

Cement, GGBFS, coarse and fine aggregates, as well as steel fibres were dry-mixed for 5 minutes using a drum mixer. The superplasticizer and surfactant were added to the mixing water. Water was then added gradually to the mixture and mixing continued for another five

Table 3-1 Concrete mixture proportions

Material	Mass/Cement Mass
Cement (SG = 3.15)	1.00
Blast Furnace Slag (SG = 2.9)	0.54
Fine Aggregate (SG = 2.68)	5.00
Coarse Aggregate (SG = 2.75)	4.17
Water (SG = 1.0)	0.58
Super plasticizer	0.34 litre/m^3
Surfactant	0.43 litre/m^3
Steel Fibres (SG = 7.8)	0, 20, 40, 60 kg/m^3

SG = specific gravity

Table 3-2 Physical and mechanical properties of steel fibres used

Fibre Type	Physical Properties				Mechanical Properties	
	Shape	L_f (mm)	d_f (mm)	φ	F_f (MPa)	E_f (GPa)
A[1]	Collated-hooked end	35	0.55	65	1550	210
B[2]	Collated-hooked end	60	0.75	80	1350	210
C[3]	Dispersed-hooked end	50	1.00	50	1050	N/A
D[4]	Dispersed-crimped	50	1.04 (eq.)	44	1242	N/A

L_f = fibre length, d_f = fibre diameter, φ = fibre aspect ratio, F_f = fibre tensile strength, E_f = fibre modulus of elasticity. [1] Dramix RC-65/35-CN. [2] Dramix RC-80/60-CN. [3] Novocon 1050. [4] Novocon XR.

minutes. The average measured air content was 3.5%. All mixtures exhibited a zero slump. Cylindrical 100 mm × 200 mm and prismatic 150 x 150 x 500 mm specimens were cast from each batch. Specimens were cast and compacted in accordance with the common practice for SFRC (i.e. no rodding or internal vibration). In agreement with previous work on dry-cast

concrete and SFRC pipes (e.g. Haktanir *et al*., 2007 and Wilson, 2012) specimens' compaction was done using a vibrating table. The vibrating table had dimensions of 500x500 mm and a motor with frequency between 2600 and 3600 RPM. Its maximum load capacity is 140 kg. Immediately after casting, specimens were covered with plastic caps and wet burlap to prevent surface drying. All specimens were de-moulded after 24 hours and moved to a moist curing room (T = 25°C and RH = 98%) until the testing age.

At 28 days, the compressive strength *(C_s)*, modulus of elasticity (E_s) and splitting tensile strength (T_s) were evaluated for the various mixtures according to the guidelines of ASTM C39 (Standard Test Method for Compressive Strength of Cylindrical Concrete Specimens), ASTM C469 (Standard Test Method for Static Modulus of Elasticity and Poisson's Ratio of Concrete in Compression) and ASTM C496 (Standard Test Method for Splitting Tensile Strength of Cylindrical Concrete Specimens), respectively. Each reported result represents the average values obtained on four identical specimens.

The flexural performance of DCSFRC prism specimens was evaluated as per the procedure of ASTM C1609 (Standard Test Method for Flexural Performance of Fibre-Reinforced Concrete (Using Beam with Third-Point Loading)). A controlled displacement load was applied at a rate of 0.05 mm/min. The first crack load was identified as the load whereby the initial linear elastic slope of the load displacement plot ends, while the peak/ultimate load was considered as the maximum load of the load-mid span displacement curve. Three replicate prismatic specimens from each mixture were tested to evaluate the flexural performance. **Tables 3-3** and **3-4** show the average and coefficient of variation (COV) for each of the conducted tests.

3.2.3 Full-Scale Pipe Production and Testing

Full-scale 300 mm DCSFRC pipes using discrete steel fibres as the main reinforcement were cast at a commercial precast plant in Oakville, Ontario. The plant uses the dry-cast production method. Pipes were cast vertically in a mould consisting of an inside core and an outside mold. This assembly was placed vertically on a supporting ring and the reinforcement cage, if any, with its spacers was placed within the mould. Then, concrete was poured in

Table 3-3 Mixtures prepared and their mechanical properties

Mix. no.	Group	Fibre Type	W_f kg/m³	C_s		T_s		E_s	
				MPa	COV	MPa	COV	GPa	COV
1	Control	-	-	45.80	3.04	5.59	1.33	35.79	6.26
2	Collated Fibres	A	20	45.80	3.29	6.86	6.36	37.53	4.61
3			40	48.92	1.85	7.07	5.96	33.53	7.03
4			60	49.65	1.30	7.85	4.51	34.78	3.87
5		B	20	47.39	4.56	6.21	7.53	32.05	1.70
6			40	51.99	2.52	8.71	3.20	37.17	2.34
7			60	53.98	8.17	8.99	6.52	35.62	5.28
8	Dispersed Fibres	C	20	52.88	4.33	6.76	0.38	34.85	5.80
9			40	58.02	6.38	7.32	4.22	37.77	2.53
10			60	61.64	2.40	7.92	0.94	34.37	2.80
11		D	20	52.74	4.83	6.29	5.19	35.15	2.54
12			40	56.24	1.09	6.89	1.95	34.82	3.26
13			60	60.00	4.31	6.95	4.80	N/A	N/A
14	Hybrid	A+B	20+20	50.00	1.79	6.93	9.18	N/A	N/A
15		A+B	20+40	51.99	4.38	9.05	6.52	N/A	N/A

Table 3-4 Summary of flexural performance test results

Mix no.	First Peak			Second Peak		at δ of L/600 (0.762 mm)	at δ of L/150 (3.05 mm)
	f_1 (MPa)	COV	δ_1 (mm)	f_2 (MPa)	δ_2 (mm)	f^{D}_{600} (MPa)	f^{D}_{150} (MPa)
1	4.76	6.55	0.08	---	---	---	---
2	5.23	9.93	0.09	---	---	---	1.09
3	5.90	0.46	0.09	---	---	3.25	2.45
4	6.81	1.58	0.09	---	---	4.92	3.80
5	5.44	1.39	0.08	---	---	2.96	1.26
6	6.41	2.38	0.07	---	---	4.50	4.00
7	6.85	3.76	0.09	7.75	0.57	6.64	5.61
8	5.38	0.59	0.07	---	---	2.94	1.56
9	6.26	1.32	0.06	---	---	4.26	3.62
10	6.58	5.23	0.07	6.58	0.70	6.20	4.64
11	4.98	8.41	0.05	---	---	---	0.56
12	5.13	7.46	0.06	---	---	3.34	0.74
13	6.69	1.24	0.07	---	---	3.46	1.45
14	6.57	1.94	0.08	6.73	0.79	5.81	3.91
15	6.61	2.28	0.07	7.46	0.85	7.35	4.44

under mechanical vibration. When the mould was filled, a circular ring descends onto the top of the concrete and applies pressure. An electronic management system regulates the supply of concrete and the application of the pressure head. The form was removed immediately after casting, as the newly formed pipe could support its self-weight. Pipes were then transferred to a curing room. The curing regime lasted for eight hours where the temperature was raised gradually up to 55^{o} under a relative humidity of 95%**.** After this steam curing, pipes were stored at the plant yard until being shipped to the Structures Laboratory of Western University for testing. All pipes had an inside diameter D_i of 300 mm and a Type C wall (D_i/12 + 44 mm). Two duplicates of PC, RC, and DCSFRC pipes were also fabricated and tested. The targeted pipe strength was Class V pipe according to ASTM C76. RC pipes had one circular reinforcement cage with a reinforcement area of 1.5 cm² per linear meter of pipe wall. **Table 3-5** shows the fabricated 300 mm diameter pipes, and their corresponding fibre type and dosage.

Table 3-5 Fabricated 300 mm diameter pipes

Fibre Type	Pipe Designation	W_f (kg/m^3)
Plain	PC	-
Regular Reinforcement	RC	-
Fibres Type A[1] (short fibres)	SS20	20
	SS40	40
	SS60	60
Fibres Type B[2] (long fibres)	SL20	20
	SL40	40
	SL60	60
Hybrid (short fibres + long fibres)	SH20 (0.5:0.5)*	20
	SH40 (0.5:0.5) *	40
	SH60 (0.33:0.67) *	60

* = hybridization ratio. [1] Dramix RC-65/35-CN. [2] Dramix RC-80/60-CN.

The mechanical performance and structural behaviour of concrete pipes were evaluated using the Three Edge Bearing Test (TEBT) as per the guidelines of ASTM C497 (Standard Test Methods for Concrete Pipe, Manhole Sections or Tile) as shown in **Fig. 2-1**. A line load was applied along the crown of the pipe using a displacement controlled universal materials testing system (MTS). A rigid steel beam was attached to the loading system. The upper bearing consisted of a 25 mm thick hard rubber strip attached to a rigid wood beam. Pipes were supported along their longitudinal axis on a lower bearing system consisting of 25 mm thick hard rubber strips attached to two rigid wood beams spaced at 50 mm apart. For each tested pipe specimen, the vertical deflection of the crown toward the invert at pipe spigot was recorded versus the load using linear displacement transducers (LVDTs). LVDTs were positioned against the inner surface of the pipe crown and attached to supports fixed at the bottom part of the pipe. In addition, concrete strain at the pipe invert at spigot (area of maximum bending moment) was recorded using strain gauges mounted on the pipe inner surface. The test setup and pipe instrumentation are shown in **Fig. 3-1.**

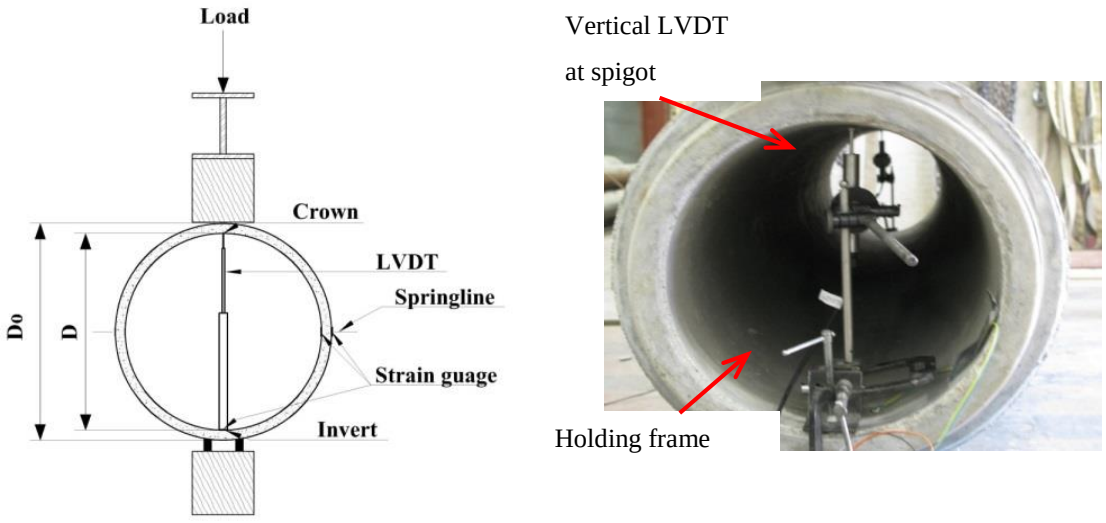

Figure 3-1 Testing setup and pipe instrumentation.

3.3 RESULTS AND DISCUSSION

3.3.1 Mechanical Characterization of DCSFRC Mixtures

3.3.1.1 Compressive Strength

Figure 3-2 illustrates the compressive strength of DCSFRC mixtures (C_s) with respect to that of the control mixture without fibre (C_p) (C_s/C_p). Generally, the compressive strength increased with the addition of steel fibres. The higher the fibre dosage, the higher was the increase. For example, for mixtures incorporating Type B steel fibres, C_s/C_p increased by about 14% as the fibre dosage increased from 20 to 60 kg/m^3. At higher fibre content, more fibres can resist crack formation in the longitudinal direction of the tested cylinders, then resulting in higher compressive strengths (Yang, 2011).

Using a hybrid fibre system did not affect C_s of DCSFRC. C_s/C_p for mixtures incorporating a hybrid system of fibres (Types A and B) was in between those for mixtures incorporating fibre A or B individually at the same fibre content. For instance, at a fibre dosage of 40 kg/m^3, C_s/C_p for mixtures incorporating Types A and B and a hybrid fibre was 1.06, 1.14, and 1.09, respectively.

It has been reported elsewhere (Ezeldin and Lowe, 1991, and Gao *et al.*, 1997) that an increase in the steel fibre content resulted in an increase in the compressive strength. For mixtures with low fibre content ($V_f < 1$), an increase in the compressive strength up to 25%, depending on the fibre type and content, can be found in the literature (Ezeldin and Lowe, 1991; Gao *et al.*, 1997; Yao *et al.*, 2003; Song and Hwang, 2004; and Nehdi and Ladanchuk, 2004). In addition, ACI Committee 544 (2009) documented an increase in the compressive strength ranging from zero to 23% for concrete with a normal range of fibre content. However, others (Beaudoin, 1990, and Johnston, 2001) reported that steel fibres had little to no effect on the compressive strength of SFRC.

Generally, these discrepancies on the effect of steel fibres on the compressive strength of concrete can be explained by the conflicting effects of fibres. Steel fibres addition arrests the development of micro-cracks in concrete, thus possibly resulting in higher compressive strength. Simultaneously, it can reduce workability and compactability of concrete, leading to

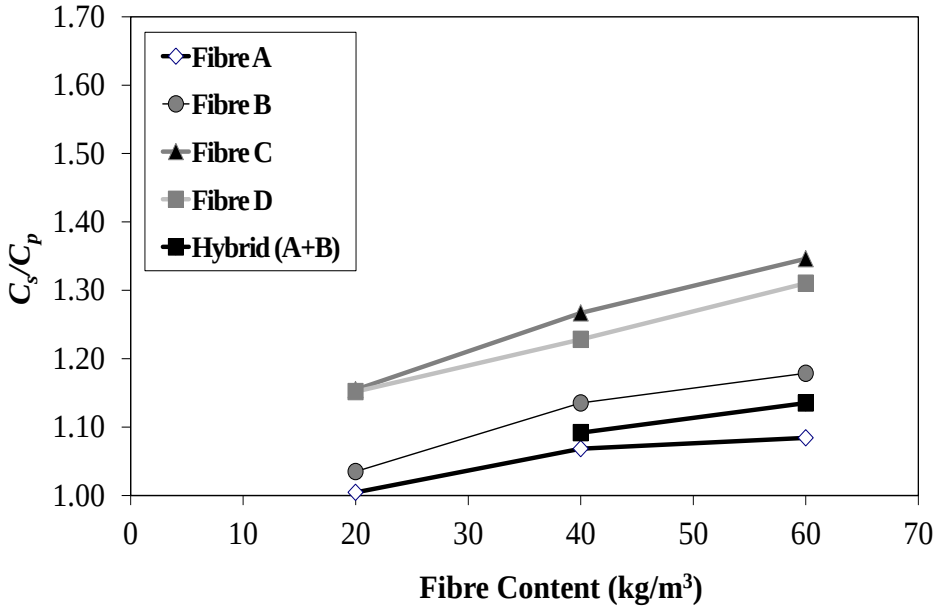

Figure 3-2 Relative compressive strength (C_s/C_p) with respect to fibre content.

perturbation of the matrix and possibly higher voidage, which in turn reduces compressive strength. In addition to the fibre dosage, perturbation of the cementitious matrix will depend on its ability to accommodate fibres (Neves and Fernandes, 2005). Unlike normal concrete, zero-slump concrete relies more on vivid mechanical vibration for its consolidation and less on its inherent flow properties. Since the detrimental effect of fibre addition on consolidation by energetic mechanical vibration is less significant than that on conventional workability, the positive effect of steel fibre addition on the compressive strength of DCSFRC can be more significant than that observed in normal slump concrete.

To account for the effects of both the fibre dosage and aspect ratio, the compressive strength of DCSFRC mixtures was expressed as a function of the fibre-reinforcing index as shown in **Eq. 3-1** (Harajli *et al*., 2002; Ou *et al*., 2012):

$$RI_v = \sum_{i=1}^{n} V_{f,i} \frac{L_{f,i}}{d_{f,i}} \qquad \textbf{Eq. 3-1}$$

where V_f is the fibre volume fraction in percentage and n is the total number of fibre types used in the mixture. The effect of the reinforcing index on the DCSFRC compressive

strength is illustrated in **Fig. 3-3**. Generally, no correlation was found between the DCSFRC compressive strength and the reinforcing index. This behaviour is expected since the fibre length (L_f) showed no effect on the compressive strength (C_s) of DCSFRC as reported in **Table 3-3**. For example, at a fibre content of 60 kg/m^3, mixtures incorporating different fibre types, including A (L_f = 35 mm- hooked ends) and B (L_f = 60 mm- hooked ends), exhibited C_s values of 49.7 and 54.0 MPa, respectively (i.e. only 8% difference). Moreover, at the same fibre content, the larger diameter fibre is preferred as it performs better under a buckling failure mode, leading to higher compressive strength (Beaudoin, 1991).

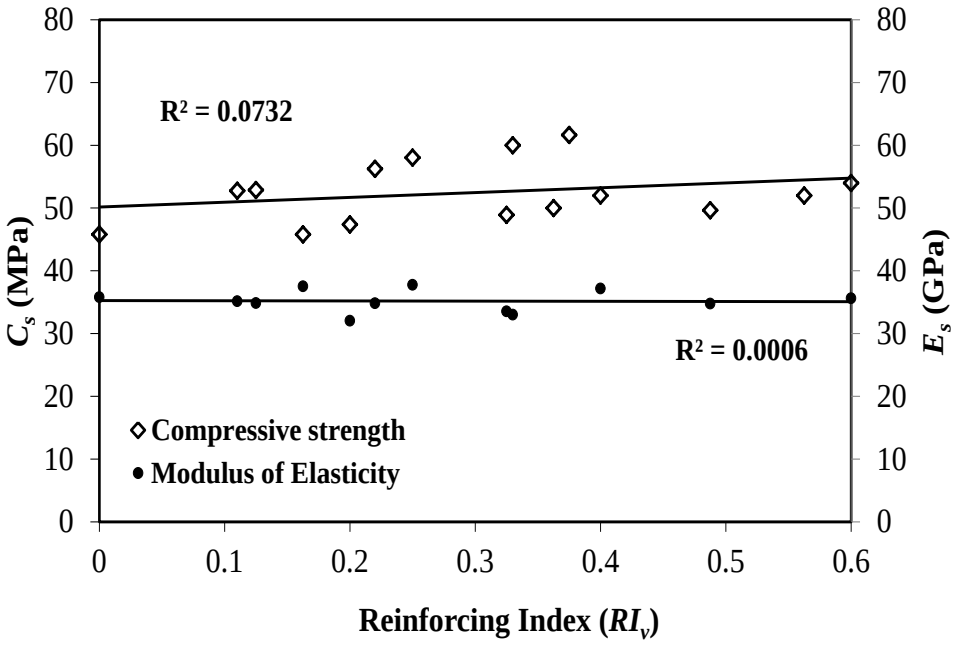

Figure 3-3 Effect of fibre reinforcing index on compressive strength and modulus of elasticity of DCSFRC.

3.3.1.2 Splitting Tensile Strength

Figure 3-4 illustrates the splitting tensile strength of the tested DCSFRC mixtures (T_s) with respect to that of the control mixture without fibre (T_p) (T_s/T_p). Regardless of the fibre type,

increasing the fibre content led to higher splitting tensile strength. This can be attributed to the presence of fibres in the matrix, which intersect, block, and arrest the propagation of cracks (Song and Hwang, 2004). The increase in relative splitting tensile strength ranged between 1.13 and 1.60. This range is in agreement with previous findings (Wafa and Ashour, 1992; Song and Hwang, 2004; Bentur and Mindess, 2007; Yazici *et al*., 2007; Mohan and Parthiban, 2011).

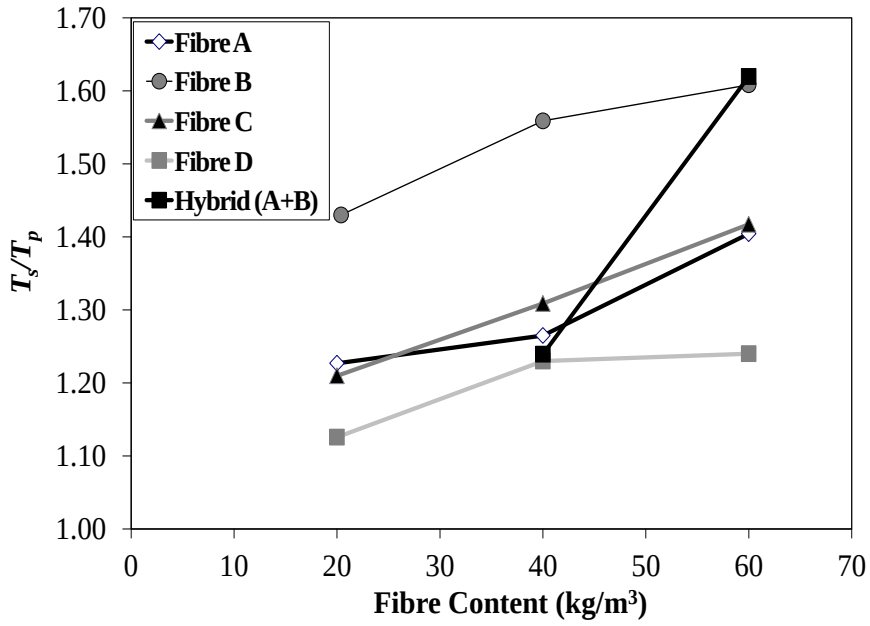

Figure 3-4 Relative splitting tensile strength (T_s/T_p) with respect to fibre content.

Mixtures incorporating Type B fibre exhibited the highest T_s/T_p increase. This can be attributed to its longer length, which is more effective at bridging micro-cracks. For mixtures incorporating a hybrid fibre system (i.e. one third of the long fibres (Type B) was replaced with shorter fibres (Type A)), the increase in T_s/T_p was not affected if compared with that of mixture incorporating fibre B only. At a fibre content of 60 kg/m^3, the increase in T_s/T_p for mixtures incorporating the Type B fibre or hybrid fibres was 60%. However, T_s/T_p dropped significantly when the hybridization ratio became 50:50 (i.e. from 1.60 to 1.24). This finding

suggests the existence of a threshold limit in replacing long fibres with short ones, beyond which fibre hybridization becomes inefficient.

In addition, **Fig. 3-4** reveals that hooked end fibres were more effective in enhancing the splitting tensile strength of DCSFRC mixtures than the crimped fibres. Type C and D fibres had the same length and comparable aspect ratio (φ); however, T_s/T_p increased in the range of 1.21 to 1.42 and 1.13 to 1.24 as the fibre dosage increased from 20 to 60 kg/m^3, respectively. This confirms that fibres with deformed ends are more effective than those with deformations over their entire length. This is because crimped fibres will transfer stresses through anchorage along its entire length, initiating crushing, and/or splitting of the matrix, which reduces its effectiveness in stress transfer (Trottier and Banthia, 1994).

Figure 3-5 shows the effect of the reinforcing index, RI_v on T_s. Unlike the case of compressive strength, the tensile strength of DCSFRC mixtures increased linearly with the increase of RI_v. This is expected since T_s increases with the increase of both V_f and φ.

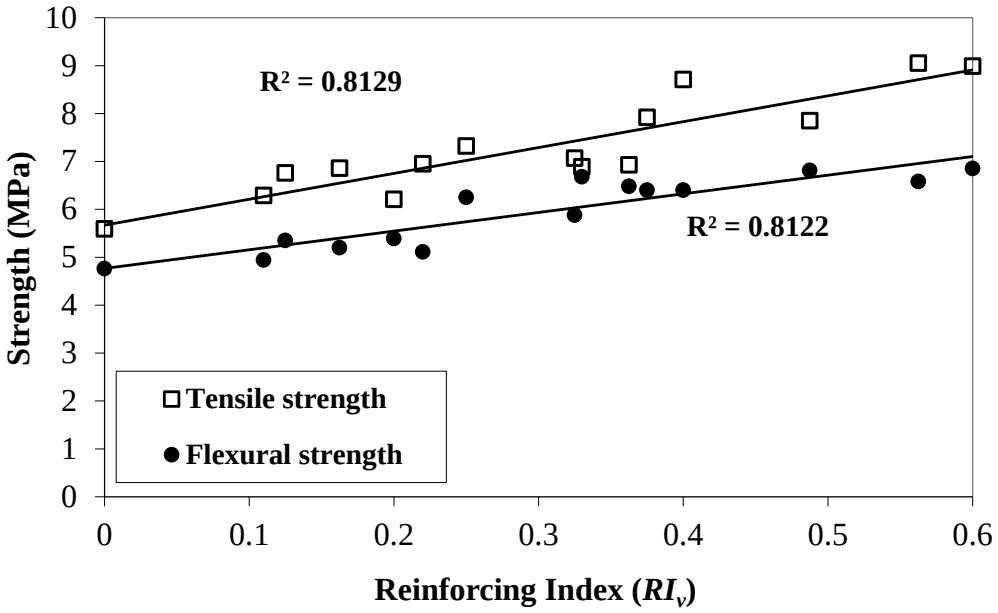

Figure 3-5 Effect of fibre reinforcing index on tensile strength and flexural strength of DCSFRC.

3.3.1.3 Modulus of Elasticity

Figure 3-3 shows the effect of RI_v on the modulus of elasticity (E_s) of DCSFRC mixtures. It can be observed that E_s fluctuated as the reinforcing index increased. The modulus of elasticity of DCSFRC mixture was independent of the fibre length and shape. Moreover, for the tested range of fibre dosage, E_s was only marginally affected by the change in the fibre dosage (i.e. ± 10% compared to that of the control mixture without fibres) (**Table 3-3**). This is in agreement with previous results (Chem *et al*., 1992; Jo *et al*., 2001). This behaviour is expected since E_s values were measured up to only 40% of the compressive strength (i.e. prior to concrete cracking). Hence, fibres were not fully activated (Ou *et al.*, 2011).

3.3.1.4 Flexural Strength

The flexural behavior of PC and DCSFRC mixtures was evaluated based on the first-peak strength (f_1), second-peak strength (f_2) and residual strengths at deflection of $L/600$ (f^{D}_{600}) and $L/150$ (f^{D}_{150}) values. The following formula was used to calculate the flexural strength at different points (**Eq. 3-2**):

$$f = \frac{PL}{bd^2} \qquad \textbf{Eq. 3-2}$$

where f is the flexural strength (MPa), P is the load (N), L is the span length (457 mm), b is the specimen's average width at fracture (152 mm), and d is the specimen's average depth at fracture (152 mm). **Eq. 3-2** is derived from the flexural stress equation $f = M.y/I$, where M is the bending moment, y is the distance between the section centroid and the extreme fibre subjected to either tension or compression, and I is the second moment of the area of the section. In the case of a third point-loading flexural test, $M = PL/6$, $y = d/2$ and $I = bd^3/12$.

Although **Eq. 3-2** is based on linear stress-strain distribution, which is no longer valid after the first crack formation, the calculated values for residual and peak stresses can be acceptable for the sake of comparison (ACI 544.4, 2009). Flexural results for different mixtures are summarized in **Table 3-4**. Similar to splitting tensile strength results, the first peak strength of DCSFRC mixtures (f_{1s}) increased linearly as the RI_v (**Fig. 3-5**) and fibre

dosage increased (**Fig. 3-6**) increased. This is because f_{1s} is directly proportional to both V_f and φ. This increase varied between 5% and 44% depending on the fibre length and shape. Interestingly, increasing the fibre dosage from 20 to 40 kg/m^3 resulted in higher first-peak strength than that induced when the fibre dosage increased from 40 to 60 kg/m^3. This suggests that a fibre content of 20 kg/m^3 or less is insufficient to improve the flexural or post-cracking behaviour of DCSFRC mixtures compared to that of the control mixture. This observation was confirmed by load-deflection curves and residual strength results as discussed below.

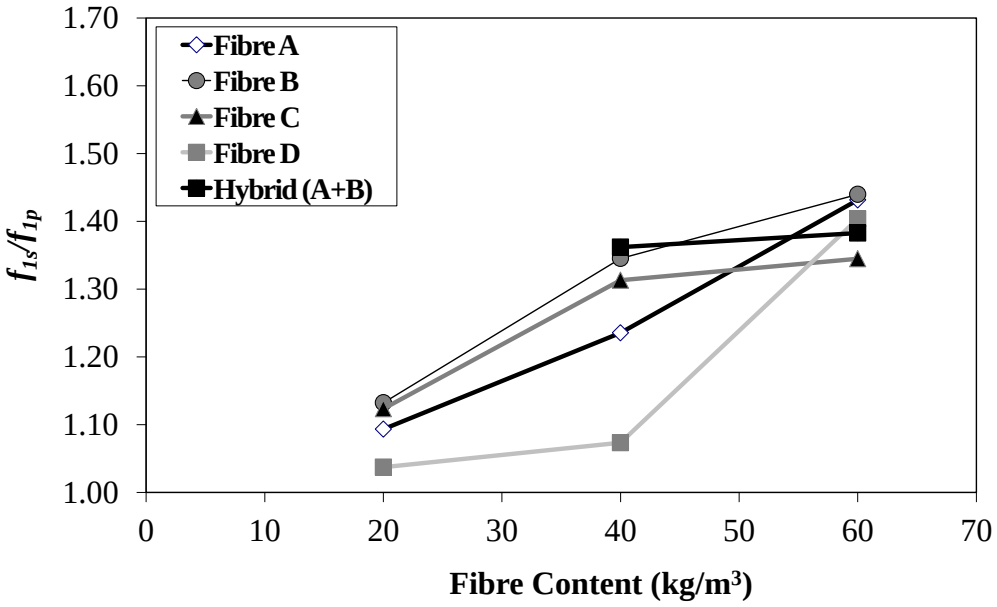

Figure 3-6 Effect of fibre content on relative flexural strength.

3.3.1.5 Load- Deflection Curves

Figure 3-7 (a-d) shows the mid-span deflection of tested prismatic specimens versus the applied load under the three-point bending test. Generally, the specimen's deflection increased linearly as the load increased until reaching the peak load. Thereafter, the load dropped while the specimen exhibited a progressive deflection. Such load drop represented the onset of cracking due to matrix failure. For control specimens, the test was terminated at

the peak load since the specimen was broken into two pieces and no post-peak behaviour could be recorded. Conversely, steel fibres in DCSFRC specimens started bridging the developed cracks at this point. The deflection of DCSFRC specimens decreased as the fibre dosage increased. Beyond the peak load, the main crack formed at mid-span started to widen and move towards the top edge of the specimen.

However, specimens incorporating 20 kg/m^3 of fibre exhibited large instability regions (i.e. abrupt increase in deflection accompanied by a reduction in load capacity) regardless fibre type. Mixtures incorporating higher fibre dosage showed more stable behavior and some exhibited a second peak load, f_2 after the initial peak (**Figs. 3-7b** and **3-7c**), a phenomenon known as deflection hardening (Naaman, 2003, and Kim *et al.*, 2010). For instance, for mixtures incorporating Type A fibre, the average residual load at a deflection of (L/150) = 3.05 mm was 8.47, 18.95 and 29.41 kN for fibre dosages of 20, 40 and 60 kg/m^3, respectively. Therefore, a fibre content greater than 20 kg/m^3 was required to achieve stable post-peak flexural behaviour.

Moreover, longer fibre length enhanced the post-peak behaviour and energy absorption capacity of DCSFRC specimens greater than that of shorter fibres (**Figs**. **3-7a** and **3-7b**). For example, at a fibre dosage of 40 kg/m^3, the average residual load immediately dropped after the first peak load to 25.82 kN and 33.20 kN at corresponding deflections of 0.71 and 0.42 mm for specimens incorporating Type A (L_f = 35 mm) and B (L_f = 60 mm) fibres, respectively. Unlike specimens incorporating 60 kg/m³ of fibre A, specimens made with similar dosage of fibre B exhibited a second peak load of 60.70 kN. Therefore, longer steel fibres are recommended to achieve better post-peak flexural behaviour and higher energy absorption capacity. Hybridization of two different fibre lengths in the same mixture was found to improve the post-peak behaviour of DCSFRC specimens, leading to higher residual loads at similar deflection (**Fig. 3-7b**). In addition, using fibres with different lengths can better control the micromechanics of crack formation at different strain levels than single-type fibres (Nehdi and Ladanchuk, 2004). This explains the comparable average second peak load (60.7 and 60.13 kN, respectively) for mixtures incorporating fibre Type B alone and hybrid fibre system (A (20 kg/m^3) + B (40 kg/m^3)).

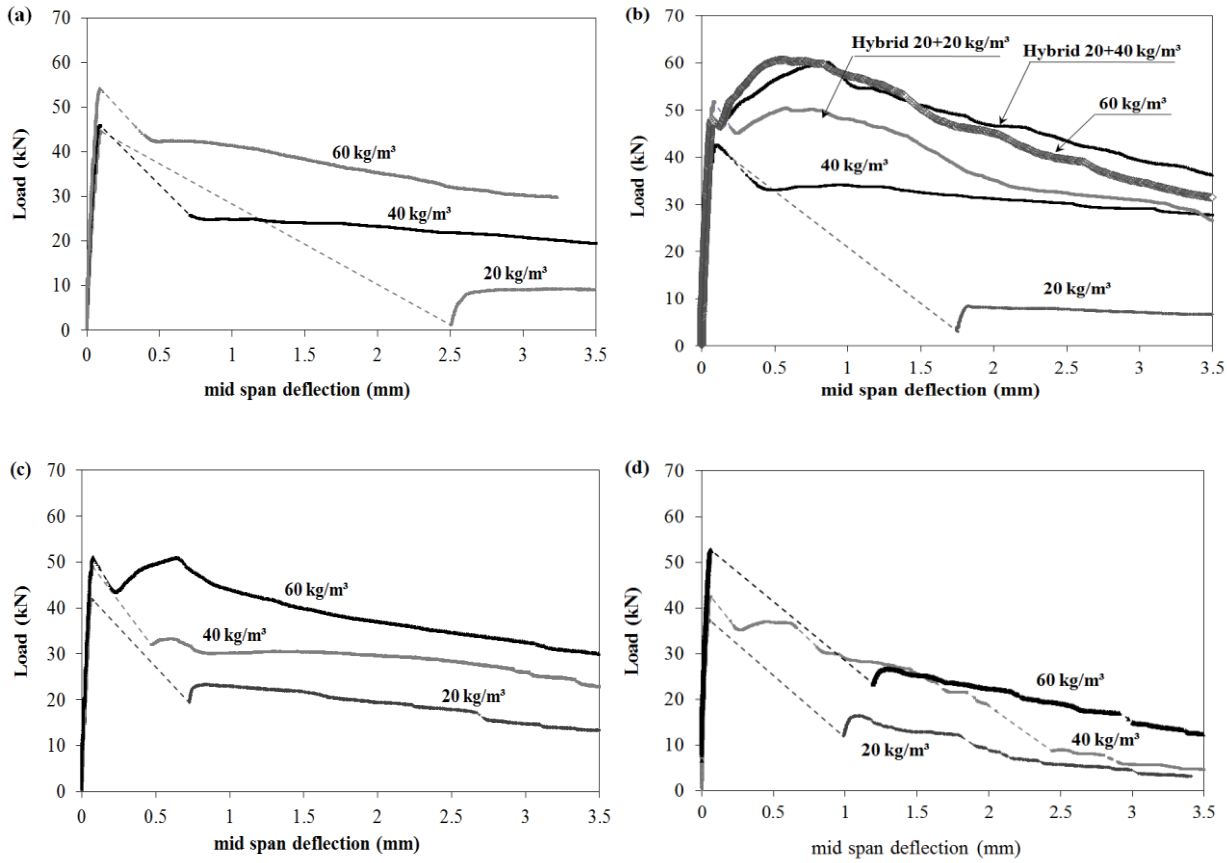

Figure 3-7 Representative load-deflection curves of DCSFRC specimens under three-point bending test for different types of fibre: a) Type A, b) Type B and hybrid fibre system (A+B), c) Type C, and d) Type D.

In addition to the fibre dosage and length, its shape was found to affect the flexural behavior of DCSFRC specimens. As shown in **Figs. 3-7c** and **3-7d**, while both fibres had similar length and comparable aspect ratio, Type C fibres achieved better post-peak behaviour and higher energy absorption capacity than that imparted by Type D fibres. For instance, at a fibre dosage of 60 kg/m^3, DCSFRC with Type C fibres achieved a second peak load (P_2 = 51.10 kN) equivalent to the first cracking load (P_1 = 51.10 kN), while DCSFRC specimens with Type D fibres did not exhibit such a behaviour. This can be ascribed to the low stress transfer effectiveness of crimped fibre as explained earlier, in agreement with previous study (Soroushian and Bayasi, 1991).

Further analysis of the flexural behaviour of DCSFRC mixtures based on residual strength is shown in **Fig. 3-8**. Residual strength represents the ability to sustain load after first crack at different specific deflection values. Generally, residual strength results confirm earlier findings: a fibre dosage of 20 kg/m^3 was unable to improve the post-peak behaviour; and at higher fibre dosage, fibres with higher aspect ratio (especially Type B) maintained higher residual strength at larger deflections. For example, for DCSFRC specimens incorporating 60 kg/m^3 of fibre, the average residual strengths were 6.6 and 5.6 MPa for Type B fibres (L_f = 60 mm- φ = 80), 6.2 and 4.6 MPa for Type C (L_f = 50 mm- φ = 50) and 4.9 and 3.8 MPa for Type A (L_f = 35 mm- φ = 65) fibres, respectively at a deflection of (L/600) = 0.76 mm and (L/150) =3.05 mm.

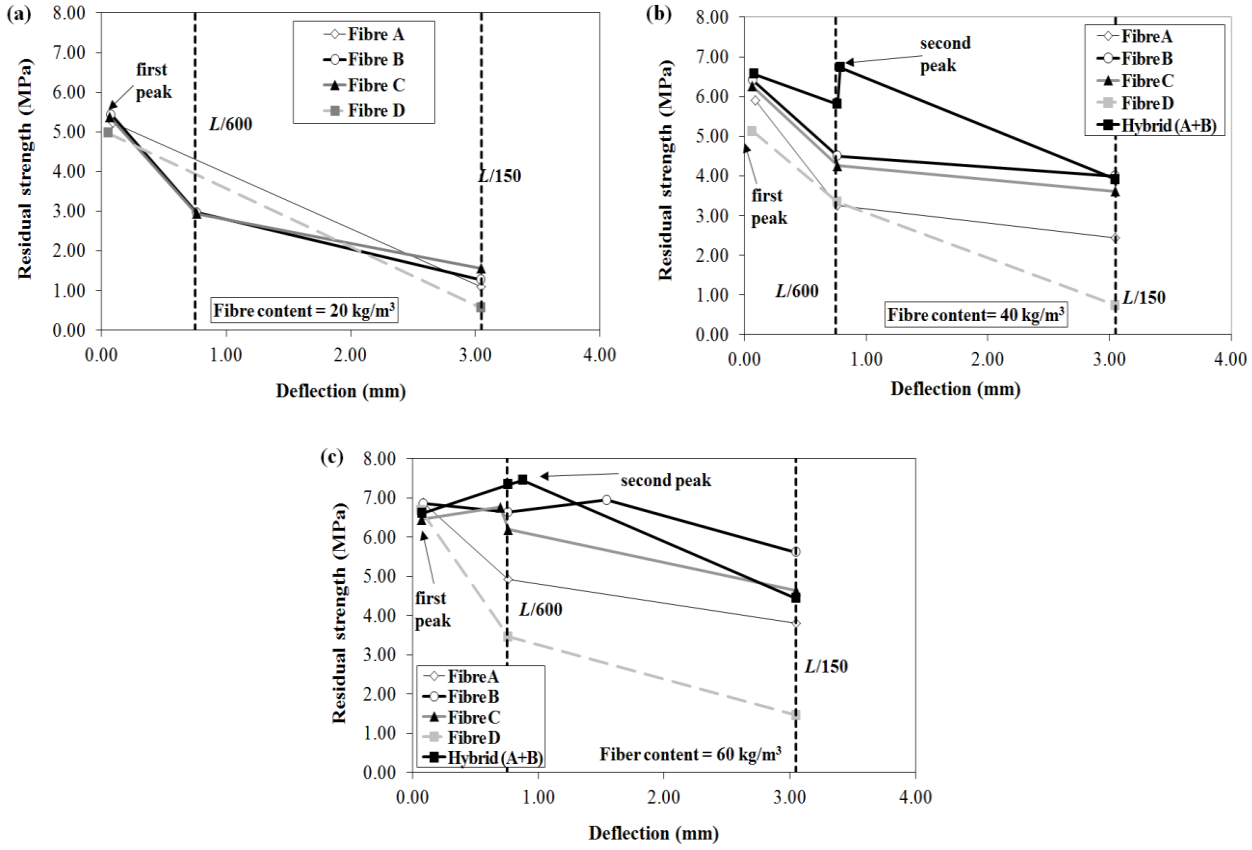

Figure 3-8 Residual strengths at different deflections for DCSFRC mixtures with fibre contents: a) 20 kg/m^3, b) 40 kg/m^3, and c) 60 kg/m^3.

The purpose of the preliminary study was to recommend a steel fibre type and dosage to be used in the fabrication of full-scale DCSFRC pipes. Thus, the flexural performance, in terms of first peak strength (f_{1s}) and the softening/hardening response in the post-cracking stage, was used in ranking the various fibres investigated. The observed performance ranked as follows: Type B fibres > Type C > Type A > Type D. Therefore, Type B fibres were recommended for the full-scale production stage. However, SFRC pipes have a known issue with fibres sticking out of the surface, especially at the spigot, which may potentially harm pipe joints during installation. Therefore, the industry partner requested using short fibres (Type A fibres) as well, especially in the fabrication of small size pipes (D_i = 300 mm) having a relatively smaller wall thickness (h = 69 mm). Thus, it was decided to use both fibres A and B for the full-scale pipe production.

3.3.2 Mechanical Characterization of Full-Scale DCSFRC Precast Pipe

3.3.2.1 Failure Mechanism

Flexural failure was the governing failure mechanism for all tested full-scale precast pipes. Such failure was characterized by the formation of longitudinal cracks at the inner crown and inner invert, as well as on the outer spring-lines of the precast pipe (**Fig. 3-9)**. Other failure mechanisms associated with conventional precast concrete pipes reinforced with steel cages (i.e. diagonal and radial tension) were not observed. DCSFRC pipes were capable to undergo large vertical and horizontal displacements without collapsing. In fact, none of the tested DCSFRC pipes collapsed during the testing. Tests were stopped due to excessive deformation beyond the ultimate load, which was accompanied by very large crack widths (> 10 mm). Examining the opened crack zones showed that both failure mechanisms (fibre pullout and rupture) had occurred (**Fig. 3-10**).

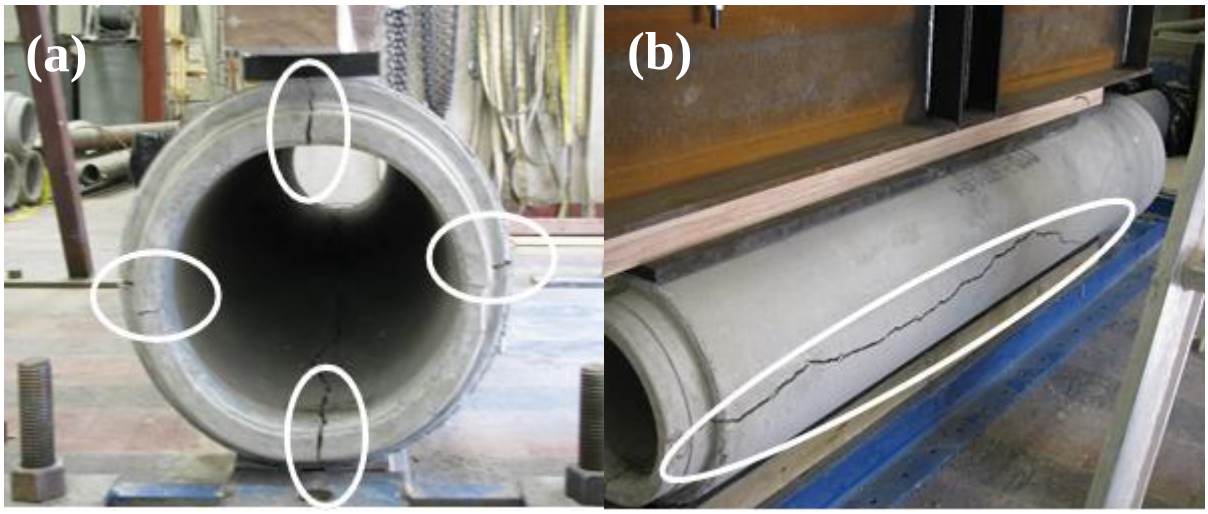

Figure 3-9 Flexural failure mechanism: (a) cross-sectional cracks, and (b) longitudinal cracks.

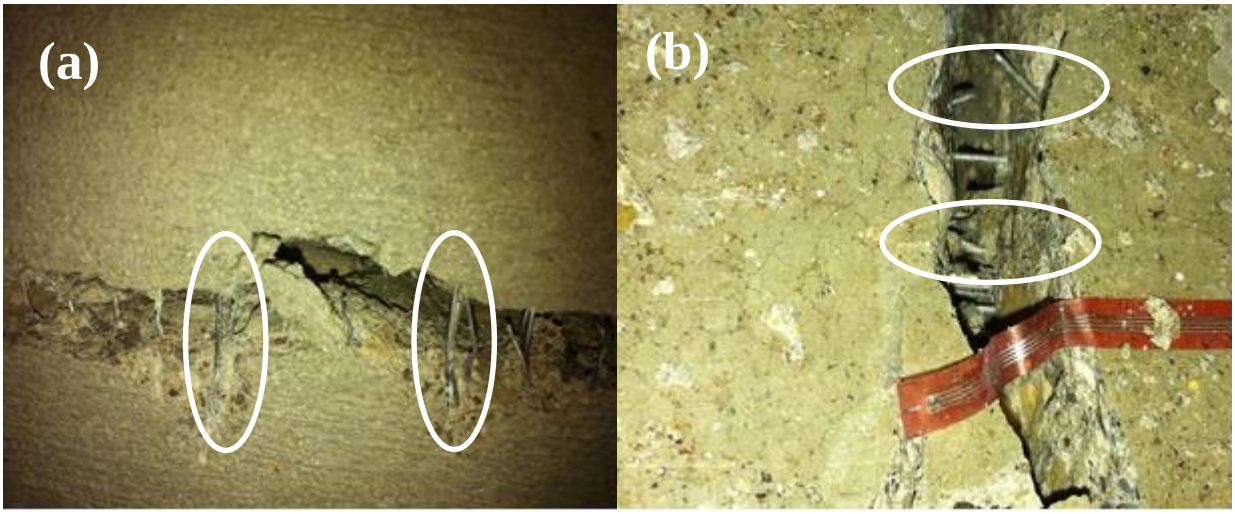

Figure 3-10 DCSFRC failure mechanism: (a) fibres pull-out, and (b) fibres rupture.

3.3.2.2 Cracking (P_{cr}) and Ultimate (P_{ult}) Loads

The cracking and ultimate strength results for all tested pipes are summarized in **Table 3-6.** The average coefficient of variation (COV) was about 1.49% and 2.17% for the crack and ultimate loads, respectively. All tested pipes, including PC pipes, exhibited substantially higher loads than the specified crack (P_{cr}) and ultimate (P_{ult}) strength for Class V pipes (highest strength class) according to ASTM C76 (i.e. P_{cr} = 104 and P_{ult} = 130 kN). For

instance, the average ultimate loads for DCSFRC pipes fabricated with 20 kg/m^3 of fibres Type A, B, and hybrid A-B fibres were 362, 371, and 346 kN, respectively. This represents an increase in the ultimate strength of the pipe of about 8% and 12.4% for fibre Type A, 10.8% and 15.2% for fibre Type B and 3.3% and 7.5% for hybrid A-B fibres compared to that of the PC and RC pipes, respectively. This can be attributed to the enhancement of the concrete tensile and flexural strengths due to fibres intersecting, blocking, and arresting the propagation of cracks (Song and Hwang, 2004). This is in agreement with results of the tested DCSFRC mixtures explained earlier.

Similar to the trend observed for DCSFRC beam specimens, the higher the fibre content, the higher was the increase in ultimate load of the precast pipes regardless the fibre type. For instance, increasing the fibre dosage from 20 to 40 and 60 kg/m³ resulted in an increase in the ultimate load by 4.1% and 24.1% for pipes fabricated with Type A (short fibre), 6.0% and 41.5% for pipes fabricated with Type B (long fibre), and 5.5% and 34.4% for pipes fabricated with hybrid fibres, respectively. Values shown in **Table 3-6** reveal that using longer fibres resulted in higher ultimate load compared to loads achieved when short or hybrid fibres were used. Short fibres were less effective since they tended to slip out of the matrix with less contribution to strength (Bentur and Mindess, 2007), which concurs with earlier findings from DCSFRC beam specimens.

Table 3-6 Summary of the crack and ultimate loads of tested pipes

Pipe	P_{cr} (kN)				P_{ult} (kN)			
	Pipe 1	Pipe 2	avg.	COV	Pipe 1	Pipe 2	avg.	COV
PC	337	333	335	0.84	337	333	335	0.84
RC	318	316	317	0.45	318	328	322	2.19
SS20	360	360	360	0.00	364	360	362	0.78
SS40	355	364	360	1.77	366	388	377	4.13
SS60	391	398	395	1.25	473	481	477	1.19
SL20	372	366	369	1.15	372	369	371	0.57
SL40	355	355	355	0.00	393	392	393	0.18
SL60	384	388	386	0.73	531	519	525	1.62
SH20	336	355	346	3.88	336	355	346	3.88
SH40	370	350	360	3.93	374	356	365	3.49
SH60	362	350	356	2.38	448	482	465	5.17

Notes: wall type: C; wall thickness = 69 mm.

Furthermore, it was observed that ultimate loads coincided with cracking loads for PC, RC, and DCSFRC pipes fabricated with a fibre content of 20 kg/m³. This indicates that pipes made with this fibre dosage exhibited a strain softening behaviour. DCSFRC pipes made with higher fibre dosage, especially at 60 kg/m³, exhibited a deflection hardening behaviour since the pipes were able to sustain higher loads after first crack. In the case of DCSFRC pipes with a fibre dosage of 40 kg/m³, P_{ult} was reached shortly after reaching the P_{cr}.

Generally, the findings reported above agree with previous studies (MacDonald and Trangsrud, 2004; Haktanir *et al.*, 2007; de la Fuente *et al*., 2012; and Abolmaali *et al.*, 2012) that steel fibres can be used to successfully replace regular reinforcement in precast concrete pipes. The achieved ultimate loads are a function of the pipe size, pipe wall thickness, steel fibres type and content, and the compressive strength of the original concrete mixture. D_i of 400 mm was the nearest SFRC pipe size to be reported in the literature (Abolmaali *et al.*, 2012). The fibre content was 26 kg/m³ and the pipe wall thickness was 50 mm (Type B wall). These pipes achieved ultimate loads from 129 to 150 kN, which is significantly lower than the range of ultimate loads reported herein. This is due to the larger pipe diameter and lesser wall thickness and fibre content used in Abolmaali *et al.* (2012).

3.3.3 Pipe Load-Deformation Curves

3.3.3.1 Effect of Fibre Content

Figure 3-11a shows the load versus deflection at the spigot's crown curves for RC and DCSFRC pipes. For all pipes, the vertical deflection at the crown increased linearly as the applied load increased up to the proportionality limit. Thereafter, an instability region was observed for all pipes except for DCSFRC pipes with a fibre dosage of 60 kg/m³, which showed a deflection hardening behaviour instantly after reaching the proportionality limit. For DCSFRC pipes incorporating 40 kg/m³ of fibres, the instability region was smaller than that of DCSFRC pipes with a fibre content of 20 kg/m³. In addition, a hardening behaviour was also observed at a fibre dosage of 40 kg/m³. This can be explained as follows: For all DCSFRC mixtures there is a critical fibre volume $V_{f\ (crit)}$, which after matrix cracking, will carry similar load to that carried by the composite before cracking (Hannant, 1978).

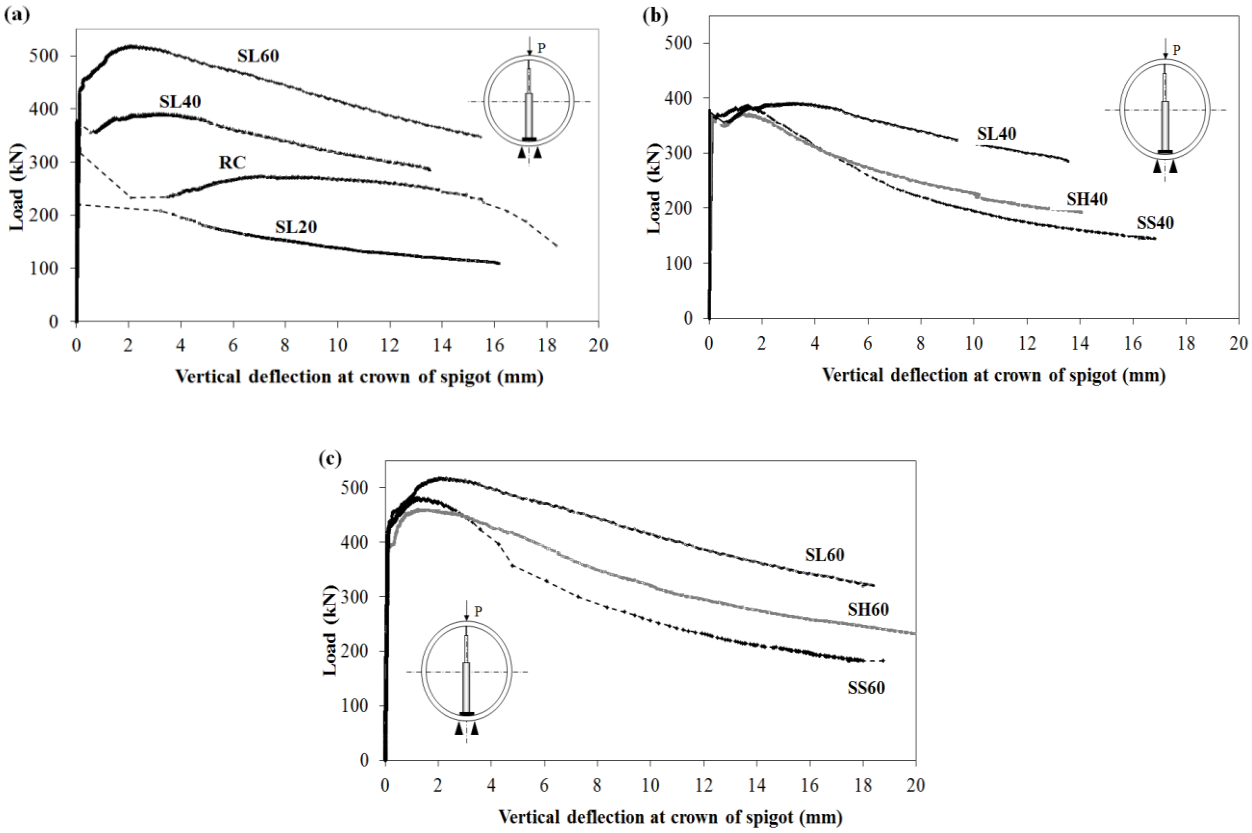

Figure 3-11 Load vs. deflection at crown of spigot for RC and SFRC pipes: (a) RC and DCSFRC pipes reinforced with 20, 40, and 60 kg/m³ of Type B fibres, (b) DCSFRC pipes reinforced with 40 kg/m³ of short (Type A), hybrid (0.5: 0.5) and long (Type B) fibres, and (c) DCSFRC pipes reinforced with 60 kg/m³ of short (Type A), hybrid (0.5: 0.5) and long (Type B) fibres.

For steel fibres, $V_{f\ (crit)}$ is about 0.31% (i.e. 25 kg/m³). Hence, DCSFRC pipes with a fibre dosage greater than 25 kg/m³ (i.e. 40 and 60 kg/m³) exhibited a deflection hardening behaviour, while specimens with lower fibre content (i.e. 20 kg/m³) exhibited a strain softening behaviour.

Interestingly, an instability region was observed for the RC pipe also (**Fig. 3-11a**). This can be attributed to the manufacturing process of precast RC pipes since the reinforcing steel cage is positioned around the mid-section of the pipe wall (near the neutral axis) in order to satisfy the minimum cover requirement. Thus, the reinforcement becomes active at high levels of cracking and displacement (de la Fuente *et al.*, 2012).

3.3.3.2 Effect of Fibre Type

The effect of the fibre type on the load-deflection curves at the spigot's crown for DCSFRC pipes is illustrated in **Fig. 3-11b**. The strain softening branch of the load-deflection curve for the SL40 specimen started at a deflection of 3.0 mm, while for both the SS40 and SH40 specimens, it started at 1.50 mm. The use of longer fibres extended the hardening region compared to those of the short and hybrid fibres as it required higher pullout energy (Beaumont and Aleszka, 1978). In addition, the behaviour of pipes reinforced with hybrid fibres (0.50:0.50) is comparable to that of the pipes reinforced with short fibres (i.e. similar residual loads at the same deflections) (**Fig. 3-11b**). This indicates that the behaviour of hybrid fibre specimens was governed by the failure of the short fibres since they would slip out of the matrix before the longer fibres. Furthermore, as the fraction of the longer fibre was increased in the hybrid system from 0.50 to 0.67, the softening branch of the average load deflection curve of the SH60 pipes was slightly improved and the residual loads obtained were higher than those of SS60 pipes at the same deflection (**Fig. 3-11c**). However, the softening branch for both the SS60 and SH60 pipes started at a deflection of 1.5 mm, which indicates that short fibres still governed the ultimate load capacity of the pipes. These findings suggest that the hybrid fibre system used herein did not result in significant synergetic effects and the improvement in the post-peak behaviour of the pipes was dependant on the fraction of long fibres used in the composite.

3.3.4 Post-Cracking Behaviour Analysis

The post-cracking strength (*PCS*) analysis proposed by Banthia and Trottier (1995) was adopted in this study to characterize the post-cracking behaviour of DCSFRC pipes. In this method, the load–displacement curve is converted into an equivalent flexural strength curve using simple energy equivalence. The generated post-cracking strength *PCS* can be used in comparative assessment and design, especially for serviceability considerations (Banthia and Sappakittipakorn, 2007).

The post-cracking strength at any point is calculated using the following equation:

$$PCS = \frac{(E_{post}) \times L}{(\delta - \delta_{peak}) \times b \times h^2} \qquad \textbf{Eq. 3-3}$$

where, E_{post} is the post-peak energy at any deflection δ (i.e. area under the load-deflection curve between δ_{peak} and δ), δ_{peak} is the vertical deflection at the first peak load, L is the specimen span = $(\pi Di/2)$, b is specimen width = 2450 mm and h = pipe wall thickness. In this study, for *PCS* calculations, deflection points were selected in the deflection range of 0.0 to 5.0 mm. Average *PCS* values for DCSFRC pipes are shown in **Fig. 3-12**. The first point on the *PCS* curve was obtained by replacing the term (E_{post}/δ-δ_{peak}) with the first peak load on the load deflection curve.

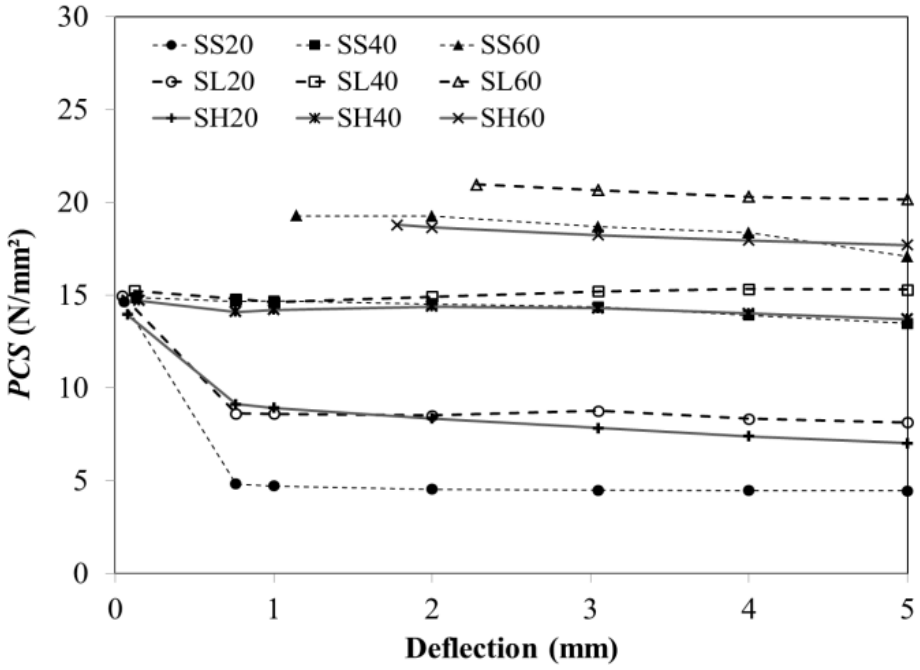

Figure 3-12 Post cracking strength PCS at different deflection values for DCSFRC pipes.

The trends of PCS curves shown in **Fig. 3-12** are generally in agreement with the previously discussed load deflection responses. For the same fibre type and at the same deflection (δ), an increase in the fibre content resulted in an increase in the post-crack

strength. For instance, the average *PCS* values were 8.76, 15.21, and 20.65 N/mm² at a deflection of 3 mm, and 8.15, 15.29, and 20.15 N/mm² at a deflection of 5 mm for SL20, SL40, and SL60, respectively (**Fig. 3-12)**. In addition, at the same fibre content and deflection, pipes incorporating the long fibres exhibited higher *PCS* values than that of similar pipes made with short or hybrid fibres. For example, at a fibre content of 20 kg/m³, the average *PCS* values were 4.49, 7.83, and 8.76 N/mm² at 3 mm deflection and 4.45, 7.01, and 8.15 N/mm² at 5 mm deflection for SS20, SL20, and SH20 pipes, respectively.

It was found that any enhancement to the post-cracking behaviour due to fibre hybridization appeared to be related to the inclusion of the long fibres only (i.e. short fibres had no synergetic effect). A synergy evaluation according to Banthia and Soleimani (2005) was performed using the following formula **(Eq. 3-4)**:

$$Synergy = \frac{PCS_{Hybrid-mix}}{\sum PCS_{\text{sin}\,gle-fibre-mix}} - 1 \qquad \textbf{Eq. 3-4}$$

where, $PCS_{Hybrid-mix}$ is the *PCS* value of the tested hybrid pipe at a certain deflection (δ), and $\sum PSC_{Single-fibre-mix}$ is the summation of the *PCS* values of tested single-fibre pipes at the same deflection. A positive value indicates the existence of a synergetic effect and vice versa. No synergy effect was observed for the selected deflection limits as shown in **Table 3-7**.

Table 3-7 Fibre synergy assessment at various deflections

Pipe	Fibre Content (kg/m³)	Synergy		
		at 1 mm	at 3 mm	at 5 mm
SH20	20	-0.33	-0.41	-0.44
SH40	40	-0.52	-0.52	-0.52
SH60	60	-1.00	-0.53	-0.12

3.3.5 Strain Measurements

Figure 3-13 shows the average strain measured at the pipe inner invert at spigot at different loading stages. The measured strain at the pipe invert was always positive (i.e. tensile strain) and increased as the load increased until the first crack formation. Subsequently, the gauge would either rupture (in most cases) or give a very low reading as an indication of stresses redistribution at the invert. The measured strain at 130 kN (required ultimate load P_{ult}) was around 60 με for all tested pipes. This value is less than the tensile strain of plain concrete at cracking (i.e. 80-200 με) (Gopalaratnam and Shah, 1985; and Belarbi and Hsu, 1994), indicating that the material was in the elastic range at this loading level. In addition, the presence of steel fibres did not affect the strain at the concrete surface for this loading level. This is because steel fibres were not contributing to the strength at this stage since they are only mobilized near the initiation of the first crack. At the cracking stage, it seems that there was an increasing trend in the strain at P_{cr} as the fibre content increased, regardless of the fibre type. This likely due to the increase of composite deformability due to the increase in the fibre content (Nataraja *et al.*, 1999, Dhakal *et al.*, 2005, Boulekbache *et al.*, 2012).

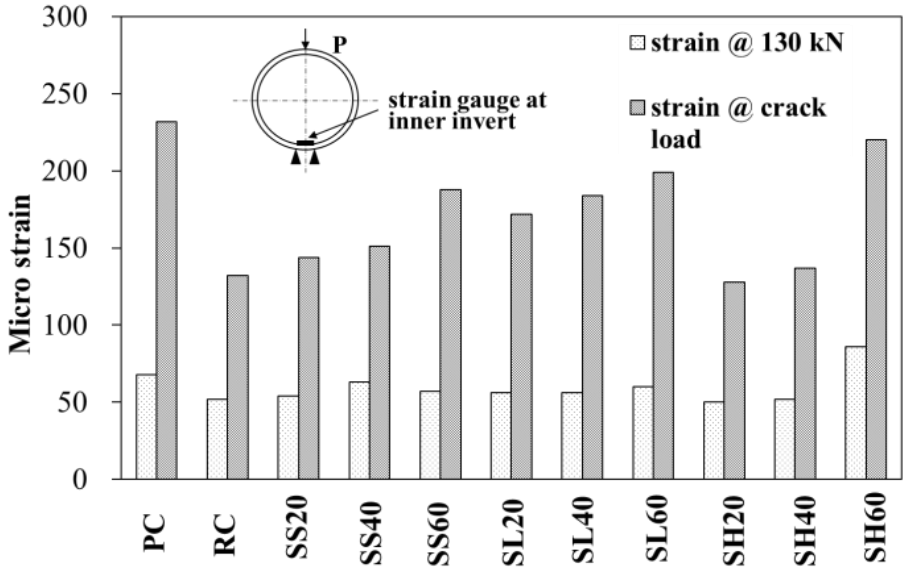

Figure 3-13 Average strain measured at the inner pipe invert at spigot at the required ultimate load (P_{ult} = 130 kN) and at the cracking load P_{cr}.

3.4 SUMMARY AND CONCLUSIONS

This chapter explored the mechanical properties of DCSFRC mixtures made with different types and dosages of steel fibres. Laboratory results on small specimens were further confirmed through full-scale production and testing of DCSFRC precast pipes. The following conclusions can be drawn based on the experimental findings:

- The engineering properties of DCSFRC mixtures were improved as the fibre dosage was increased. Consequently, DCSFRC precast pipes incorporating higher fibre content exhibited higher ultimate and post-cracking strengths.

- The reinforcing index, RI_v can be utilized for comparing the splitting tensile and flexural strengths of different DCSFRC mixtures, while it showed no defined correlation with the compressive strength and modulus of elasticity.

- A fibre dosage of 20 kg/m^3 was found to be insufficient to provide a significant improvement in the mechanical properties of DCSFRC.

- Type B fibres induced the best flexural performance of DCSFRC specimens among all fibres investigated herein. Type D fibres were the least effective at enhancing the flexural strength and the post-peak behaviour of DCSFRC.

- Using a hybrid fibre system improved the mechanical properties of the DCSFRC with respect to a mixture fabricated with one type of fibre at the same fibre content. The improvement in DCSFRC mechanical properties induced by hybridization depended mainly on the amount of long fibres in the mixture rather than a synergetic effect.

- Dispersed steel fibres can be used instead of regular steel reinforcement in precast concrete pipes depending on the target pipe strength, pipe diameter, steel fibres type and dosage.

- The reinforcement specified for Class V 300 mm diameter pipes in ASTM C76 could be achieved by a steel fibre dosage of 20 kg/m³.

3.5 REFERENCES

Abbas, S., Soliman, A.M. and Nehdi, M.L., "Mechanical performance of RC and SFRC precast tunnel lining segments: a case study." *ACI Materials Journal*, 111(5), 2014a, pp. 501- 510.

Abbas, S., Soliman, A.M. and Nehdi, M.L., "Experimental study on settlement and punching behavior of full-scale RC and SFRC precast tunnel lining segments." *Engineering Structures*, 72, 2014b, pp. 1-10.

Abolmaali, A., Mikhaylova, A., Wilson, A. and Lundy, J., "Performance of steel fibre-reinforced concrete pipes." Journal of the Transportation Research Board, 2313(1), 2012, pp. 168-177.

ACI Committee 211, "Guide for selecting proportions for no-slump concrete," (211.3R-02), American Concrete Institute, Farmington Hills, MI, USA, 2009, 26 p.

ACI Committee 544, "Design considerations for steel fibre reinforced concrete," (544.4R-88), American Concrete Institute, Farmington Hills, MI, USA, 2009, 18 pp.

ASTM C39-14, "Standard test method for compressive strength of cylindrical concrete specimens." American Society for Testing and Materials, ASTM International, West Conshohocken, PA, 2014, 7 p.

ASTM C76-13, "Standard specification for reinforced concrete culvert, storm drain, and sewer pipe." ASTM International, West Conshohocken, PA, 2013, 11 p.

ASTM C469-10, "Standard test method for static modulus of elasticity and poisson's ratio of concrete in compression." American Society for Testing and Materials, ASTM International, West Conshohocken, PA, 2010, 5 p.

ASTM C496-11, "Standard test method for splitting tensile strength of cylindrical concrete specimens." American Society for Testing and Materials, ASTM International, West Conshohocken, PA, 2011, 5 p.

ASTM C497-13, "Standard test methods for concrete pipe, manhole sections or tile." American Society for Testing and Materials, ASTM International, West Conshohocken, PA, 2013, 14 p.

ASTM C1609-12, "Standard test method for flexural performance of fiber-reinforced concrete (using beam with third-point loading)." American Society for Testing and Materials, ASTM International, West Conshohocken, PA, 2012, 9 p.

Banthia, N., and Trottier, J., "Test methods for flexural toughness characterization of fiber reinforced concrete: some concerns and a proposition." *ACI Materials Journal*, 92(1), 1995, pp. 48-57.

Banthia, N., and Soleimani, S.M., "Flexural response of hybrid fiber reinforced cementitious composites." *ACI materials journal*, 102(6), 2005, pp. 382-389.

Banthia, N., and Sappakittipakorn, M., "Toughness enhancement in steel fiber reinforced concrete through fiber hybridization," *Cement and Concrete Research*, 37(9), 2007, pp.1366 -1372.

Beaudoin, J. J., "*Handbook of fibre-reinforced concrete: principles properties, developments and applications,"* Noyes Publications, *Park* Ridge, NJ, USA, 1990, 332 pp.

Beaumont, P.W.R., and Aleszka, J.C., "Cracking and toughening of concrete and polymer-concrete dispersed with short steel wires," *Journal of Material Science*, 13(8), 1978, pp. 1749-1760.

Belarbi, A., and Hsu, T.C., "Constitutive laws of concrete in tension and reinforcing bars stiffened by concrete," *ACI structural Journal*, 91(4), 1994, pp. 465-474.

Bentur, A., and Mindess, S., "*Fibre-Reinforced Cementitious Composites."* 2nd edition; New York: Taylor & Francis, 2007, 660 p.

Boulekbache, B., Hamrat, M., Chemrouk, M. and Amziane, S., "Influence of yield stress and compressive strength on direct shear behaviour of steel fibre-reinforced concrete." *Construction and Building Materials*, 27(1), 2012, pp. 6-14.

Brandt, A.M., "Fibre-reinforced cement-based (FRC) composites after over 40 years of development in building and civil engineering." *Composite Structures*, 86(1–3), 2008, pp. 3-9.

Chem, J.C., Yang, H.J., and Chen, H.W., "Behaviour of steel fibre reinforced concrete in multi-axial loading," *ACI Materials Journal*, 89(1), 1992, pp. 32-40.

Cook, R.F., Wongaew, K., Carlson, J.E., Smith, C.R. and Cleys, T., "Design, testing, and production of steel-fibre reinforced concrete segmental tunnel lining for the east side combined sewer overflow tunnel." *Rapid Excavation And Tunnelling Conference - 2007,* Edited by Traylor, M.T., and Townsend, J.W., Society for Mining, Metallurgy and Exploration, Inc., Littleton, Colorado, USA, 2007, pp. 1192-1204.

Dhakal, R.P., Wang, C., Mander, J.B., "Behaviour of steel fibre reinforced concrete in compression." *International Symposium on Innovation & Sustainability of Structures in Civil Engineering*, Nov. 2005.

de la Fuente, A., and de Figueiredo, D., "Experimentation and numerical simulation of steel fibre reinforced concrete pipes." *Materiales de Construcción,* 61(302), 2011, pp. 275-288.

de la Fuente, A., Escariz, R.C., de Figueiredo, A.D., Molins, C., and Aguado, A., "A new design method for steel fibre reinforced concrete pipes," *Construction and Building Materials,* 30, 2012, pp. 547-555.

European Standards, EN 1916, "Concrete pipes and fittings, unreinforced, steel fibre and reinforced." European Committee for Standardization, 2002, 89 p.

Ezeldin, A.S, and Lowe, S.R., "Mechanical properties of steel fiber reinforced rapid-set materials." *ACI Materials Journal,* 88(4), 1991, pp. 384-389.

Gao, J., Sun, W., and Morino. K., "Mechanical properties of steel fiber reinforced, high strength, lightweight concrete," *Cement and Concrete Composites,* 19(4), 1997, pp. 307-313.

Gopalaratnam, V.S., and Shah, S.P., "Softening response of plain concrete in direct tension." *ACI Journal Proceedings,* 82(3), 1985, pp. 310-323.

Haktanir, T., Ari, K., Altun, F., and Karahan, O., "A comparative experimental investigation of concrete, reinforced-concrete and steel-fibre concrete pipes under three-edge-bearing test," *Construction and Building Materials,* 21(8), 2007, pp. 1702-1708.

Harajli, M., Hamad, B., and Karam, K., "Bond-slip response of reinforcing bars embedded in plain and fibre concrete." *Journal of Materials in Civil Engineering,* 14(6), 2002, pp. 503-511.

Hannant, D.J., "*Fibre Cements & Fibre Concretes*." J. Wiley & Sons, London, UK, 1978, 234 p.

Ilki, A., Yilmaz, E., Demir, C. and Kumbasar, N., "Prefabricated SFRC jackets for seismic retrofit of non-ductile reinforced concrete columns," *Proceedings of 13th World Conference on Earthquake Engineering*, Vancouver, BC, Canada, 2004, paper # 2434.

Johnston, C., "*Fibre-Reinforced Cements and Concrete.*" Gordon and Breach Science Publishers, Amsterdam, Netherlands, 2001, 364 p.

Jo, B., Young-Hyun, S., and Young-Jin, K., "The Evaluation of Elastic Modulus for Steel Fiber Reinforced Concrete" *Russian journal of non-destructive testing,* 37(2), 2001, pp. 152-161.

Kim, D.J., Naaman, A.E., and El-Tawil, S. "Correlation between tensile and bending behavior of FRC Composites with scale effect." in *Fracture Mechanics of Concrete and Concrete Structure,* Korea Concrete Institute, 2010, pp. 1379-85.

MacDonald, C. and Trangsrud, J., "Steel fiber product introduction through pre-cast reinforced concrete pipe." *ACI Special Publication,* 222, 2004, pp. 185-199.

Mohan, K.S.R., and Parthiban, K., "Strength and behaviour of fly ash based steel fibre reinforced concrete composite" *Journal of Civil & Structural Eng.*, 2(1), 2011, pp. 318-28.

Morgan, D.R., "Steel fibre shotcrete for rehabilitation of concrete structures." *International Symposium on Mechanical Properties of Special Concrete, Part of the 63rd Annual Meeting of the Transportation Research Board*, Washington DC, USA, 1984, pp. 36-42.

Murakoshi, J., Yanadori, N., and Ishii, H., "Research on steel fibre reinforced concrete pavement for orthotropic steel deck as a countermeasure for fatigue." *Stress,* (1), 2008, pp. 1-13.

Naaman, A.E., "Strain hardening and deflection hardening fiber reinforced cement composites." *High Performance Fiber Reinforced Cement Composites 4 (HPFRCC-4).* Naaman, A.E., and Reinhardt, H.W. Editors, RILEM Publications, Pro. 30, 2003, pp. 95-113.

Nataraja, M.C., Dhang, N. and Gupta, A.P., "Stress–strain curves for steel-fibre reinforced concrete under compression." *Cement and Concrete Composites,* 21(5–6), 1999, pp. 383-390.

Nehdi, M., and Ladanchuk, J.D., "Fibre synergy in fibre-reinforced self-consolidating concrete," *ACI Materials Journal*, 101(6), 2004, pp. 508-517.

Neves, R.D., and de Fernandes, A., "Compressive behaviour of steel fibre reinforced concrete," *Structural Concrete*, 6(1), 2005, pp. 1-8.

Ontario Concrete Pipe Association, "*Concrete Pipe Design Manual*." Ontario Concrete Pipe Association, Kitchener, ON, Canada, 2010, www.ocpa.com.

Ou, Y., Tsai, M., Liu, K., and Chang, K., "Compressive behaviour of steel-fibre-reinforced concrete with a high reinforcing index," *Journal of Materials in Civil Eng.*, 24(2), 2012, pp. 207-215.

Ramakrishnan, V., "Super-plasticized fibre-reinforced concretes for the rehabilitation of bridges and pavements," *International Symposium on Mechanical Properties of Special Concrete, Part of the 63rd Annual Meeting of the Transportation Research Board.* Transportation Research Board, Washington DC, USA, 1984, pp. 4-11

Roesler, J.R., Lange, D.A., Altoubat, S.A., Rieder, K., and Ulreich, G.R., "Fracture of plain and fibre-reinforced concrete slabs under monotonic loading," *Journal of Materials in Civil Engineering*, 16(5), 2004, pp. 452-460.

Song, P.S., and Hwang, S., "Mechanical properties of high-strength steel fibre-reinforced concrete," *Construction and Building Materials,* 18(9), 2004, pp. 669-673.

Soroushian, P., and Bayasi, Z., "Fiber type effects on the performance of steel fiber reinforced concrete." *ACI Materials Journal,* 88(2), 1991, pp. 129-134.

di Tommaso, A., Focacci, F., and Mantegazza, G., "PBO-FRCM Composites to strengthen rc beams: mechanics of adhesion and efficiency," *Proceedings of the International Conference on FRP Composites in Civil Engineering,* Zurich, Switzerland. 2008.

Trottier, J.F., and Banthia, N., "Toughness characterization of steel fibre reinforced concrete" *ASCE Journal of Materials in Civil Engineering*, 6(2), 1994, pp. 264-289.

Wafa, F.F., and Ashour, S.A., "Mechanical properties of high-strength fibre reinforced concrete" *ACI Materials Journal,* 89(5), 1992, pp. 449-455.

Wang, Y., and Lee, M.G., "Ultra-high strength steel fiber reinforced concrete for strengthening of RC frames." *Journal of Marine Science & Technology*, 15(3), 2007, pp. 210 - 218.

Wilson, A. "Performance evaluation and finite element analysis of fiber reinforced precast concrete underground structures" *MSc. Thesis*, Civil Engineering Department, University of Texas at Arlington, 2012.

Yan, Z., Zhu, H. and Ju, J.W., "Behaviour of reinforced concrete and steel fibre reinforced concrete shield TBM tunnel linings exposed to high temperatures." *Construction and Building Materials*, 38, 2013, pp. 610-618.

Yang, K., "Tests on concrete reinforced with hybrid or monolithic steel and polyvinyl alcohol fibres," *ACI Materials J*ournal, 108 (6), 2011, pp. 664-672.

Yao, W., Li, J., and Wu, K., "Mechanical properties of hybrid fiber reinforced concrete at low fiber volume fraction" *Cement and Concrete Research*, 33(1), 2003, pp. 27-30.

Yazici S., Inan G., and Tabak V., "Effect of aspect ratio and volume fraction of steel fibre on the mechanical properties of SFRC" *Construction & Building Materials*, 21(6), 2007, pp. 1250-1253.

CHAPTER FOUR

4 MECHANICAL PERFORMANCE OF FULL-SCALE PRECAST STEEL FIBRE-REINFORCED CONCRETE PIPES[2]

4.1 INTRODUCTION

This chapter expands on the findings of the previous chapter and explores the behaviour of SFRC pipes in greater depth. Full-scale precast SFRC pipes having internal diameters (D_i) of 450 and 600 mm were fabricated and tested. In addition, PC and RC pipes of the same diameters were cast and tested for comparison. Precast pipes were tested using both the continuous and cyclic loading procedures as per the ASTM C497 and EN 1916 guidelines, respectively. The steel fibre content needed to satisfy the strength requirements for Class V 450 and 600 mm diameter pipes according to ASTM C76 was identified. Moreover, the continuous TEBT test and the cyclic TEBT test, specified in ASTM C497 and EN 1916, respectively, were compared, which provided insight into how SFRC pipes should be tested in the future.

[2] A version of this chapter was published in the Journal of *Engineering Structures* (2015). Part of this chapter was published in the *ACI-fib workshop on FRC*, Ecole Polytechnique de Montreal, Montreal, Canada (2014).

4.2 EXPERIMENTAL PROGRAM

4.2.1 Materials and Mixture Proportions

SFRC pipes were cast at an industrial precast concrete plant in Oakville, Ontario. Two pipe diameters were manufactured; namely, 450 mm and 600 mm. All pipes were 2.45-m in length. All pipes had a Type C wall. Class V pipe was the target pipe strength (i.e. $D_{0.3}$ and D_{ult} are 140 and 175 N/m/mm, respectively) according to ASTM C76.

In this study, SFRC pipes with the same diameter were produced in a single day in order to minimize the influence of intervening variables in the pipes production. Detailed description of materials used in concrete fabrication was given earlier in **Section 3.2.1**. Two types of steel fibres (Dramix RC-65/35-CN and Dramix RC-80/60-CN) were added manually as partial replacement for the coarse aggregate at W_f (fibre mass per 1 m^3) of 20, 30 and 40 kg/m^3, i.e. equivalent to 0.25, 0.38, and 0.50 % by concrete volume (V_f). The compositions of the control fibreless mixture and other tested SFRC mixtures are shown in **Table 4-1**. The physical and mechanical properties of steel fibres used in this study were given earlier in **Table 3-2**. Pipes were produced and cured in the same manner described earlier in **Section 3.2.3**. Simultaneously, 100 x 200 mm cylinders were cast for measuring the compressive strength of the mixtures. **Tables 4-2** and **4-3** list the fabricated 450 and 600 mm diameter pipes, their fibre type and content, and the compressive strength of corresponding mixtures, respectively. Three pipe replicates were cast for each mixture composition for a total of 66 full-scale pipes.

Table 4-1 Concrete mixture proportions

Material	Mass/Cement mass
Cement	1.00
Blast Furnace Slag	0.54
Fine Aggregate	5.00
Coarse Aggregate	4.17
Water	0.58
Super plasticizer	0.0016
Air entraining admixture	0.002
Steel Fibres	0, 20, 30, 40 kg/m^3

Table 4-2 Fabricated 450 mm diameter pipes and their achieved loads

Reinforcement	Pipe Designation	V_f (kg/m^3)	f_c' (MPa)	COV	P_{cr} (kN)	P_{ult} (kN)	$P_{post,\ max}$ (kN)
None	PC45	-	66.0	3.40	280	280	-
Regular	RC45	-	47.0	4.86	265	265	210
Short fibre (Dramix RC-65/35-CN)	SS4520	20	74.1	6.84	304	304	147
	SS4530	30	42.5	6.01	266	283	249
	SS4540	40	61.0	6.17	330	360	339
Long fibre (Dramix RC-80/60-CN)	SL4520	20	66.0	8.97	316	316	210
	SL4530	30	35.8	1.28	286	302	273
	SL4540	40	46.2	9.24	330	344	-
Hybrid (Short + Long fibres)	SH4520	20	48.3	2.97	240	251	214
	SH4530	30	52.5	3.82	315	320	294
	SH4540	40	62.1	6.33	327	362	325

Notes:

- Pipe Wall Thickness = 82 mm
- ASTM C76: $P_{0.3}$ = 156 kN, P_{ult} = 195 kN for class V (class 140D) 450 mm diameter pipe
- BS 5911: P_c = 108 kN, P_{ult} = 135 kN for 450 mm diameter pipes of class 120 for trench use

Table 4-3 Fabricated 600 mm diameter pipes and their achieved loads

Reinforcement	Pipe Designation	V_f (kg/m^3)	f_c' (MPa)	COV	P_{cr} (kN)	P_{ult} (kN)	$P_{post,\ max}$ (kN)
None	PC60	-	64.8	5.26	253	253	-
Regular	RC60	-	43.8	3.28	192	294	-
Short fibre (Dramix RC-65/35-CN)	SS6020	20	61.6	13.71	227	227	206
	SS6030	30	58.0	7.23	275	277	239
	SS6040	40	73.0	1.89	266	330	294
Long fibre (Dramix RC-80/60-CN)	SL6020	20	56.0	10.60	237	237	217
	SL6030	30	44.9	5.26	260	288	262
	SL6040	40	65.2	2.44	325	352	324
Hybrid (Short + Long fibres)	SH6020	20	72.1	4.62	251	254	224
	SH6030	30	70.7	0.09	261	320	-
	SH6040	40	71.7	1.74	262	329	295

Notes:

- Pipe Wall Thickness = 94 mm
- ASTM C76: $P_{0.3}$ = 208 kN, P_{ult} = 258 kN for class V (class 140D) 600 diameter mm pipe
- BS 5911: P_c = 142 kN, P_{ult} = 177 kN for 600 diameter mm pipes of class 120 for trench use

4.2.2 Pipe Testing Procedures and Specimen Instrumentation

The mechanical performance and structural behaviour of the full-scale precast concrete pipes were evaluated using the TEBT according to the EN 1916 standard. However, in the present study, one additional step was added to the EN 1916 testing procedure according to the Brazilian standard NBR 8890 (Precast Circular Concrete Pipes for Pluvial and Sanitary Drainage: Requirements and Test Methods) (Brazilian Association of Technical Standards, 2008). After the one minute sustained loading, the load is increased until the pipe reaches the maximum measured post-peak load ($F_{post,\,max}$). The $F_{post,max}$ must be greater than 1.05 F_c. This procedure was adopted to ensure adequate fibre-bond in the post-cracking stage of SFRC pipes (de Figueiredo *et al., 2012*). In addition, selected specimens were evaluated using the crushing test method according to the ASTM C497 method for comparison.

Figure 4-1 shows the load profile versus time for the 450-mm diameter pipes tested according to the ASTM C497 (continuous test) and EN 1916 (cyclic test) procedures. It also shows the design and ultimate D-loads specified in ASTM C76 for 450 mm Class V pipes. The change in slope at 50 kN corresponds to the change in the loading rate from 5 mm/min to 1 mm/min. The loading rate was reduced to better capture the full behaviour of the pipe. The horizontal line in **Fig. 4-1b** represents the one minute period during which the load was held constant at 156 kN (= 64 kN/m). This corresponds to F_c = 0.8 F_n > 0.67 F_n. This further modification to the EN 1916 standard was adopted so that the proof load F_c specified in EN 1916 could coincide with the design load specified in ASTM C76. Furthermore, EN 1916 specifies that the proof load F_c should be equal to 0.8 F_n in the case of "tightened inspection". Tightened inspection is required when a new production or a change in process occurs (European Committee for Standardization, 2002). In the present study, the cracking load (F_{cr}) is the load at which the first crack took place and always occurred at the pipe invert at the spigot.

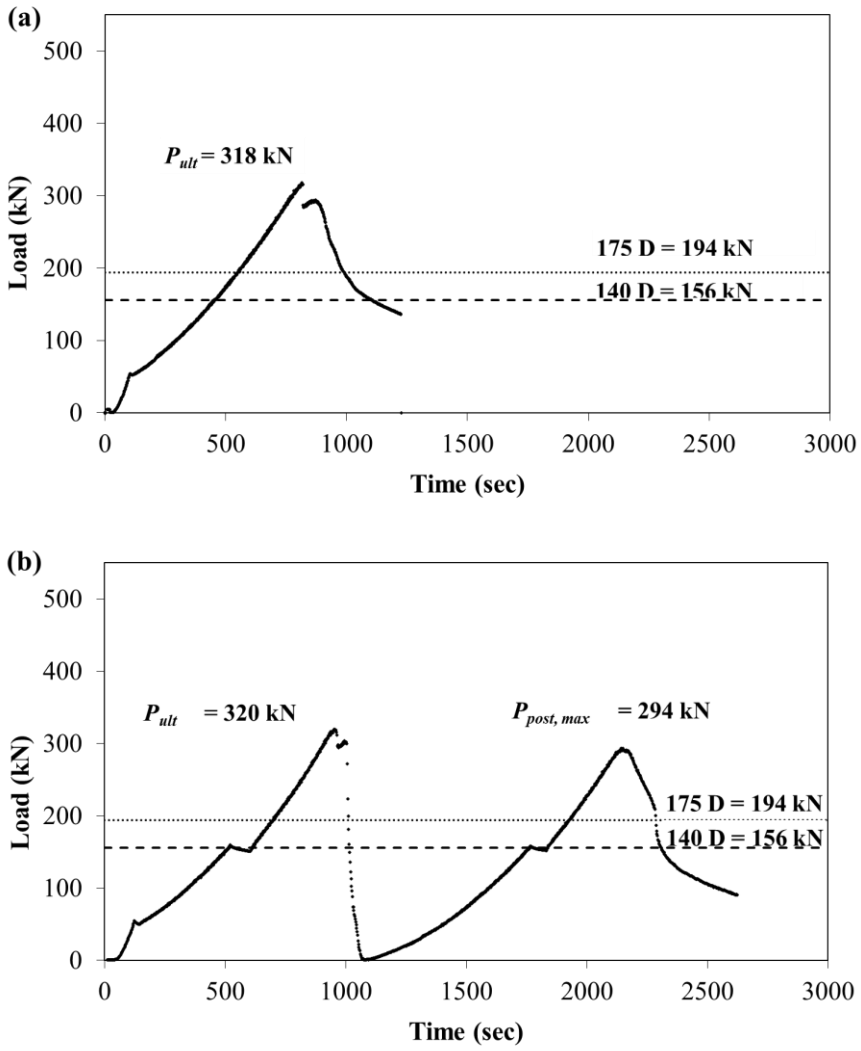

Figure 4-1 Load vs. time for TEBT according to (a) ASTM C497, and (b) modified European EN: 1916 test procedures for SH4530 pipes.

It is worthy of noting that the British Standard BS 5911 (Concrete Pipes and Ancillary Concrete Products Specification for Unreinforced and Reinforced Concrete Pipes (including jacking pipes) and fittings with flexible joints (complementary to EN 1916:2002)) (British Standards Institution, 2002) indicates that pipes used in trenches shall satisfy the strength class of 120 N/m/mm, which falls in between Class III and Class IV of the ASTM C76. Contrary to ASTM C76, EN 1916 does not provide guidelines regarding the amount of reinforcement required for a pipe to achieve a certain required strength.

Details of the test setup and pipes instrumentation were given earlier in **Section 3.2.3**. In addition, the horizontal deformation of the spring-lines were recorded using two LVDTs. LVDTs were positioned against the upper and the two sides of the inner surface of the pipe and attached to supports fixed at the bottom part of the pipe at the spigot section. Furthermore, strains on the concrete surface at critical points (e.g. invert, inside of spring-lines, outside of spring-lines, etc.) were recorded using strain gauges mounted on the pipe surface at spigot. The test setup and pipe instrumentation are shown in **Fig. 4-2**.

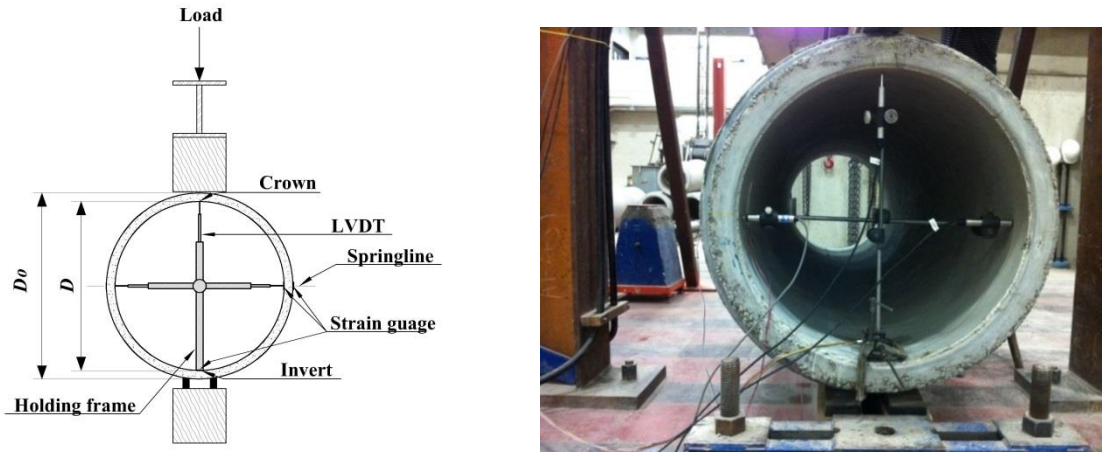

Figure 4-2 Test setup and pipe instrumentation.

4.3 RESULTS

4.3.1 Failure Mechanism and Cracking Pattern

All tested SFRC pipes exhibited a flexural failure mechanism, which was characterized by the occurrence of longitudinal cracks at the crown, invert, and spring-lines, as shown in **Fig. 4-3**. Other failure mechanisms typically associated with conventional concrete pipes

reinforced with steel cages (i.e. diagonal tension and radial tension) were not observed. **Figure 4-4** shows typical crack openings at failure for SFRC pipes.

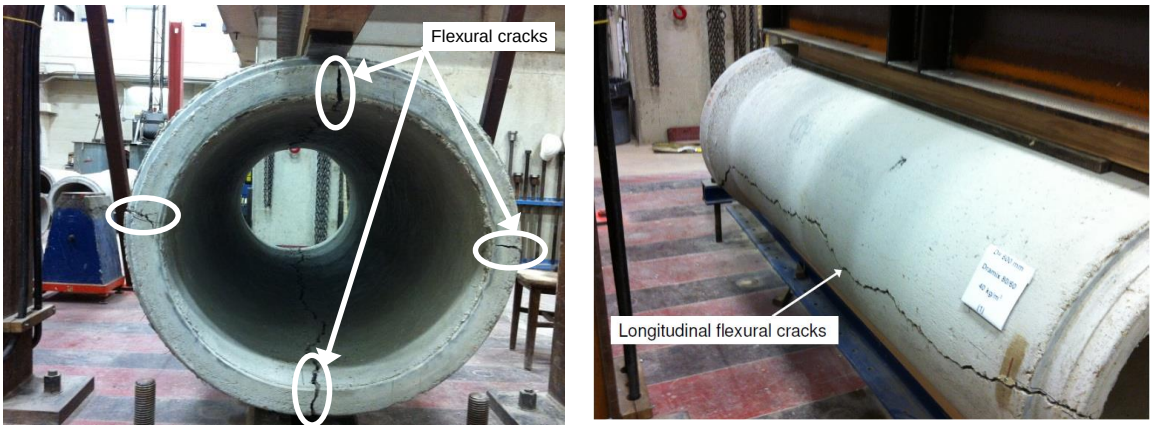

Figure 4-3 Flexural failure mechanism (SL6040 pipes).

In the first loading cycle, the first crack always developed at the spigot in the inner side of the pipe's invert between the two supporting blocks, followed by a crack at the outer side of the pipe's wall of the spring-lines at spigot. Both cracks increased in width and length gradually with load increase. By the end of this cycle, for most pipes, the crack at the invert reached the bell end of the pipe, while cracks at the spring-lines stopped at nearly the pipe's half-length. No secondary cracks were observed during this loading cycle. The average crack width in the spring-line at the ultimate load ranged between 1.0 and 2.0 mm. The effect of the fibre type and dosage on the cracking pattern could not be identified in this first load stage. In the second loading cycle, both cracks did not increase in length and width until $P_{post,\,max}$ was reached. Afterwards, the crack at the invert increased in width; only a few short hairline secondary branched cracks were observed in this area. Simultaneously, the crack at the spring-line started to propagate towards the pipe bell. Secondary cracks started to form thereafter in the spring-lines at various locations along the pipe's length (i.e. $L/2$, $2L/3$, $3L/4$). While propagating towards the bell end, these cracks inclined between 0^0 and 90^0. The number of these secondary cracks seemed to increase with higher fibre dosage; however, the effect of changing the fibre type was not tangible.

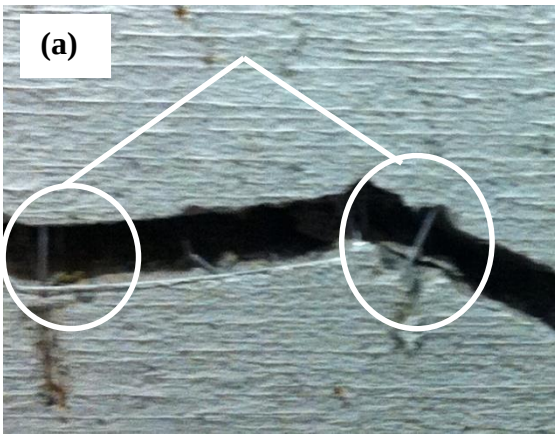

(a) Crack bridging by steel fibres

(b) Steel fibres pull out failure mechanism

(c) Steel fibres rupture failure mechanism

(d) Excessive crack opening

Figure 4-4 Cracking patterns at failure of SFRC pipes.

Examining the opened crack zones showed that both failure mechanisms of fibre pullout and fibre rupture co-existed. SFRC pipes were able to undergo large vertical and horizontal displacements without collapse. Tests were stopped due to excessive deformation beyond the ultimate load and substantial increase in crack widths (typically at vertical deflection of about 20 mm). The average crack width at the spring-line ranged between 8.0 and 12.0 mm when the test was terminated.

4.3.2 Effect of Fibre Type and Dosage on Ultimate Load

Table 4-2 and **Table 4-3** show the average crack, ultimate, and post-peak loads and coefficient of variation for ultimate loads achieved from TEBT for 450 mm and 600 mm pipes, respectively. Some inconsistency can be observed for the ultimate loads reported in **Tables 4-2** and **4-3**. For instance, the achieved ultimate loads, P_{ult} for 450 mm diameter SFRC pipes fabricated with 20, 30, and 40 kg/m³ of Dramix 65/35 steel fibres were 304, 283, and 360 kN, respectively (**Table 4-2**). This can be due to variability in the strength of the original concrete matrix itself. Hence, to minimize this effect, the normalized ultimate loads were used for evaluation. The normalized ultimate load is the ultimate load P_{ult} divided by the square root of the compressive strength, f_c' of the concrete mixture. This is in agreement with previous work (Cho and Kim, 2003; Dhakal *et al.*, 2005; and Ou *et al., 2011*).

Figure 4-5 shows the change of the normalized ultimate load, $P_{ult} / f_c'^{0.5}$ ($N^{0.5}$.m) with respect to the fibre content and type. Generally, the normalized ultimate load increased as the fibre content was increased, regardless of the fibre type. This can be attributed to the presence of fibres in the matrix, which intersect, block, and arrest the propagation of cracks, leading to enhanced structural performance (Song and Hwang, 2004). For instance, the calculated normalized ultimate load for 450 mm diameter pipes fabricated with 20 kg/m³ of Dramix 65/35 fibres increased by 22.9% and 30.5% when the fibre content was increased to 30 and 40 kg/m^3, respectively. Similarly, the normalized ultimate load for the 600 mm diameter pipes fabricated with 20 kg/m³ of Dramix 80/60 fibres increased by 35.7% and 37.6% when the fibre content was increased to 30 and 40 kg/m^3, respectively. Moreover, the addition of long fibres (Dramix 80/60) led to higher normalized ultimate loads. For example, at a fibre content of 30 kg/m^3, the normalized ultimate loads for 450 mm diameter pipes were 50.47, 44.16, and 43.41 $N^{0.5}$.m for Dramix 80/60, hybrid (Dramix 65/35 and Dramix 80/60 at 0.5:0.5 hybridization ratio) and Dramix 65/35 fibres, respectively.

Regardless of the fibre length, it was noticeable that the gain in the normalized ultimate load, $P_{ult} / f_c^{0.5}$ was insignificant when the fibre content increased from 30 to 40 kg/m³. For instance, for the 600 mm diameter pipes, the gain in the normalized ultimate load when the fibre content increased from 30 to 40 kg/m³ was only 6% and 1.2% for short and long fibres, respectively. This was true for both pipe diameters under investigation (**Fig. 4-5**). This is in

agreement with findings of Haktanir *et al*. (2007). Furthermore, no increase in $P_{ult} / f_c'^{0.5}$ was observed when the hybrid fibre system was used, compared to using the short fibre alone (Dramix 65/35). Again, this was true for both pipe diameters under investigation. It seems that the normalized ultimate load was governed by the dosage of the long fibre.

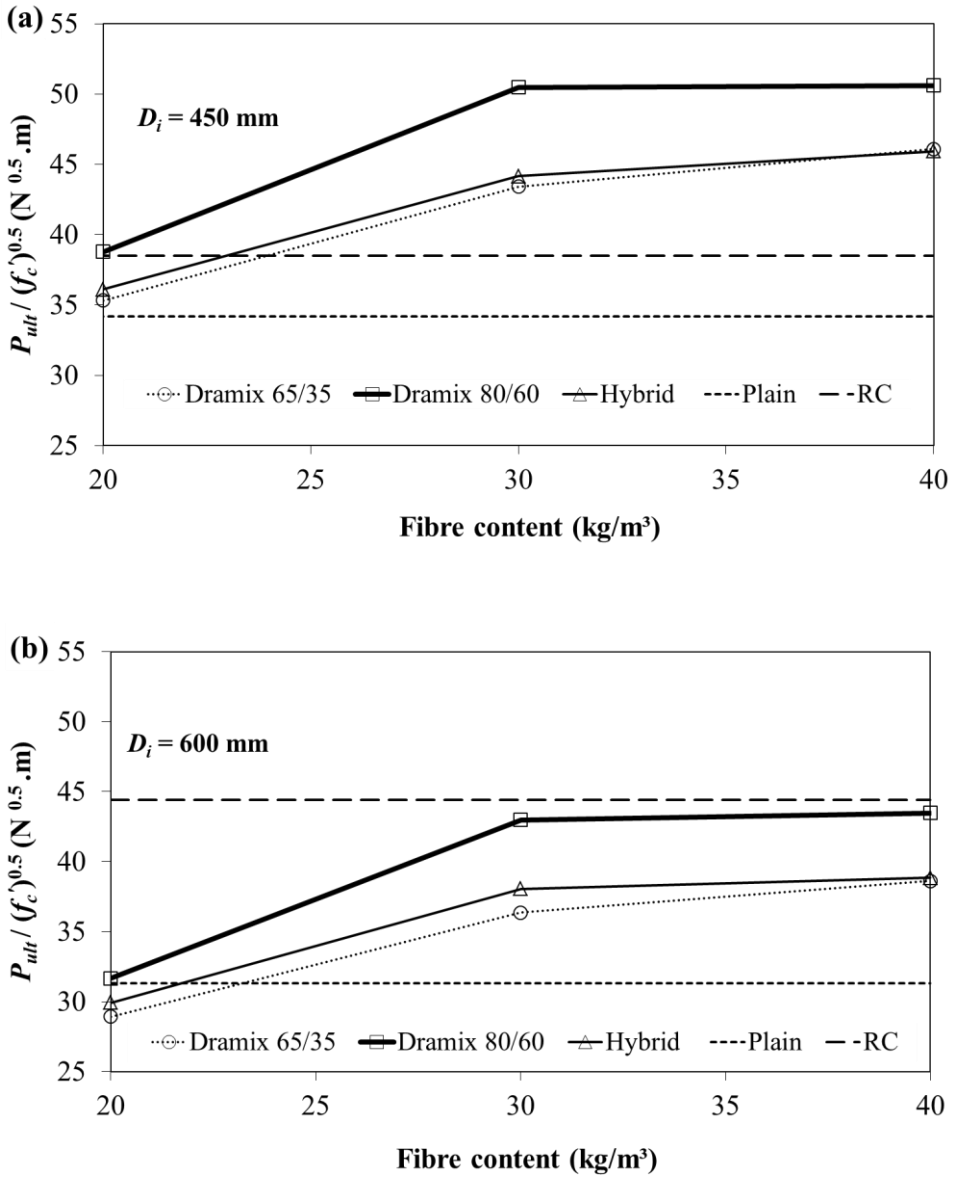

Figure 4-5 Normalized ultimate load change with fibre dosage in precast SFRC (a) 450 mm, and (b) 600 diameter mm pipes.

4.3.3 Structural Behaviour of 450 mm Precast Concrete Pipes

The required ultimate D-load strength for Class V pipes according to ASTM C76 is 175 N/m/mm, which corresponds to an applied load of about 195 kN. The ultimate strengths for all tested 450 mm SFRC pipes were substantially higher than the strength requirements specified for ASTM C76 Class V pipes (**Table 4-2)**. However, ASTM C76 lacks criteria for accepting SFRC pipes. Therefore, the load-deformation curves under continuous loading were selected to characterize the post-crack behaviour of the SFRC pipes.

Figure 4-6 shows typical load deformation curves for SFRC and RC precast pipes tested using the continuous TEBT. In all cases, the deflection was found to increase linearly as the load was increased, until reaching the cracking load or the peak load. It can be observed that the recorded P_{ult} for all SFRC pipes, even at the lowest fibre content (i.e. 20 kg/m^3), were higher than the P_{ult} of the RC pipes. This implies a strength increase due to fibre inclusion in the matrix. In addition, an instability region, marked by an abrupt decrease in the load carrying capacity accompanied by a very large increase in deflection, was observed for the RC45 pipe. This can be attributed to the manufacturing process of precast RC pipes since the reinforcing steel cage is positioned around the mid-section of the pipe wall (near the neutral axis) in order to satisfy the minimum cover requirement. Thus, the reinforcement becomes active at high levels of cracking and displacement (de Figueiredo *et al.*, 2012). Conversely, steel fibres effectively contribute to the strength of the pipe even before the initiation of the first major crack.

Generally, the post-cracking behaviour depended on the fibre content. At a fibre content of 20 kg/m^3, an abrupt increase in vertical deflection occurred immediately after cracking. Conversely, as the fibre content was increased to 40 kg/m^3, the behaviour changed to a deflection hardening and a second peak load of 334 kN was observed. **Figure 4-6** suggests that for a 450 mm diameter SFRC pipe, a fibre of content between 20 and 40 kg/m^3 would be sufficient for providing stress-strain behaviour comparable to that of conventional RC45 pipes with similar diameter.

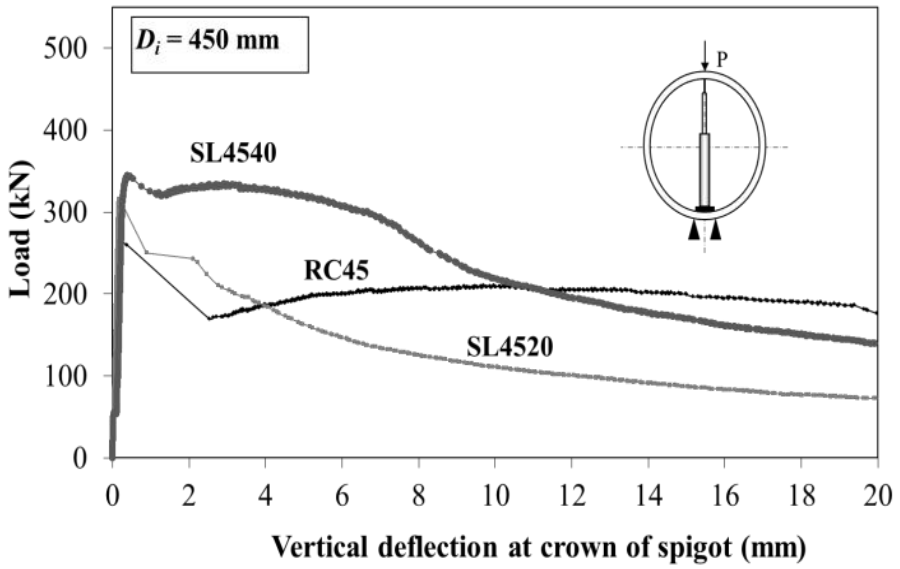

Figure 4-6 Load vs. deflection at crown of spigot for RC45, SL4520, and SL4540 pipes (ASTM C497 continuous TEBT).

Figure 4-7 shows the applied load versus time for the 450 mm diameter SFRC pipes reinforced with short (Dramix 65/35) fibres at a dosage of 20 and 30 kg/m^3. Considering the acceptance criteria described in EN 1916, the SS4520 pipe incorporating 20 kg/m^3 of Dramix 65/35 fibres did not meet the required proof load in the second load cycle (i.e. $P_{post,\,max}$ = 147 kN < P_c = 156 kN). When the fibre content was increased to 30 kg/m^3, the SS4530 pipe not only met the required P_c load, but also exhibited $P_{post,\,max}$ load that was 70% higher than that of the SS4520 pipe. However, no cracks were detected on the concrete surface of both pipes when the load was held for one minute at P_c = 156 kN (i.e. both pipes passed the first load cycle successfully). Thus, it can be argued that a fibre content of 30 kg/m^3 would be sufficient to substitute for the regular reinforcement in Class V 450 mm diameter pipes.

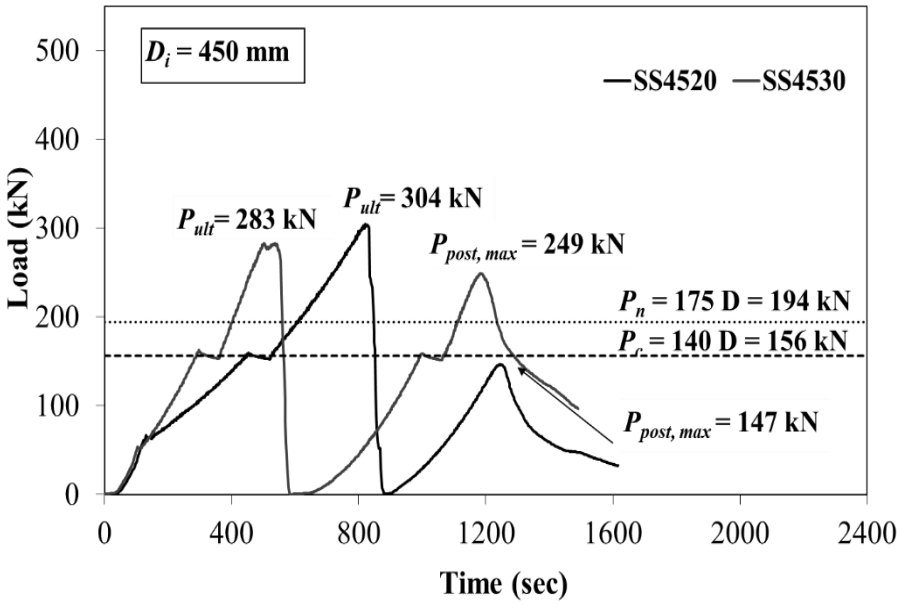

Figure 4-7 Load vs. time (modified EN: 1916 cyclic TEBT) for SS4520 and SS4530 pipes.

Figure 4-8 exhibits the cyclic load versus deflection at the crown of the spigot for the SS4530, SH4530, and SL4530 pipes. In the first loading cycle, a linear elastic behaviour is observed for all pipes up to the cracking load (P_{cr}). Once the first crack was initiated, all pipes showed a deflection hardening behaviour, indicating that fibres effectively contributed to the ultimate load capacity of the pipes by transferring stresses across cracks. When the load bearing capacity dropped to 0.95 P_{ult}, the load was released completely, leading to the recovery of some deformation as shown in **Fig. 4-8**.

In the second load cycle, which is specified in EN 1916 to ensure that fibres are able to prevent the pipe from collapsing after P_{ult} is reached (Abolmaali *et al.*, 2012), a nearly linear response was recorded until $P_{post,\ max}$ was reached. Two components contributed to this response: (i) bridging cracks by fibres up to the $P_{post,\ max}$, and (ii) aggregate interlocking which had a relatively much smaller contribution to the overall response. After $P_{post,\ max}$, a softening behaviour was recorded regardless of the fibre type and dosage. This is expected since deflection-hardening behaviour would have occurred in the first cycle.

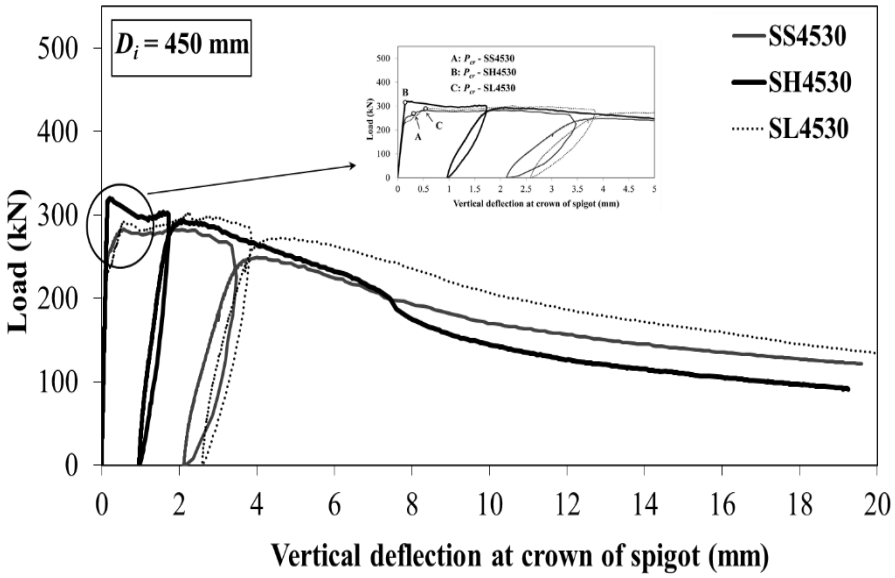

Figure 4-8 Load vs. deflection at crown of spigot SS4530, SH4530, and SL4530 pipes (modified EN: 1916 cyclic TEBT).

In addition, it was observed that there were no instability regions in any of the second load cycles. The same observation was reported elsewhere (de Figueiredo and Gettu, 2008).

4.3.4 Structural Behaviour of 600 mm Diameter Precast Concrete Pipes

The required ultimate D-load for Class V 600 mm diameter pipes according to ASTM C76 is 175 N/m/mm, which corresponds to an applied load of 258 kN. **Figure 4-9** shows the load deformation curves for 600 mm SFRC pipes. Similar to the 450 mm diameter pipes, the deflection in the first load cycle was found to increase linearly with increasing load until reaching the cracking load. After cracking, all pipes showed a deflection hardening behaviour. However, the post-cracking behaviour better improved at higher fibre content. Unlike pipes with fibre contents of 20 and 30 kg/m³, the deflection hardening at a fibre content of 40 kg/m³ was accompanied by increasing load carrying capacity as the deflection increased. For example, the load capacity was 225, 277, and 301 kN at a deflection of 1.0

mm and 218, 273, and 324 kN at a deflection of 2.0 mm for the SS6020, SS6030, and SS6040 pipes, respectively (**Fig. 4-9a**).

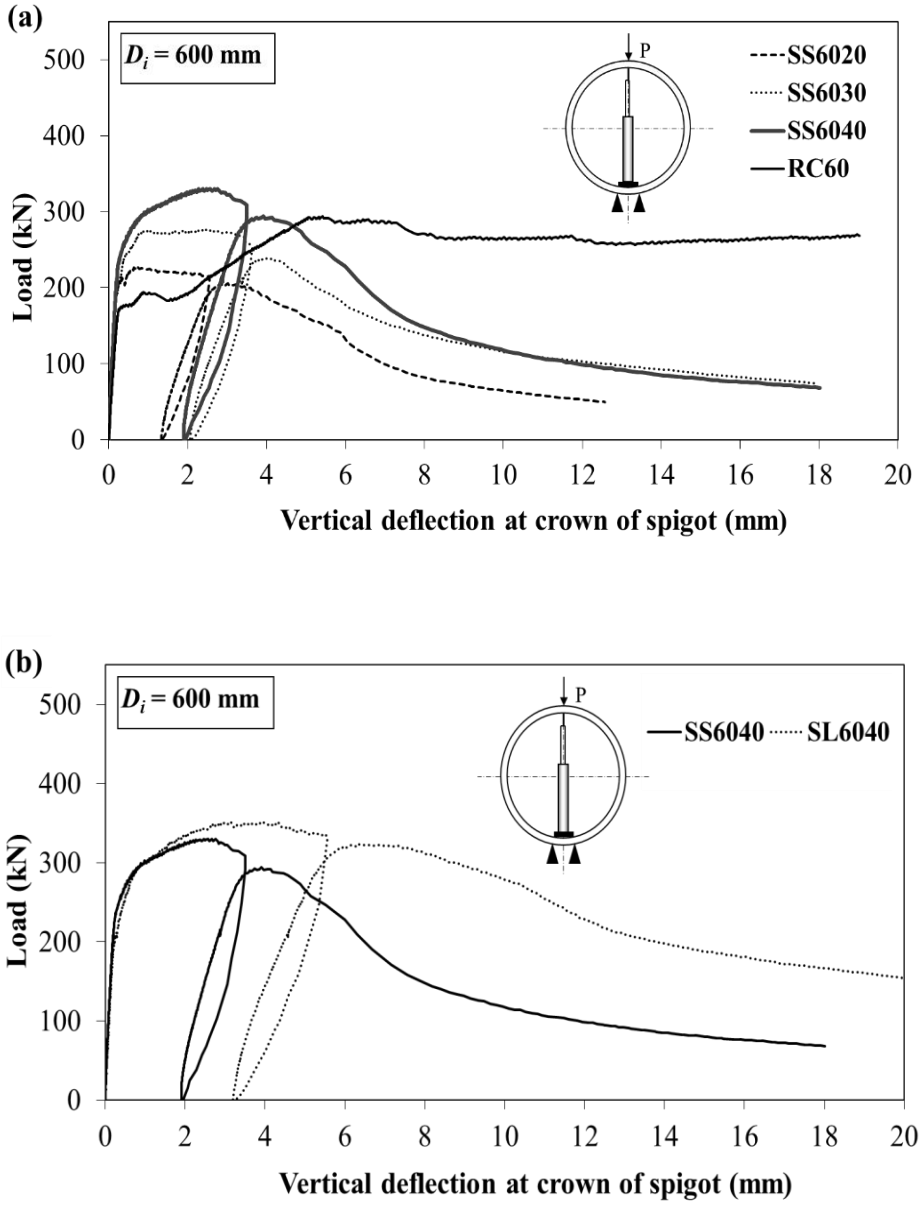

Figure 4-9 Load vs. deflection at crown of spigot (EN: 1916 cyclic TEBT) for (a) RC60, SS6020, SS6030, and SS6040 pipes and (b) SS6040 and SL6040 pipes.

The load- deflection curve for the control RC60 pipe was plotted on the same graph as that of the SFRC pipes for comparison (**Fig. 4-9a**). Unlike the RC45 pipe, no instability regions were observed on the load-deflection curve of the RC60 pipe because the reinforcement consisted of three steel rebar cages (inner, outer and elliptical) that were positioned closer to the extreme fibres (ASTM C76). It can be deduced from **Fig. 4-9a** that the SFRC pipes showed superior behaviour (higher load bearing capacity at similar displacement level) to that of the conventionally reinforced pipes at small displacements (2.5 to 5.0 mm depending on the fibre content). Similar observation was also reported by others (de Figueiredo *et al.*, 2012).

Examining **Fig. 4-10** reveals that a fibre content of 20 kg/m³ failed to achieve the required ultimate strength for Class V 600 mm diameter pipes (P_{ult} = 227 kN < P_n = 258 kN), despite the fact that the pipe sustained the required design strength (P_{cr} = 227 kN < P_c = 208 kN) with no visible cracks on the concrete surface. In the second load cycle, the pipe did not reach the required proof load (i.e. $P_{post,\ max}$ = 206 kN < 208 kN). When the fibre content was increased to 30 and 40 kg/m³, P_{ult} increased to 277 and 330 kN and $P_{post,\ max}$ increased to 239 and 294 kN, respectively. These findings suggest that a fibre content of 30 kg/m³ would be sufficient for 600 mm diameter SFRC pipes to achieve the required strength for Class V pipes according to ASTM C76 requirements. In addition, data presented in **Table 4-3** and **Fig. 4-9a** show that, similar to P_{ult}, the maximum post-peak strength, $P_{post,\ max}$ increased with the increase of the fibre content, regardless of the fibre type.

The benefit of using longer fibres (Dramix 80/60) over short fibres (Dramix 65/35) is illustrated in **Fig. 4-9b.** Pipes incorporating both types of fibres achieved the required strength in the first and second load cycles (P_{ult} = 330, 352 kN and $P_{post,\ max}$= 294, 324 kN for Dramix 65/35 and Dramix 80/60 fibres, respectively). The increases in ultimate and maximum post-peak load were 7% and 10%, respectively. Likewise, using longer fibres enhanced the toughness or fracture energy (i.e. area under load-deflection curve) for SFRC pipes. For example, the average measured toughness at deflections of 3.1 mm (i.e. $\pi D_i/600$) and 12.5 mm (i.e. $\pi D_i/150$) was 0.93×10^6 and 0.94×10^6 N.mm for SS6040 pipe and 2.72×10^6 and 3.93×10^6 N.mm for SL6040 pipe, respectively. Changes in residual strength of -2, 115, 131, and 144% were recorded at deflections of 5, 8, 12, and 18 mm, compared to that observed for pipes made with short fibres, respectively.

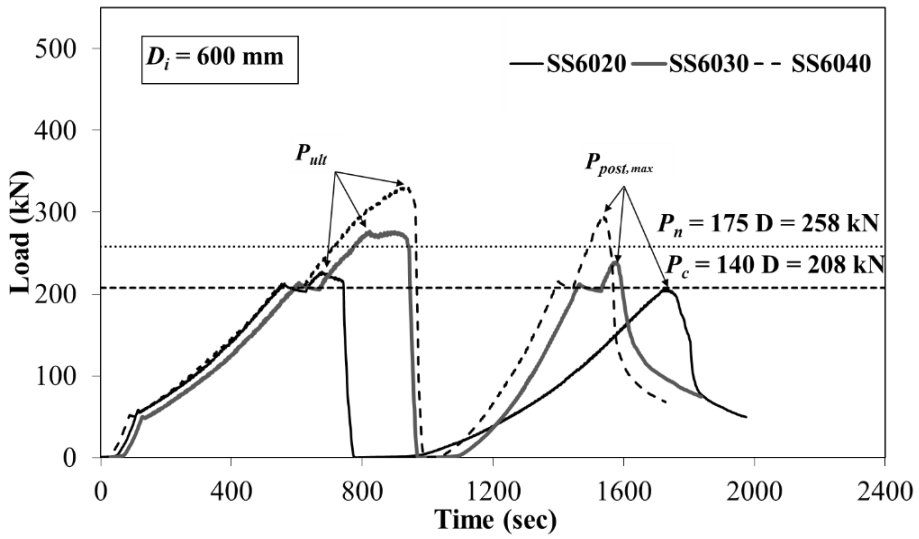

Figure 4-10 Load vs. time (modified EN: 1916 cyclic TEBT) for SS6020, SS6030, and SS6040 pipes.

This can be ascribed to the efficiency of long fibres in bridging cracks since they require higher pullout energy than that of short fibres (Beaumont and Aleszka, 1978).

4.3.5 Post-Cracking Behaviour Analysis

The post-cracking strength (PCS) analysis was explained earlier in **Section** 3.3.4. The trends of PCS curves shown in **Fig. 4-11** are generally in agreement with the previously discussed load deflection responses. For the same fibre type and at the same deflection (δ), an increase in the fibre content resulted in an increase in the post-crack strength. For instance, for the 450 mm diameter pipes, the average *PCS* values were 11.0, 13.2, and 14.2 N/mm² at a deflection of 2 mm, and 9.6, 11.7, and 14.0 N/mm² at a deflection of 5 mm when long fibres were added at rates of 20, 30, and 40 kg/m³, respectively (**Fig. 4-11-a)**. In addition, at the same fibre content and deflection, pipes incorporating the long fibres exhibited higher *PCS* values than that of similar pipes made with the short or hybrid fibres. For example, at a fibre content of 30 kg/m³, the average *PCS* values were 10.6, 11.8, and 11.8 N/mm² at 5 mm deflection and 9.1, 9.6, and 10.5 N/mm² at 10 mm deflection for pipes made with short, hybrid, and long

fibres, respectively (**Fig. 4-11b)**. These values are of great importance when considering the design of SFRC elements from serviceability limits perspective.

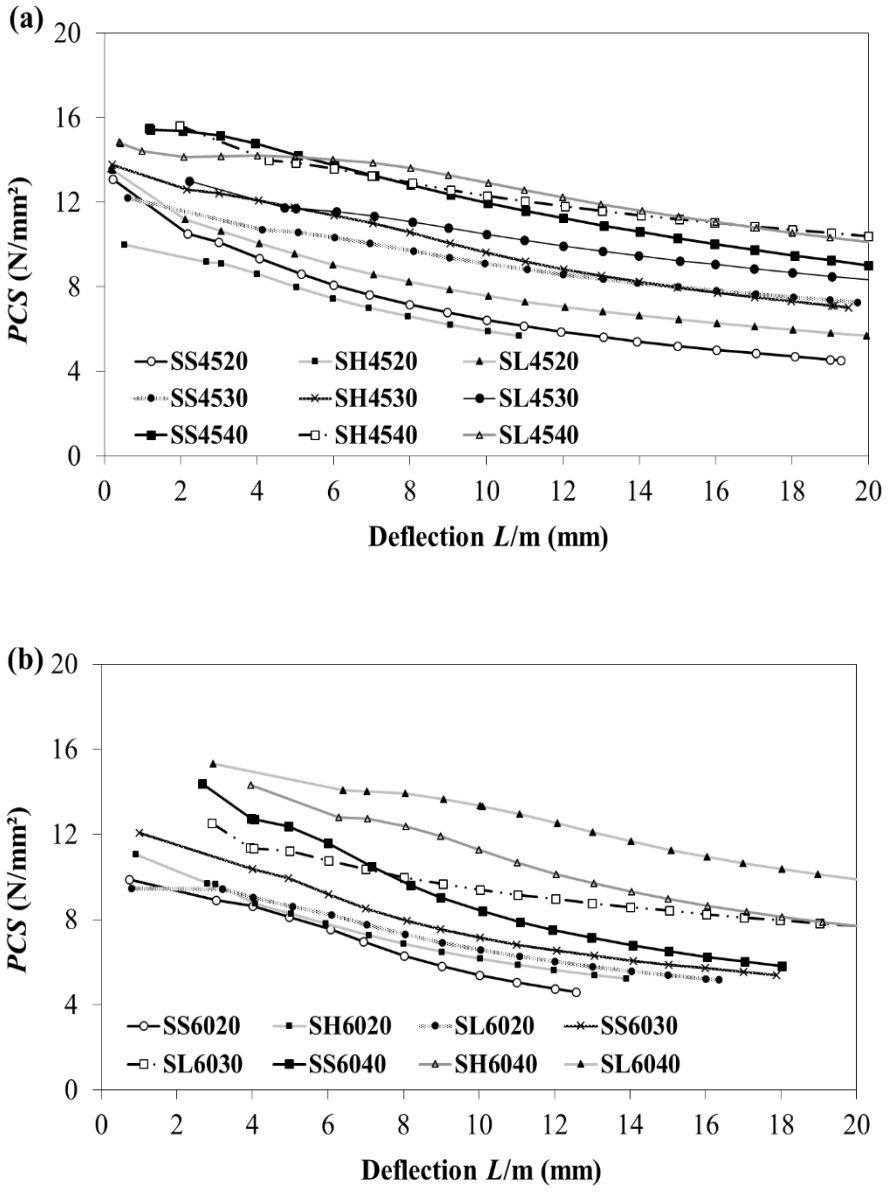

Figure 4-11 Post-crack strength PCS at different deflection values for (a) 450 mm diameter SFRC pipes and (b) 600 mm diameter SFRC pipes.

The synergy analysis was explained earlier in **Section 3.3.4**. No synergy effect was observed for the selected deflection limits for mixtures used in the fabrication of the 450 and 600 mm diameter pipes as shown in **Table 4-4**. It was found that any enhancement to the post-cracking behaviour due to fibre hybridization appeared to be related to the inclusion of the long fibres only (i.e. short fibres had no synergetic effect).

Table 4-4 Fibre synergy assessment at various deflections

Pipe	Fibre Content (kg/m^3)	Synergy		
		at 3.0 mm	at 5 mm	at 10 mm
SH4520	20	-0.56	-0.49	-0.47
SH4530	30	-0.48	-0.48	-0.51
SH4540	40	-0.49	-0.51	-0.51
SH6020	20	-0.47	-0.51	-0.49
SH6030	30	-0.51	-0.48	-0.49
SH6040	40	-0.49	-0.50	-0.48

Note: hybridization ratio = 0.5:0.5

4.3.6 Strain Measurements for 450 mm Diameter Pipes

Figure 4-12 illustrates the strains measured at the inner invert (SG #1), the inner spring-lines (SG #2) and the outer springs (SG #3) of the 450 mm diameter pipes at the ultimate D-Load (175 D) for Class V pipes, and at the ultimate load P_{ult}. **Figure 4-12a** indicates that the measured strains on the concrete surface corresponding to the ultimate D-Load level at the inner invert and outer spring-lines were positive (i.e. tensile strains). SG #1 and SG #3 readings increased with increasing load until the formation of the first crack.

After first crack formation, SG #1 either ruptured or gave a very low reading (positive or negative) as an indication of stresses redistribution at the inside invert area. Similarly, with loading increase, SG #3 either ruptured or indicated a redistribution of stresses at the outer spring area. This can be ascribed to the fact that the bending moment at the invert section is typically higher than that at spring-lines, resulting in higher stresses at the invert section. The average measured strain values for SG#1 and SG#3 were less than 100 με (<<concrete

ultimate tensile strain = 900 to 1600 με (Gopalaratnam and Shah, 1985)), indicating that the material was well in the elastic range at such a loading level.

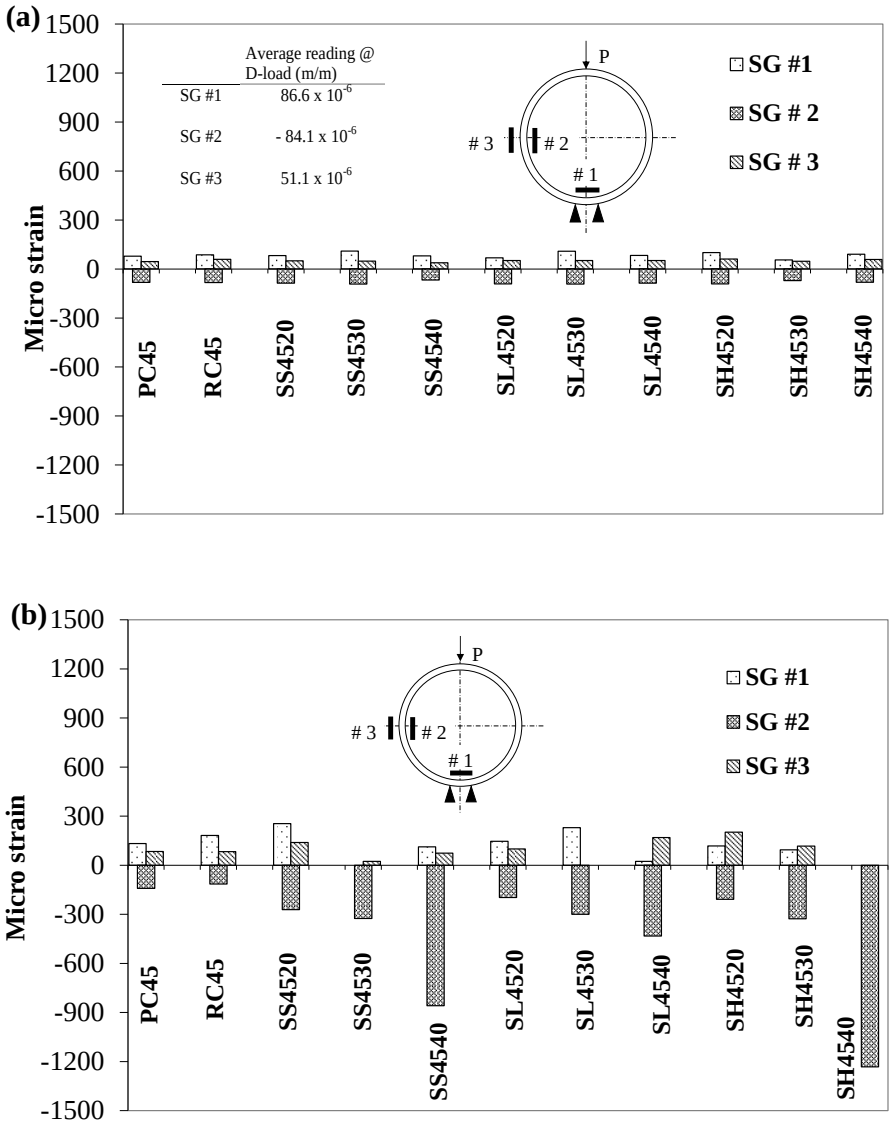

Figure 4-12 Measured strain at concrete surface of 450 mm diameter pipes at inner invert (SG #1), inner spring-line (SG #2), and at outer spring-line (SG #3) at (a) ultimate required D-load = 194 kN and (b) at ultimate load P_{ult}.

Conversely, the reading of SG #2 progressed until the end of the test, indicating that a concrete compression failure did not occur at the spring-lines. For instance, average SG #2 readings at P_{ult} for PC45 and RC45 pipes were -141 and -115 με (which is significantly lower than the concrete's ultimate compressive strain = 3500 με), respectively. After reaching P_{ult}, the PC45 pipe collapsed, while the RC45 pipe exhibited a deflection hardening behaviour (**Fig. 4-6**). The maximum compressive strain measured at the inner spring-lines was 1360 με at P = 190 kN, before it started to decrease due to a reduction of residual strength induced by yielding of the wire reinforcement.

A similar behaviour to that of the RC45 pipe was observed for the SFRC pipes; however, the maximum measured compression strain was significantly higher than that of the RC45 pipe. For instance, at a fibre content of 40 kg/m^3, the maximum strain readings for SG #2 were -4447, -2112 and -4954 με at P = 136, 172 and 204 kN for pipes incorporating short, long, and hybrid fibres, respectively. These values are well below reported values for maximum compressive strain for SFRC incorporating similar range of steel fibres (= 15000 με) (Fanella and Naaman, 1985; Ezeldin and Balaguru, 1992; Nataraja *et al.*, 1999).

SG #2 readings for SFRC pipes decreased due to reduction of the residual strengths caused by fibres pullout and rupture. **Figure 4-12b** shows a pattern of increased compressive strain at P_{ult} as the fibre content increased for all fibre types. This is ascribed to improvements of the matrix deformability due to the addition of higher amount of fibres (Nataraja *et al.*, 1999; Dhakal *et al.*, 2005; and Boulekbache *et al.*, 2012).

4.3.7 Strain Measurements for 600 mm Diameter Pipes

Figure 4-13 displays typical strains measured at the inner invert (SG #1), inner spring-lines (SG #2) and outer spring-lines (SG #3) of the 600 mm diameter pipes at the ultimate required D-Load (175 D) for Class V pipes and at the ultimate load P_{ult}. The behaviour of the 600 mm diameter pipes was comparable to that of the 450 mm diameter pipes. However, the 600-mm diameter pipes with a fibre dosage of less than 30 kg/m³ failed to reach the required ultimate load (no reading reported in **Fig. 4-13a**). The average strain reading of SG #2 for SFRC pipes at the required D-load was -260 με, which is higher than that of the 450 mm diameter pipes

(-84 με). This is due to the larger pipe diameter, which dictates higher D-loads and bending moments. Similar to 450 mm diameter pipes, **Fig. 4-13b** shows an increasing trend of compressive strain at P_{ult} with increased fibre content.

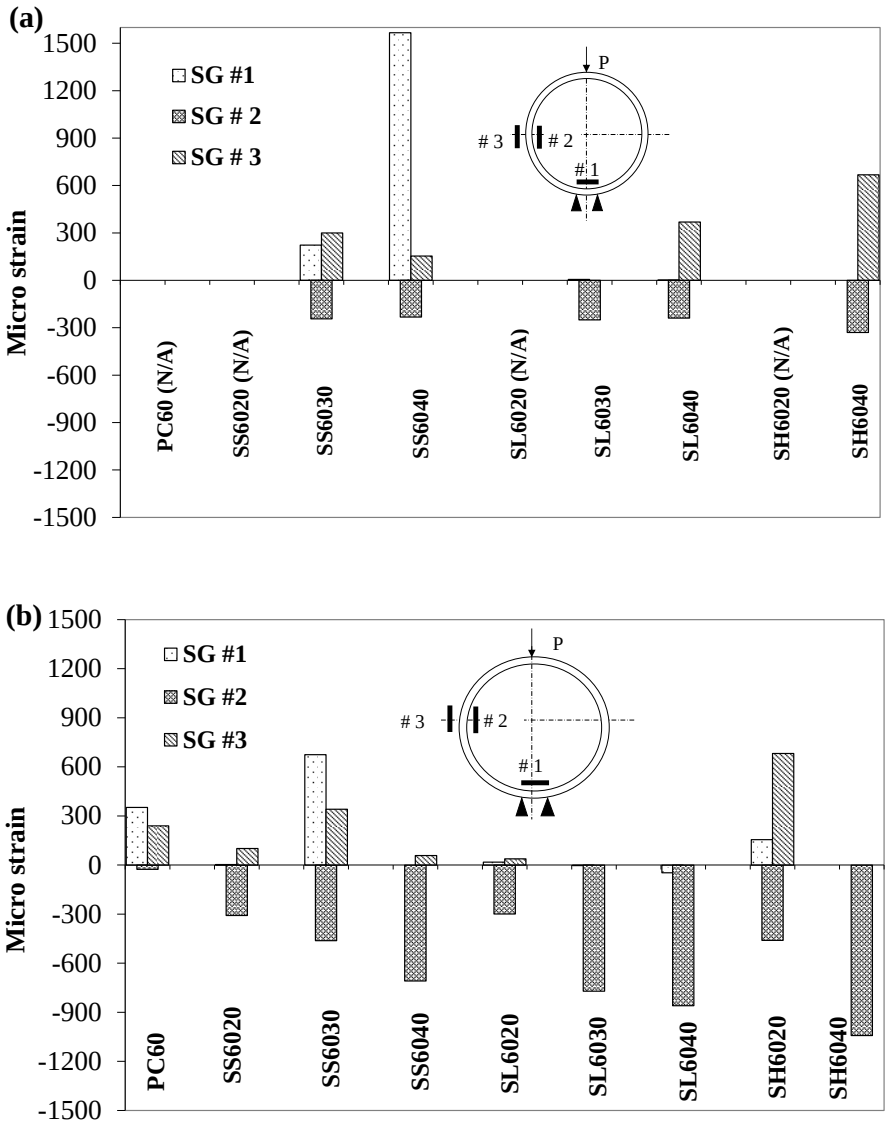

Figure 4-13 Measured strain at concrete surface of 600 mm pipes at inner invert (SG #1), inner spring-line (SG #2), and at outer spring-line (SG #3) at (a) ultimate required D-load = 258 kN, and at (b) ultimate load P_{ult}.

4.3.8 Diametrical Deformation of 450 and 600 mm Diameter SFRC pipes

Figures 4-14 and **4-15** illustrate the cross-sectional deformations at the two load cycles specified in EN 1916 TEBT for SFRC 600 mm and 450 mm diameter pipes, respectively. Four loading points were selected, which correspond to the ASTM design load (140 D) and P_{ult} in the first loading cycle, and proof strength (140 D) and $P_{post,\ max}$ in the second loading cycle. At the end of the first loading cycle, the vertical and horizontal deformations were gaged to zero and considered as initial values for the second loading cycle in order to compare the deformability of the pipe during the two cycles.

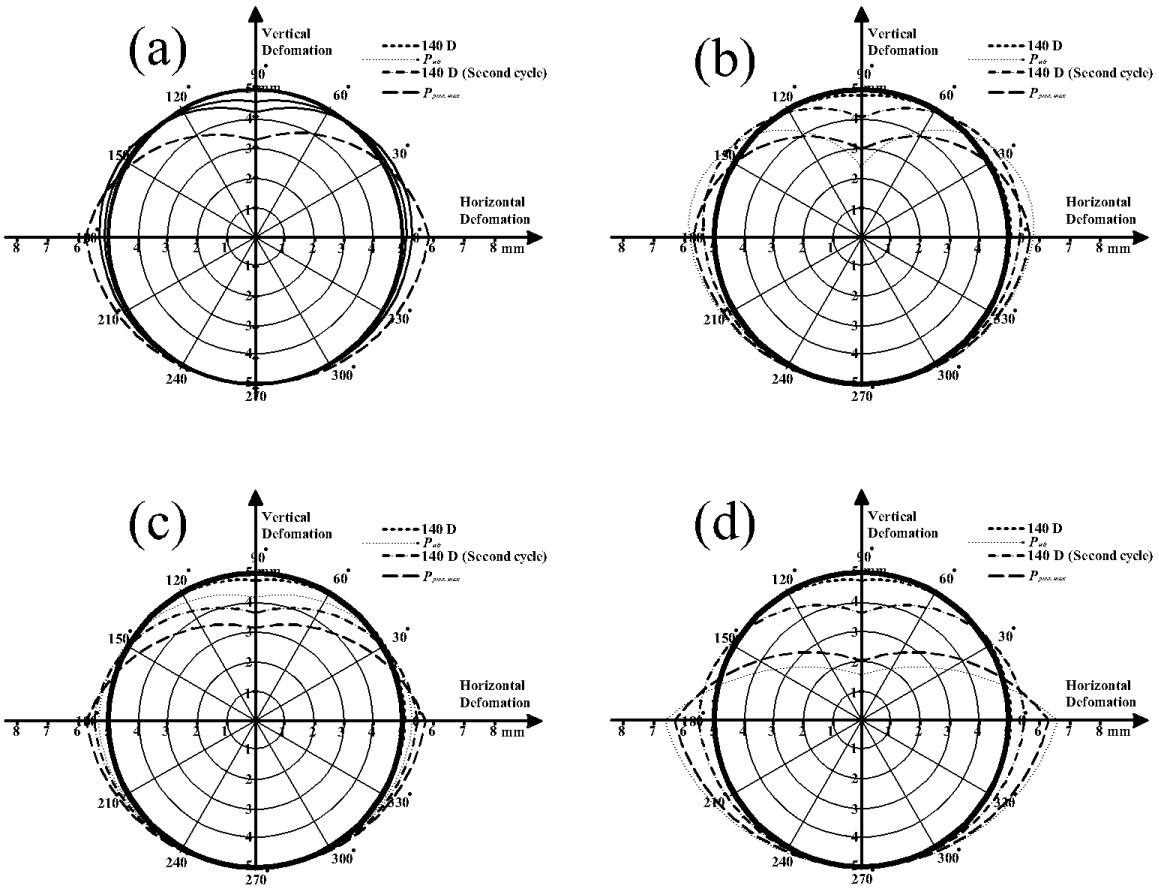

Figure 4-14 Cross-section vertical and horizontal deformations of 600 mm SFRC pipes with a) 20 kg/m^3 and b) 40 kg/m^3 of Dramix 65/35 fibres, c) 20 kg/m^3, and d) 40 kg/m^3 of Dramic 80/60 fibres.

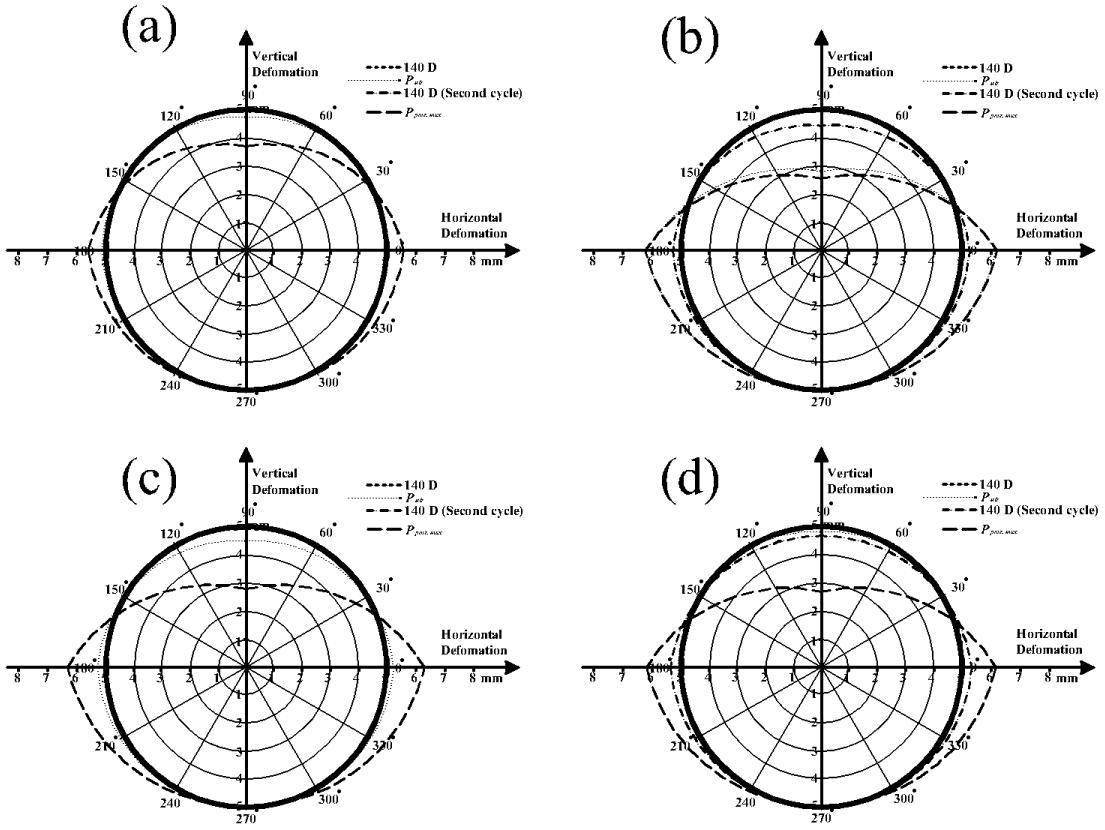

Figure 4-15 Cross-section vertical and horizontal deformations of 450 mm SFRC pipes with a) 20 kg/m^3 of Dramix 65/35 fibres b) 30 kg/m^3 of Dramix 80/60 fibres, c) 20 kg/m^3, and d) 30 kg/m^3 of Hybrid Dramix fibres.

In the first load cycle, it can be observed that there was no significant difference between pipe deformations at the design load 140D (156 kN and 208 kN for 450 and 600 mm diameter pipes, respectively) (**Figs. 4-14** and **4-15)**. This is because the load was carried primarily by the concrete matrix and fibres were not mobilized at this stage. At the ultimate loads of the first load cycle (P_{ult}), pipes with higher fibre content exhibited higher corresponding diametrical deformations. For instance, for the 600 mm diameter pipes, the vertical and horizontal deformations at P_{ult} increased from 0.805 and -0.332 mm (negative sign indicates outward displacement) to 3.95 and - 1.656 mm, respectively when the long fibre content increased from 20 to 40 kg/m^3 (**Fig. 4-14**). This amounts to about five times increase in deformability when the fibre content was doubled, which further explains the

increase in compressive strain values at the pipe inner springs when the fibre content increased (**Fig. 4-13b**).

In addition, pipes incorporating longer fibres exhibited more ductile behaviour, which is in agreement with findings discussed earlier. For instance, at a fibre content of 40 kg/m³, the vertical and horizontal deformations at P_{ult} increased from 2.573 and - 0.835 mm to 3.950 and - 1.656 mm when short fibres were replaced by longer fibres. **Figure 4-15** indicates that combining long and short fibres did not create a synergetic effect. For example, for the 450 mm diameter pipes incorporating 30 kg/m³ of fibres, the vertical and horizontal deformations at P_{ult} were 0.20 and - 0.075 mm when long fibres were used, and 2.155 and -1.219 mm for hybrid fibres, respectively.

In the second load cycle, the ability of SFRC pipes to deform was mainly dependant on the properties and dosage of the steel fibres used, unlike in the first load cycle where the interaction between the matrix and fibres had a predominant effect. It was observed that pipes incorporating high dosage (i.e. 30 and 40 kg/m³) of long fibres exhibited comparable cross-section deformations at the ultimate loads in both load cycles (P_{ult} and $P_{post,\ max}$). This was true for both the 600 mm (**Fig. 4-14d**) and 450 mm diameter pipes (**Fig. 4-15b**).

4.4 DISCUSSION

4.4.1 Continuous TEBT versus Cyclic TEBT

The procedures of ASTM C497 and EN 1916 pipe crushing tests were illustrated earlier. In their work, Abolmaali *et al.* (2012) used the cyclic EN 1916 test reporting that the second cycle loading is used to ensure that fibres are able to prevent pipe collapse after the ultimate load is reached. Conversely, de Figueiredo *et al.* (2012) used the continuous ASTM C497 crushing test in their work. They reported that there was no influence of the number of cycles (one or two) used in the test on the response of SFRC pipes based on de Figueiredo and Gettu (2008) previous findings.

Results of the current study align with de Figueiredo and Gettu (2008) and de Figueiredo *et al.* (2012) findings. **Figure 4-16** shows the load deflection curves for two 450

mm diameter pipe specimens fabricated with 30 kg/m³ of hybrid fibres under continuous and cyclic TEBT. It can be observed that the second load cycle did not alter the post-cracking behaviour since the pipe specimen in the second load cycle was able to pick up the load from where it ended in the first load cycle. This suggests that the behaviour of SFRC pipes can be explored using the continuous TEBT without need for an extra loading cycle. However, in an industrial realm, if the second loading cycle is to be eliminated, an acceptance criterion for the post-peak behaviour of SFRC pipes must be agreed upon between the owner and the manufacturer depending on the pipe application. This criterion could be in the form of a minimum required residual strength at a specified deflection related to the pipe diameter.

Recently ASTM C1765-13 (standard specification for "Steel Fiber Reinforced Concrete Culvert, Storm Drain, and Sewer pipe) (ASTM, 2013) was published after the completion of the experimental program reported in the present study. SFRC pipe classes specified in ASTM C1765 are similar to classes specified in ASTM C76 for RC pipes. Similar to the EN 1916 standard, the ASTM C1765 standard specifies two loading cycles, however, it does not require the load to be held constant at any loading stage.

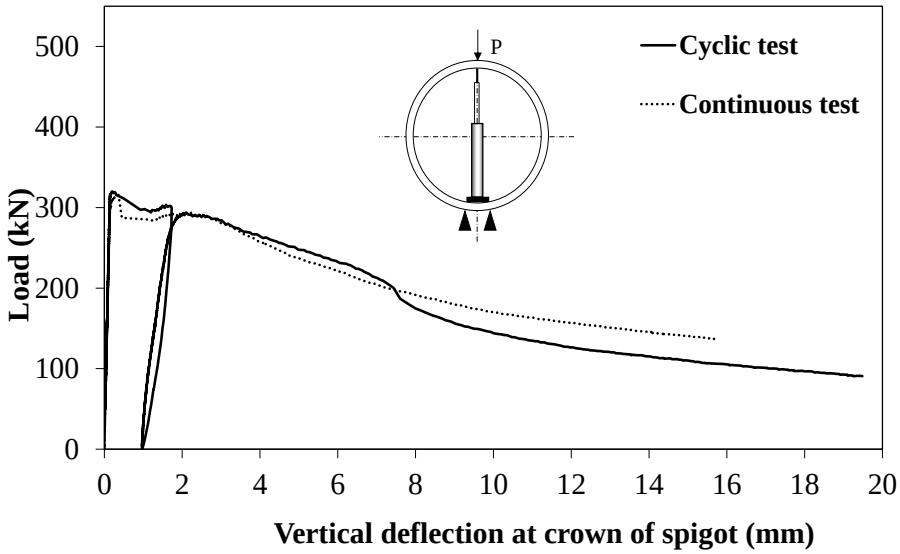

Figure 4-16 Load vs. deflection for TEBT continuous and cyclic test for 450 mm SFRC pipe fabricated with 30 kg/m³ of hybrid Dramix fibres

4.4.2 $P_{0.3}$ versus P_{cr}

ASTM C497 specifies the pipe design (crack) strength for RC pipes based on the 0.3 mm crack width criterion, where the design load is the maximum load reached before a crack having a width of 0.3 mm and a continuous length of 300 mm occurs. The crack is considered 0.3 mm in width when the tip of the 0.3 mm measuring gage will, without forcing; penetrate 1.5 mm at close intervals throughout the specified distance of 300 mm. This procedure is operator sensitive (de Figueiredo and Gettu, 2008). In addition, Erdogmus and Tadros (2009) reported that the 0.3 mm crack width criterion is arbitrary and it is not technically supported that it constitutes the limit of allowance for water ingress to cause corrosion. Thus, it is recommended to alter the 0.3 mm crack width criterion and adopt an alternative criterion stating "no visible cracks on the concrete surface" for SFRC pipes (similar to EN 1916), since the inclusion of steel fibres in the cementitious matrix shall significantly increase the ability of the composite to resist crack formation and propagation (Bischoff, 2003; Jiang *et al.,* 2008; and Buratti, *et al.,* 2013). Indeed, crack occurrence at this load stage would indicate inadequate fibre dosage in the matrix.

4.5 SUMMARY AND CONCLUSIONS

This chapter presents the results of an experimental program that was carried out on full-scale 450 mm and 600 mm diameter SFRC pipes using both the continuous and cyclic three-edge bearing tests. A Post-Cracking Strength (PCS) analysis was conducted in order to evaluate the effects of the reinforcement strategy on the post-cracking behaviour of SFRC pipes. The following conclusions emerged from the experimental results:

- Steel fibres could be successfully used in producing precast concrete pipes to replace the regular steel cage reinforcement. Results showed that a fibre dosage of 30 kg/m³ should be sufficient for 450 and 600 mm diameter pipes to satisfy the strength requirements of ASTM C76 Class V pipes.

- At relatively small displacements (2.0 to 5.0 mm), SFRC pipes fabricated with a fibre content of 30 kg/m³ or more exhibited residual strengths higher than that of RC pipes.

- For SFRC pipes, PCS values at the same deflections increased with the increase of fibres length and dosage.

- Using a hybrid system of long and short steel fibres did not result in synergetic effects. Improvements due to the usage of a hybrid fibre system over short fibres were due to the inclusion of long fibres.

- In the second loading cycle of the cyclic TEBT, diametrical deformations of SFRC pipes were dependant only upon the employed fibre type and dosage and were not affected by the hosting matrix.

- The behaviour of SFRC pipes can be fully explored using the continuous TEBT without the need of an extra loading cycle.

4.6 REFERENCES

Abolmaali, A., Mikhaylova, A., Wilson, A. and Lundy, J., "Performance of steel fibre-reinforced concrete pipes," *Transportation Research Record: Journal of the Transportation Research Board,* 2313(1), 2012, pp. 168-177.

ASTM C497-13, "Standard test methods for concrete pipe, manhole sections, or tile," American Society for Testing and Materials, ASTM International, West Conshohocken, PA, 2013, 14 p.

ASTM C76-13, "Standard specification for reinforced concrete culvert, storm drain, and sewer pipe," American Society for Testing and Materials, ASTM International, West Conshohocken, PA, 2013, 11 p.

ASTM C1765-13, "Standard specification for steel fibre reinforced concrete culvert, storm drain, and sewer pipe." American Society for Testing and Materials, ASTM International, West Conshohocken, PA, 2013, 6 p.

Beaumont, P.W.R., and Aleszka, J.C., "Cracking and toughening of concrete and polymer-concrete dispersed with short steel wires." *Journal of Materials Science,* 13(8), 1978, pp. 1749-60.

Bischoff, P.H., "Tension stiffening and cracking of steel fibre-reinforced concrete." *Journal of Materials in Civil Engineering,* 15(2), 2003, pp. 174-182.

Boulekbache, B., Hamrat, M., Chemrouk, M. and Amziane, S., "Influence of yield stress and compressive strength on direct shear behaviour of steel fibre-reinforced concrete." *Construction and Building Materials,* 27(1), 2012, pp. 6-14.

BS 5911-1:2002 "Concrete pipes and ancillary concrete products (part 1: specification for unreinforced and reinforced concrete pipes (including jacking pipes) and fittings with flexible joints)." British Standards Institution, London, UK, 2002, 21 p.

Buratti, N., Ferracuti, B., and Savoia, M., "Concrete crack reduction in tunnel linings by steel fibre-reinforced concretes." *Construction and Building Materials,* 44(0), 2013, pp. 249-259.

Cho, S., and Kim, Y., "Effects of steel fibres on short beams loaded in shear," *ACI Structural Journal,* 100(6), 2003, pp. 765-774.

Dhakal, R.P., Wang, C., Mander, J.B., "Behaviour of steel fibre reinforced concrete in compression," International *Symposium on Innovation & Sustainability of Structures in Civil Engineering*, Nov. 2005.

Erdogmus, E., and Tadros, M., "Behavior and design of buried concrete pipes phase II-final report." Nebraska Department of Roads, 2009, 124 p.

European Standards, EN 1916, "Concrete pipes and fittings, unreinforced, steel fibre and reinforced." European Committee for Standardization, 2002, 89 p.

Ezeldin, A. S., and Balaguru, P.N., "Normal-and high-strength fiber-reinforced concrete under compression," *Journal of Materials in Civil Engineering*, 4(4), 1992, pp. 415-429.

Fanella, D.A., and Naaman, A.E., "Stress-strain properties of fiber reinforced mortar in compression," *ACI Journal proceedings*, 82 (4), 1985, pp. 475-483.

de Figueiredo, A. and Gettu, R., "Evaluation of the test method for crushing strength of steel fibre reinforced concrete pipes." *Seventh RILEM International Symposium on Fibre Reinforced Concrete*, RILEM Publications SARL, 2008, pp. 989-1000.

de Figueiredo, D., De La Fuente, A., De Cea, A., Borrell, C., and Chama Neto, P., "Steel fiber reinforced concrete pipes. Part 1: technological analysis of the mechanical behaviour." *IBRACON Structures and Materials Journal*, 5 (1), 2012, pp. 1-11.

Gopalaratnam, V. S., and Shah, P.S., "Softening response of plain concrete in direct tension," *ACI Journal Proceedings*, 82 (3), 1985, pp. 310-323.

Haktanir, T., Ari, K., Altun, F. and Karahan, O., "A Comparative experimental investigation of concrete, reinforced-concrete and steel-fibre concrete pipes under three-edge-bearing test" *Construction and Building Materials,* 21(8), 2007, pp. 1702-1708.

Jiang, J., Sun, W., Zhang, Y., Chen, C. and Wang, J., "Cracking resistance performance of super vertical-distance pumped SFRC," *Frontiers of Architecture and Civil Engineering in China*, 2(2), 2008, pp. 179-83.

NBR 8890 "Concrete pipe of circular section for storm water and sanitary sewers - requirements and test methods." Brazilian Association of Technical Standards, 2008, 30 p.

Nataraja, M.C., Dhang, N. and Gupta, A.P., "Stress–strain curves for steel-fibre reinforced concrete under compression," *Cement and Concrete Composites,* 21(5–6), 1999, pp. 383-390.

Ou, Y., Tsai, M., Liu, K. and Chang, K., "Compressive behaviour of steel-fibre-reinforced concrete with a high reinforcing index." *Journal of Materials in Civil Engineering,* 24(2), 2011, pp. 207-215.

Song, P.S. and Hwang, S., "Mechanical properties of high-strength steel fibre-reinforced concrete," *Construction and Building Materials,* 18(9), 2004, pp. 669-673.

CHAPTER FIVE

5 FIELD PERFORMANCE OF BURIED FULL-SCALE STEEL FIBRE REINFORCED CONCRETE PIPES[3]

5.1 INTRODUCTION

Reinforced concrete pipes are typically installed following the procedures of the Standard Installations Direct Design (SIDD) method. The SIDD method is the state-of-the art in the area of reinforced concrete pipe design and it is used to determine the actual moments, thrusts, and shears in a buried pipe (ACPA, 1993). The SIDD method introduced the four standard installations (I to IV) based on Heger's earth pressure distribution around a buried pipe (**Fig. 2-4**). The four standard installations cover a wide range of installation effort, site management, and soil quality. Type I requires the highest quality of bedding material and compaction effort, while Type IV assumes little or no effort with no imported bedding materials (Wong *et al*., 2006).

Over the last two decades, several authors have experimentally investigated the soil-pipe interaction of conventionally reinforced concrete pipes through long-term field monitoring (e.g. Hill *et al.*, 1999; McGrath *et al.*, 2000; Smeltzerl and Daigle, 2005; Wong *et al.*, 2006; Maximos *et al.*, 2008; Erdogmus and Tadros, 2009) and short-term laboratory testing (e.g. Sargand *et al.,* 1995; Lay and Brachman, 2014). However, no studies could be found in the open literature that investigate the soil-pipe interaction of SFRC pipes.

[3] A version of this chapter was submitted for publication to the *Construction and Building Materials Journal*.

This chapter presents an exploratory investigation providing novel data on the behaviour of buried full-scale 600-mm diameter SFRC pipes under actual and simulated live loads. The first phase of this study monitored the behaviour of SFRC pipes under standard CL 625 truckloads. In the second phase, the post-cracking behaviour of SFRC pipes under artificial live loads was examined. The soil-pipe interaction for SFRC pipes was analyzed in light of the established analysis procedures. Plain concrete (PC) and conventionally reinforced concrete (RC) pipes were also tested for comparison.

5.2 EXPERIMENTAL PROGRAM

5.2.1 Precast Concrete Pipes Fabrication

PC, RC, and SFRC pipes were fabricated at an industrial precast concrete plant in Oakville, Ontario, operating with the dry-cast production method. Pipes' internal diameter (D_i) was 600 mm. All pipes had a Type C wall (wall thickness h = 94 mm). The Class V pipe (i.e. ultimate D-load = 175 N/m/mm) was the target pipe strength according to ASTM C76. Two types of steel fibre (Dramix RC-65/35-CN and Dramix RC-80/60-CN) were added manually as partial replacement for the coarse aggregate in SFRC pipes at W_f (fibres mass per 1 m^3) of 20 and 40 kg/m^3 (i.e. equivalent to 0.25 and 0.50 % by concrete volume (V_f)). Detailed description of materials used in concrete fabrication was given earlier in **Section 3.2.1**. The compositions of the control fibreless mixture and other tested SFRC mixtures are shown in **Table 5-1**. The physical and mechanical properties of steel fibres used in this study are shown in **Table 3-2**. Full-scale field-testing was conducted at Western University's Field Site. **Table 5-2** summarizes experimental details, including the tested pipes, reinforcement type and dosage, and installation types according to the SIDD method.

5.2.2 Instrumentation and Specimens Preparation

In the first experimental phase, only PC60 and SS6020 pipes were tested. A total of 24 electrical foil resistance strain gauges were mounted on the circumference direction at the spigot and mid-span sections to measure hoop strains. For each pipe segment, at both

sections, strain gauges were mounted on the interior and exterior wall surfaces of the pipe at its crown, spring-lines, and invert regions to measure flexural strains. After mounting, strain gauges were treated with polyethylene and melting wax for waterproofing and protection from soil friction.

Table 5-1 Concrete mixture proportions

Material	Mass/Cement mass
Cement	1.00
Blast Furnace Slag	0.54
Fine Aggregate	5.00
Coarse Aggregate	4.17
Water	0.58
Super plasticizer	0.0016
Air entraining admixture	0.002
Steel Fibres	0, 20, 40 kg/m^3

Table 5-2 Tested pipes and Installation types

Phase	Pipe Designation	Reinforcement	W_f (kg/m^3)	Installation Type
1st	PC60	None	-	IV
	SS6020	Dramix 65/35	20	IV
2nd	SL6020	Dramix 80/60	20	IV
	SL6040	Dramix 80/60	40	IV
	PC60	None	-	IV
	RC60	Regular	-	IV
	SS6020	Dramix 65/35	20	III
	SS6040	Dramix 65/35	40	III

In the second phase, RC and SFRC pipes were subjected to the three-edge bearing test TEBT in the laboratory prior to being transported and tested in the field. SFRC pipes were loaded up to their ultimate loads (P_{ult}), and then the load was released when the load carrying capacity dropped to 0.95 P_{ult}. This procedure is similar to the first loading cycle described in both standards ASTM C1765 (Standard Specification for Steel Fiber Reinforced Concrete Culvert, Storm Drain, and Sewer Pipe) and EN 1916 (Concrete Pipes and Fittings, Unreinforced, Steel Fiber and Reinforced), while the second loading cycle was replaced with

the field-testing. The RC60 pipe was loaded up to $P_{ult,}$ and then the load was released when the reinforcement started yielding. The PC60 pipe was not loaded in the laboratory prior to field-testing.

In both experimental phases, during pipe installation, linear variable differential transducers (LVDTs) were used to measure vertical pipe deflections. A special central holder truss frame with three spokes radiating from the holder hub were designed and built to hold the LVDTs during loading at the pipe spigot (**Fig. 5-1**). Measured strains and displacements were recorded automatically using a data acquisition system.

Figure 5-1 Pipe segment instrumented with LVDTs.

In the second experimental phase, 230 mm diameter Geokon earth pressure cells (model 4810E Vibrating Wire Contact Pressure Cell) were used to monitor the stresses in the soil around the outside walls of the buried pipe during installation and live load application. The operating range of the pressure cells was from zero up to 700 kPa; however, they are capable of accommodating a 50% overload as per manufactures specifications. All cells used vibrating wires sensors to determine the pressure and were accurate up to 0.25% as indicated

by the manufacturer. All cells were calibrated by the manufacturer prior installation and Geokon's calibration curves were used in analyzing the recorded data. The pressure cells were positioned approximately at the middle of the pipe length from one end. A portable GK403 readout unit was used to monitor earth pressure cells during installation and loading. **Figure 5-2** shows a schematic cross-sectional view of a typical pipe segment and pressure cells positions in this stage. Pressure cells installed in the horizontal direction were used to measure the vertical earth pressure at the pipe invert and crown. Pressure cells installed in the vertical orientation were used to measure the horizontal earth pressure at the pipe spring-lines. Pressures cells were installed following the same procedure described by Sargand *et al.* (1995) and Wong *et al.* (2006). Furthermore, to ensure uniform contact pressure on the cell surface, the following installation procedure was adopted:

- Compaction of all areas surrounding the pressure cell prior to installation using a plate vibratory compactor.
- Digging a hole of 400 x 400 x 100 mm dimensions and the removal of any visible cobblestones in the hole.

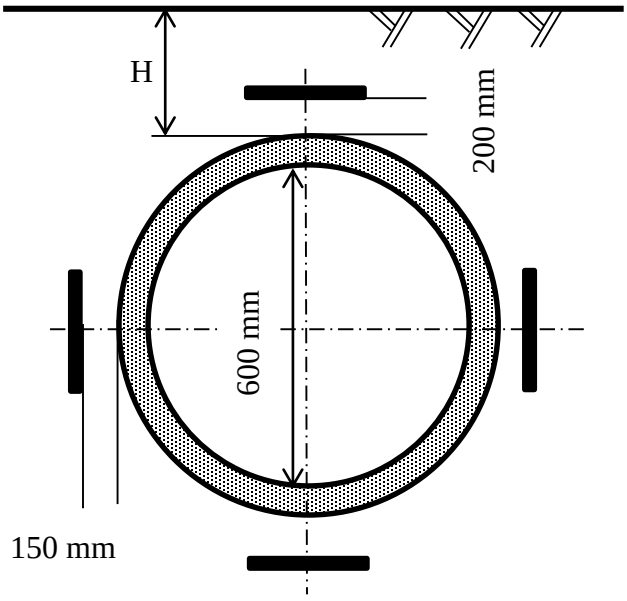

Figure 5-2 Arrangement of earth pressure cells around the pipe in the second experimental campaign.

- Filling the hole with fine white sand and burying the pressure cell in fine sand.
- Finally, covering the hole with the excavation and compacting by hand.

Using white sand facilitated locating the pressure cell during pipe removal after testing.

5.2.3 Installation Type and Procedure

Type III and IV standard installations according to the SIDD method were tested (**Table 5-2**). In Type IV installation, available soil from the site excavation was compacted to a standard Proctor compaction of 85%. The soil was classified as clayey sand (SC) according to ASTM D2487 (Standard Practice for Classification of Soils for Engineering Purposes (Unified Soil Classification System)). For Type III installation, well-graded river sand (SW) was imported and compacted to a standard Proctor compaction of 85%. The particle size distribution of both soils is given in **Fig. 5-3.** These installations match the C and D installations according to Marston/Spangler design method (ACPA, 2007). **Figure 5-4** shows the original trench dimensions and pipe after installation.

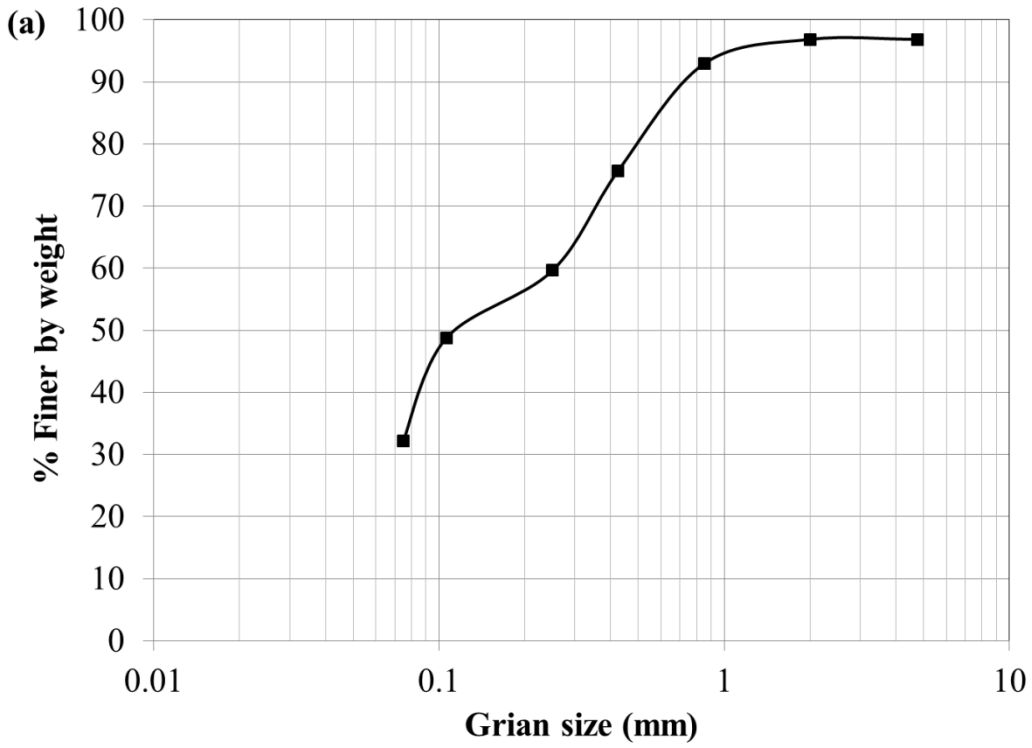

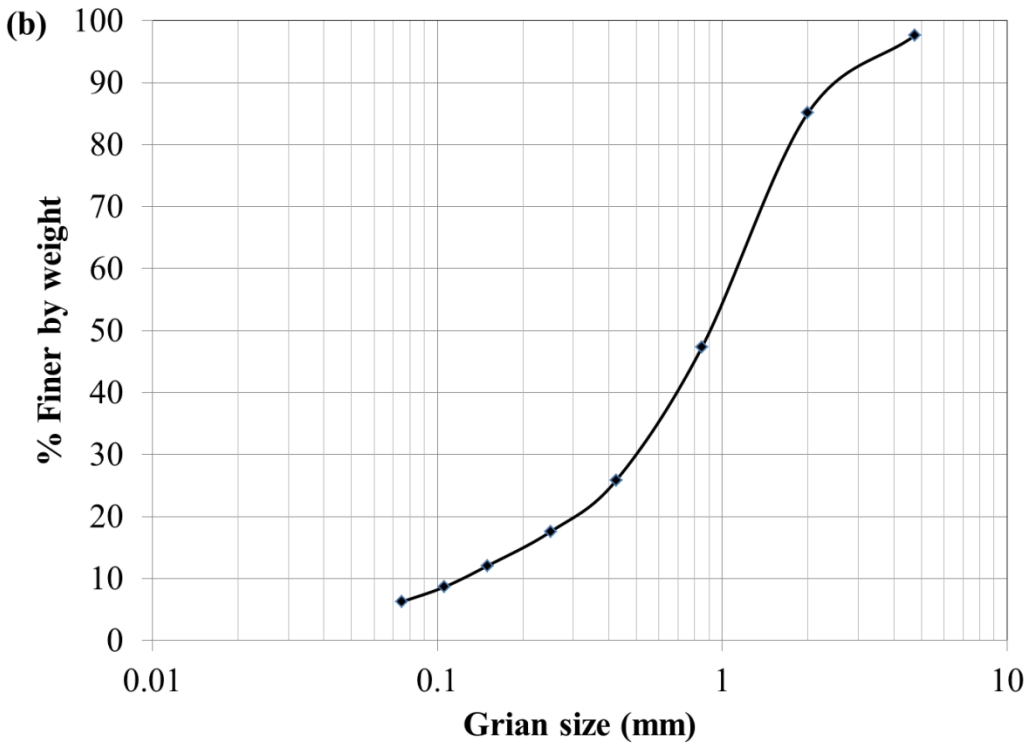

Figure 5-3 Grain size distribution for soil type a) Clayey sand (SC) and b) Well-graded sand (SW)

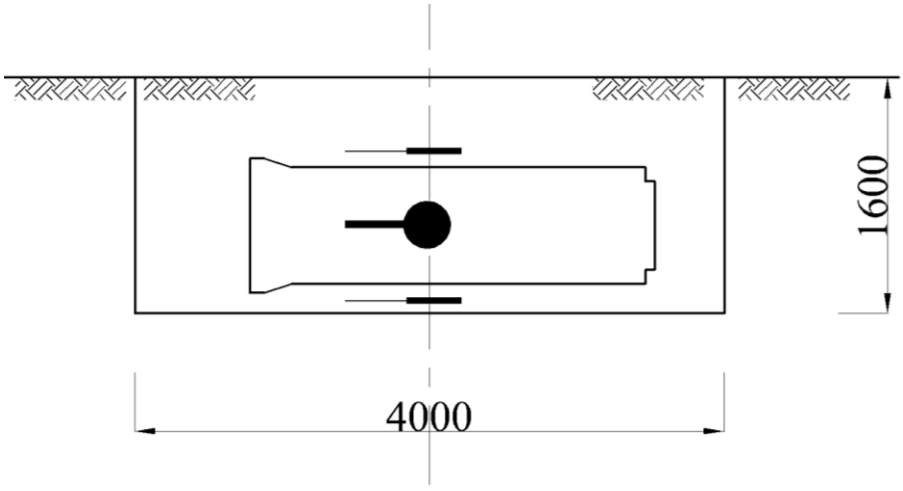

Figure 5-4 Trench dimensions (mm) in the second experimental campaign.

5.2.4 Testing Procedure

5.2.4.1 First experimental phase

Pipes were tested for service performance using a standard fully loaded CL 625 Ontario truck that was about 35 tons (343 kN), which is the maximum allowable weight for such truck. This was equivalent to front and rear axle loads of 68 kN and 137 kN, respectively. Two loading orientations were applied: a) Truck travels transverse to the centerline of the pipe, and b) parallel to the centerline of the pipe. Four stations (i.e. truck stops) along the buried pipe were explored: 1) tires of the rear axle of the truck were exactly over the center of the buried pipe, 2) tires of the front axles were exactly over the center of the buried pipe, 3) tires of one side of the two rear axles were exactly along the center of the buried pipe, and 4) tires of the two rear axles of each tandem dump truck were positioned symmetrically with respect to the buried pipes. **Figure 5-5** shows a schematic of a buried pipe under truck loading and tire/load configuration of the loading truck.

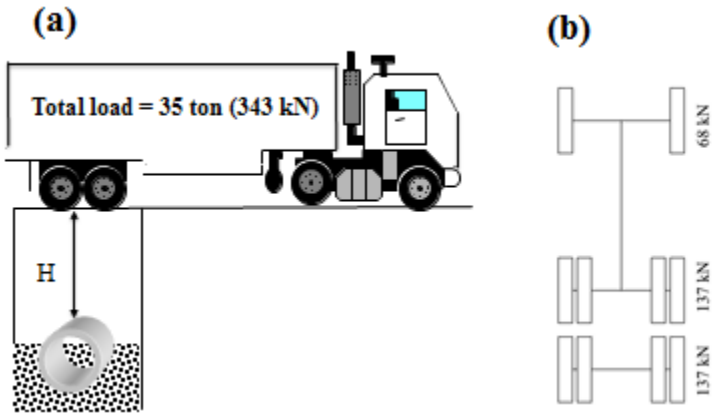

Figure 5-5 a) Schematic of pipe under truck loading b) tire/load configuration of the loading truck

5.2.4.2 Second experimental phase

Loading was done using precast concrete blocks. Loading increased/ decreased incrementally by 75 kN. Readings of pressure cells and LVDTs were recorded at the end of each step after a period of five to ten minutes to allow the system to stabilize. **Figure 5-6** shows a schematic of a pipe buried in the trench with concrete blocks loading.

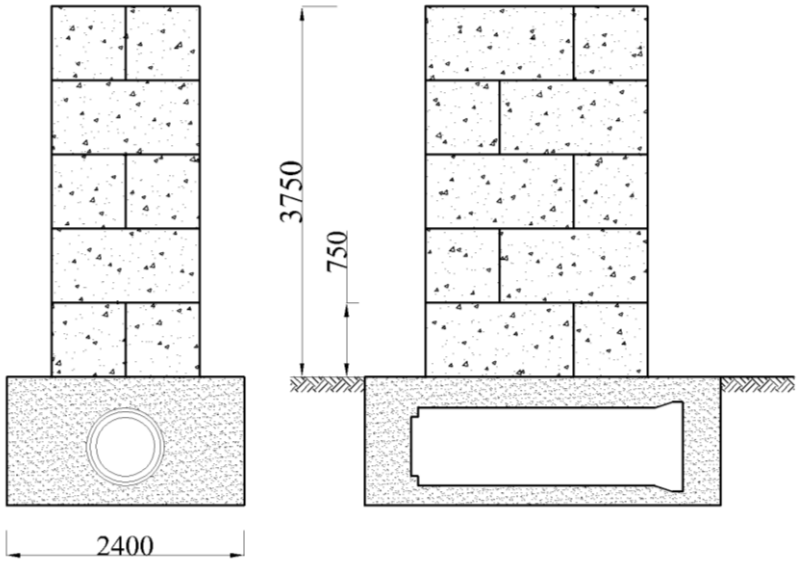

Figure 5-6 Schematic of loading using concrete blocks in the second experimental campaign (mm).

5.3 RESULTS AND DISCUSSION

5.3.1 First Experimental Phase

Table 5-3 shows the average measured internal (ε_{in}) and external (ε_{out}) circumferential strains at the invert and spring-line sections for the PC60 and SS6020 tested pipes. Positive sign indicates tension strains and vice versa. Regardless of the pipe type, the measured tensile strain values were lower than the tensile cracking strain of plain concrete (i.e. 100-200 με) (Gopalaratnam and Shah, 1985; and Kaklauskas, and Ghabouss, 2001). Furthermore, the

measured vertical displacement at crown for all loading cases was less than 0.1 mm. This explains the absence of cracks or permanent deformations on the concrete surface when the pipes were visually inspected after extraction. To better utilize values reported in **Table 5-3**, experimental bending moments (M_{exp}) were calculated and compared to theoretical bending moments (M_{SIDD}) as shown in **Fig. 5-7**. Experimental bending moments (M_{exp}) were calculated using **Eq. 5-1** (Munro *et al.*, 2009, and Lay and Brachman, 2014).

$$M_{exp} = EI\left(\frac{\varepsilon_{in}-\varepsilon_{out}}{h}\right) \qquad \textbf{Eq. 5-1}$$

Table 5-3 Average flexural strains at critical sections for PC60 and SS6020 pipes

Loading case	PC60				SS6020			
	at Invert		at spring-line		at Invert		at spring-line	
	ε_{in} (με)	ε_{out} (με)	ε_{in} (με)	ε_{out} (με)	ε_{in} (με)	ε_{out} (με)	ε_{in} (με)	ε_{out} (με)
1	45	-25	-31	20	67	-22	-44	41
2	53	-30	-39	48	61	-25	-41	41
3	61	-27	-32	68	91	-50	-67	64
4	55	-12	-19	71	74	-33	-52	49

where M_{exp} is the bending moment (kN.m/m), EI is the flexural stiffness of the pipe wall section (kN.m²/m), h is the pipe wall thickness (m), ε_{in} and ε_{out} are the internal and external circumferential concrete strains, respectively. The modulus of elasticity (E) was determined experimentally using standard sized cylindrical specimens (100 mm x 200 mm) that were prepared during pipe fabrication, then cured and tested at an age of 28 days. The average modulus of elasticity value was 30 GPa. The calculated flexural stiffness (EI) was 2076 kN.m²/m. In all load cases, no significant difference in experimental bending moment values at critical sections between the two tested pipes was recognized (**Fig. 5-7**). The difference between the measured M_{exp} at critical sections for the SS6020 pipe and that for the PC60 pipe ranged from -41% to 17% of the M_{exp} values for the PC60 pipe at same sections for all

loading cases. This range is acceptable for such studies (Smeltzer and Daigle, 2005; Lay and Brachman, 2014). This is expected, since both pipes sustained the applied live load without suffering any cracks at critical sections. Consequently, the effect of fibre addition to the matrix was not clear at this stage, since the concrete properties dominated the pipe's behaviour rather than the steel fibres.

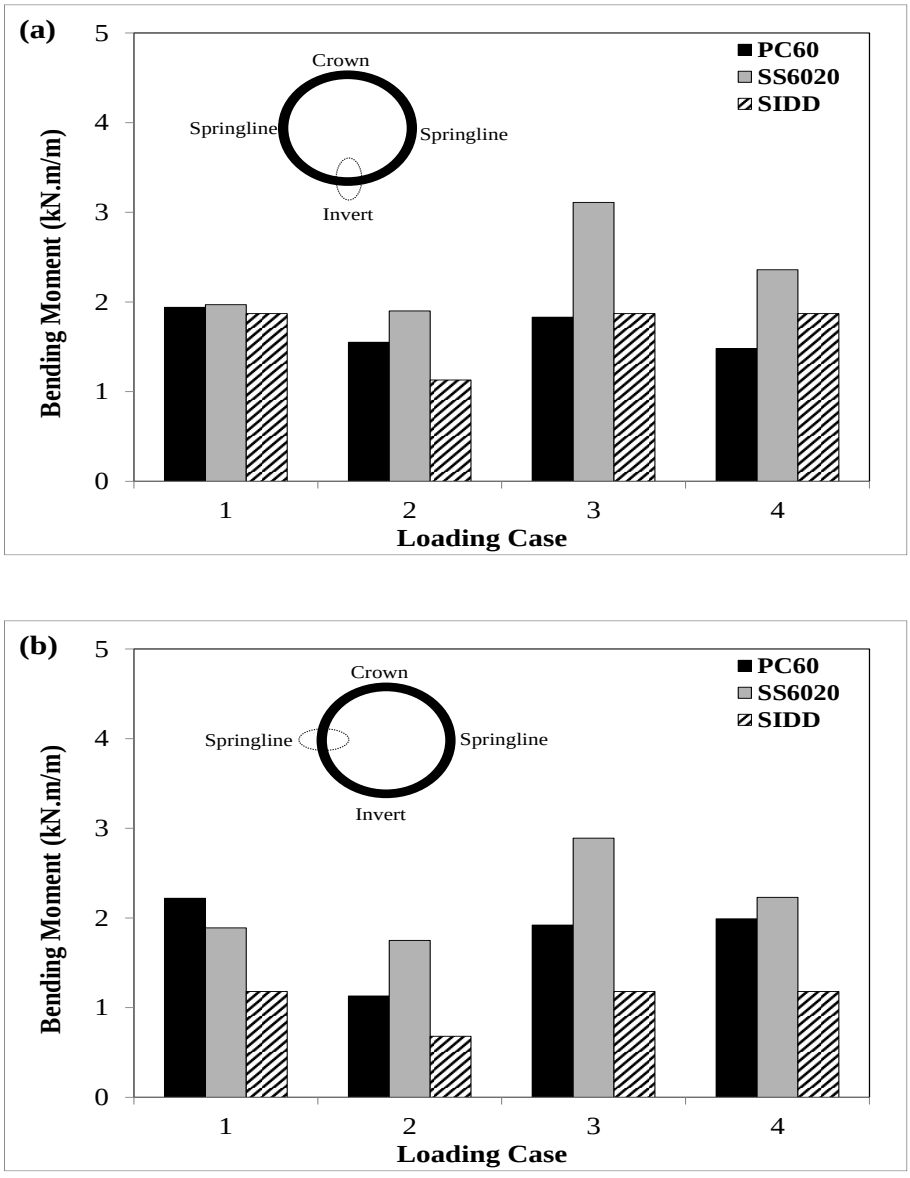

Figure 5-7 Experimental and theoretical SIDD bending moments for PC60 and SS6020 pipes at a) invert section b) spring-line section.

Furthermore, **Fig. 5-7** shows theoretical bending moments (M_{SIDD}) calculated using standard installations direct design method (SIDD) procedures. M_{SIDD} was calculated using **Eq. 5-2** (ACPA, 2001):

$$M_{SIDD} = \frac{D_m}{2} (C_{mp}\, W_p + C_{ml}\, W_l) \qquad \textbf{Eq. 5-2}$$

where M_{SIDD} is the theoretical bending moment according to the Standard Installations Direct Design method (SIDD) (kN.m/m), D_m is the mean pipe diameter (m), W_p is the pipe's weight (kN/m), W_l is the live load (kN/m), C_{mp} and C_{ml} are non-dimensional coefficients for calculating the bending moment.

The same load spreading assumptions and calculating procedures provided by ACPA (1993), which are consistent with the Canadian Highway Bridge Design Code (CHBDC) (CSA, 2006), were adopted in this study. **Table 5-4** summarizes values of parameters used to calculate SIDD bending moments. Detailed calculations of M_{SIDD} are given in Appendix A. The difference between the measured M_{exp} at critical sections and the theoretical M_{SIDD} values ranged from -20% to 157%. This range is similar to that published in the literature on regularly reinforced concrete pipes installed according to SIDD installations (Sargand *et al.*, 1995; Smeltzerl and Daigle, 2005; and Lay and Brachman, 2014). These findings confirm that the SIDD method provides reasonable approximation for bending moments acting on a buried SFRC pipe's wall before cracking.

At the end of this phase, it was concluded that, similar to the PC pipe, the SFRC pipe (fabricated with the least content of steel fibres, i.e. 20 kg/m³) can sustain a fully loaded CL 625 standard Ontario truck without any cracking or significant deformation. Thus, in order to investigate the efficiency of steel fibres in the post-cracking regime, pipes in the second phase were pre-cracked in the laboratory under the TEBT, prior to installation and testing in the field.

Table 5-4 Values of parameters used to calculate bending moments according to SIDD method

Parameter	Value
Installation type	IV
Inside diameter (D_i)	0.6 m
Mean diameter (D_m)	0.694 m
Outside diameter (D_o)	0.8 m
Wall thickness (h)	0.094 m
Concrete density (ρ)	2400 kg/m³
Backfill height (H)	0.6 m = 1.0 D_i
Moment coefficient (C_{mi})	
at Invert: C_{mp}	0.235
C_{mL}	0.211
at Spring-line: C_{mp}	-0.101
C_{mL}	-0.145
Length of tire contact area (L)	0.2 m
Width of tire contact area (W)	0.5 m
Length of distributed earth pressure area at the crown level (AL_1)	1.25 m
Width of distributed earth pressure area at the 0.75 D_o level (AL_2)	2.61 m
Impact factor (I_f)	1.2
Wheel load (P):	
Load case # 1:	68.5 kN
Load case # 2:	34.25 kN
Load case # 3:	68.5 kN
Load case # 4:	68.5 kN

5.3.2 Second Experimental Phase

5.3.2.1 TEBT load-deflection curves

In order to investigate the actual field behaviour of SFRC pipes in the post-cracking stage, these pipes were preloaded to their ultimate load capacity (P_{ult}). The regularly reinforced concrete pipe RC60 was also pre-cracked in the laboratory prior to field-testing. **Figure 5-8** shows the load deformation curves (in terms of D-loads) for SFRC pipes at the preliminary cracking stage. Regardless of the pipe type, no cracks were observed at the critical sections

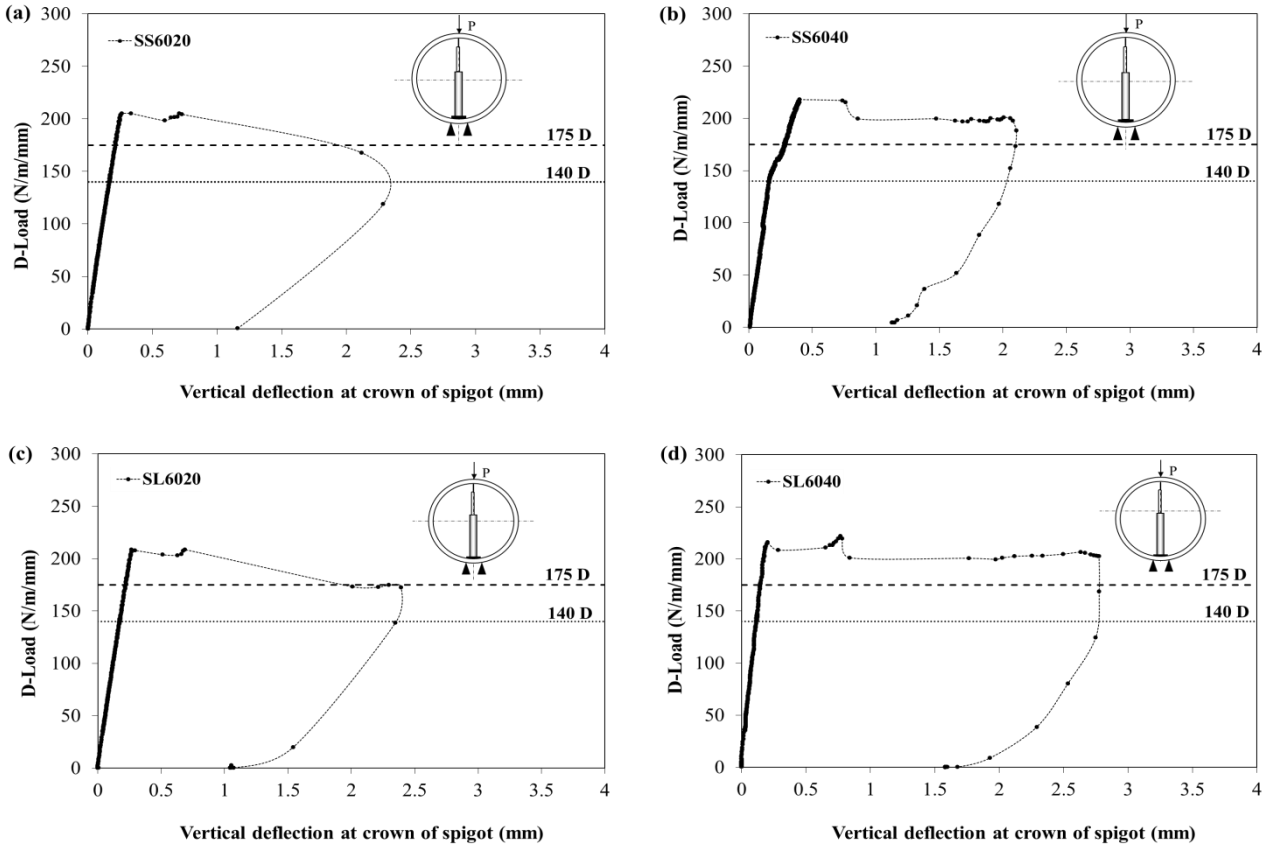

Figure 5-8 Load-deformation curves for SFRC pipes at the preliminary cracking stage.

(invert, crown, and the spring-lines) when the load was held at the 140D limit (208 kN for 600 mm diameter Class V pipe according to ASTM C76) for one minute. The first crack load (P_{cr}) was 298 kN (D-load = 200 N/m/mm) for the SS6020 pipe. A slight increase in P_{cr} was observed with increasing fibre content or using longer fibres. For instance, P_{cr} increased to 304 kN (D-load = 208 N/m/mm) and 302 kN (D-load = 206 N/m/mm) when the fibre content was increased to 40 kg/m³ (pipe SS6040), and the long fibres were used (SL6020), respectively. Similarly, the achieved ultimate load increased as the fibre content increased. For instance, the ultimate load increased from 305 kN (D-load = 208 N/m/mm) to 325 kN (D-load = 222 N/m/mm) when the fibre content was increased from 20 to 40 kg/m³ of Dramix 80/60 fibres. All SFRC pipes achieved ultimate D-loads higher than 175 N/m/mm (i.e. 258 kN for 600 mm diameter Class V pipe according to ASTM C76).

Figure 5-9 shows the load deformation curve for the RC60 pipe during the preliminary cracking stage. The first crack load (i.e. P_{cr} = 193 kN or D-load = 132 N/m/mm) was significantly lower than that of SFRC pipes (298 kN). This can be attributed to the absence of steel fibres. Steel fibres in the matrix would intersect, block and arrest the propagation of cracks leading to higher cracking loads and a better overall structural performance (Song and Hwang, 2004). **Table 5-5** summarizes the achieved ultimate loads for all of the tested pipes. The achieved ultimate load for the RC60 pipe (i.e. P_{ult} = 292 kN or D-load = 200 N/m/mm) was comparable to that reported for SFRC pipes (average variation = 4.88%); however, it was achieved at a higher deformation in the case of the RC60 pipe (i.e. 9.0 mm) when the steel reinforcement started to yield.

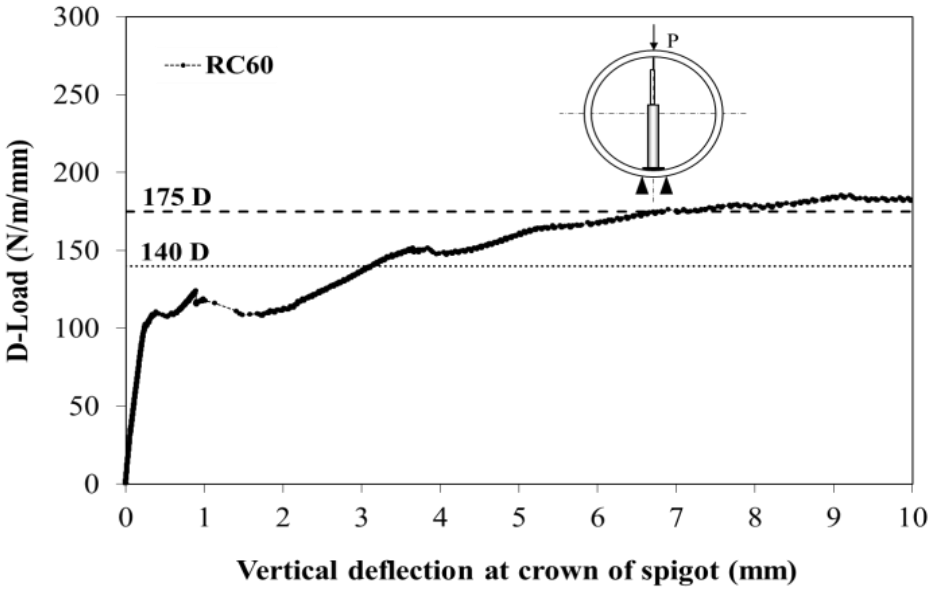

Figure 5-9 Load-deformation curve for the RC60 pipe at the preliminary cracking stage.

Table 5-5 P_{cr} and P_{ult} for pipes under investigation in the second experimental phase

Pipe	Reinforcement	P_{cr} (kN)	P_{ult} (kN)
PC60	Plain	—	—
RC60	Regular Reinforcement	193	292
SS6020	Dramix RC-65/35-CN (short fibres)	298	300
SS6040		304	319
SL6020	Dramix RC-80/60-CN (long fibres)	302	305
SL6040		314	325

5.3.2.2 Initial earth pressure measurements

In this study, pipe installations were adapted from the Standard Installation Direct Design SIDD method. This method is based on the Heger's earth pressure distribution as illustrated earlier (**Fig. 2-4**). **Tables 5-6** to **5-8** show the measured and estimated earth pressure at the pipe's invert, crown and spring-line, respectively. The estimated earth pressures were based on Heger's distribution and the calculation of the prism load (*PL*) at the top of the pipe. The prism load *PL* was calculated using the following equation **Eq. 5-3** (ASCE 15-98, 2000):

$$PL = (\gamma D_o)\,[H + 0.107\,D_o] \qquad \textbf{Eq. 5-3}$$

where *PL* is the prism load (N/m), γ is the unit weight of soil (N/m³), D_o is the outside diameter of the pipe (m), and *H* is the height of earth above the top of the pipe (m). An example of the calculated Heger's earth pressures is given in Appendix B.

Based on the results reported in **Tables 5-6** to **5-8**, it can be observed that the PC60 pipe was the only pipe that was installed in the un-cracked condition, thus it represents a true rigid pipe case. The percentage difference between the measured and estimated stresses was around 26%, -73%, and 272% at the pipe invert, crown, and spring-lines, respectively.

Hence, it can be concluded that the SIDD method provides a reasonable estimation for the vertical stress at the pipe's invert. However, the SIDD method overestimated the vertical stress at the pipe crown and underestimated the horizontal stress at the pipe spring-line level. This is in agreement with previous work (Wong *et al*., 2006).

Moreover, for the RC60 and SFRC pipes, the SIDD method overestimated the vertical stresses at the pipe's invert by about -40% to -87% (average of -64%). This can be attributed to the fact that the RC60 pipe and the SFRC pipes were tested in the cracked condition; hence, their behaviour can be approximated as semi-rigid pipes rather than rigid pipes. Therefore, stresses were dissipated in the pipe ring deformation and crack width increase rather than being transformed in the form of higher stresses in the soil around the pipe.

Table 5-6 Measured and estimated earth pressure at pipe invert

pipe	Installation type	Height (m)	Earth Pressure at Invert σ_{inv} (kPa)		
			measured	estimated	% Diff.
PC60	IV	0.9	177.20	140.71	25.93
RC60	IV	0.9	28.07	140.71	-80.05
SS6020	III	1.1	19.81	155.59	-87.27
SS6040	III	1.1	63.58	155.59	-59.14
SL6020	IV	0.6	43.87	97.95	-55.21
SL6040	IV	0.6	59.21	97.95	-39.55

Table 5-7 Measured and estimated earth pressure at pipe crown

pipe	Installation type	Height (m)	Earth Pressure at Crown σ_{crn} (kPa)		
			measured	estimated	% Diff.
PC60	IV	0.9	12.00	44.55	-73.06
RC60	IV	0.9	6.77	44.55	-84.80
SS6020	III	1.1	13.00	52.96	-75.45
SS6040	III	1.1	4.53	52.96	-91.45
SL6020	IV	0.6	7.21	31.01	-76.75
SL6040	IV	0.6	6.40	31.01	-79.36

Table 5-8 Measured and estimated earth pressure at pipe spring-lines

pipe	Installation type	Height (m)	Earth Pressure at Springs σ_{spg} (kPa)		
			measured	estimated	% Diff.
PC60	IV	0.9	7.11	1.91	272.25
RC60	IV	0.9	4.09	1.91	114.14
SS6020	III	1.1	5.00	3.47	44.09
SS6040	III	1.1	2.96	3.47	-14.70
SL6020	IV	0.6	4.05	1.33	204.51
SL6040	IV	0.6	6.63	1.33	398.50

Likewise, vertical stresses at the pipe's crown (σ_{crn}) were overestimated for all the cracked pipes under investigation. The difference ranged between -75% and -91% (average of -82%). The difference of σ_{crn} in the case of the PC60 pipe was in the same range (-73%). This indicates that the vertical stress at the pipe's crown σ_{crn} was not affected by the pipe condition. This can be attributed to the fact that σ_{crn} was measured at a level above the pipe itself, hence it was not affected by the pipe ability to deform.

Furthermore, the horizontal stresses at the pipe's spring-line level σ_{spg} were underestimated for all the cracked pipes under investigation (except for pipe SS6040). The difference ranged between 44% and 398% (an average of 169%). This can be attributed to the increased lateral support offered by the soil surrounding the pipe when the horizontal deformation of the pipe is allowed (i.e. semi-rigid pipe).

5.3.2.3 Soil-pipe response during loading

As mentioned earlier, each loading step represented an incremental load increase or decrease of 75 kN. Loading was stopped after five loading steps. At that stage, soil failure was identified by significant cracking and settlement around the loading area. Afterwards, unloading began while recording stresses and displacements at each loading step.

Figures 5-10 to **5-15** show the measured soil stresses (σ_{crn}, σ_{inv}, and σ_{spg}) around the tested pipes. **Figures 5-10a** to **5-15a** show soil stresses before loading, at the maximum load, and after fully unloading for the PC60, RC60, SL6020, SL6040, SS6020, and SS6040 pipes, respectively. Combined soil-pipe responses are presented as the change in σ_{inv} and in vertical displacement at the pipe crown (ΔD_v) as shown in **Figs. 5-10b** to **5-15b**. All stresses (σ_{crn}, σ_{inv}, and σ_{spg}) increased as the applied load increased and decreased with unloading. The highest reading was recorded at maximum load. Stress values varied depending on the pipe condition (cracked or un-cracked), type of reinforcement (regular reinforcement or steel fibres), type and dosage of steel fibres, and type of installation (Type IV or III). For instance, at maximum load, the highest σ_{inv} value was recorded for the un-cracked pipe (PC60) (i.e. 315 kPa) compared to only 58 kPa for the cracked RC60 pipe. For cracked SFRC pipes, σ_{inv} ranged from 43 to 198 kPa. Similarly, for all pipes, ΔD_v increased as the applied load was increased and vice versa.

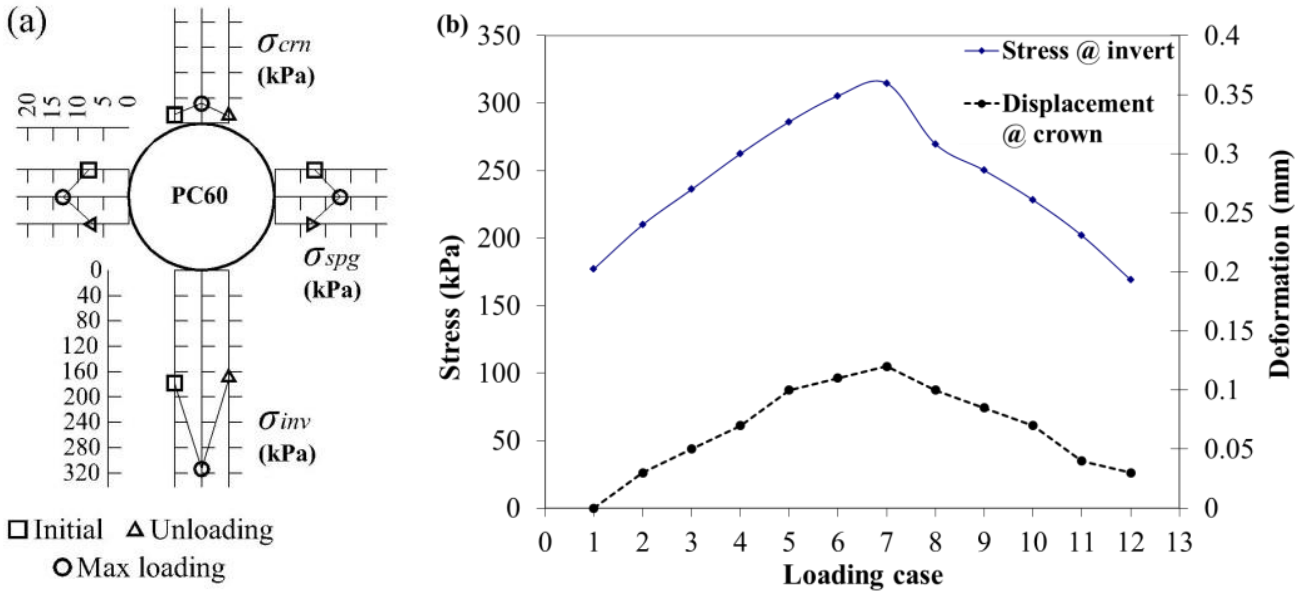

Figure 5-10 PC60 pipe (a) measured soil stresses around the pipe, and (b) Soil- pipe response during loading and unloading.

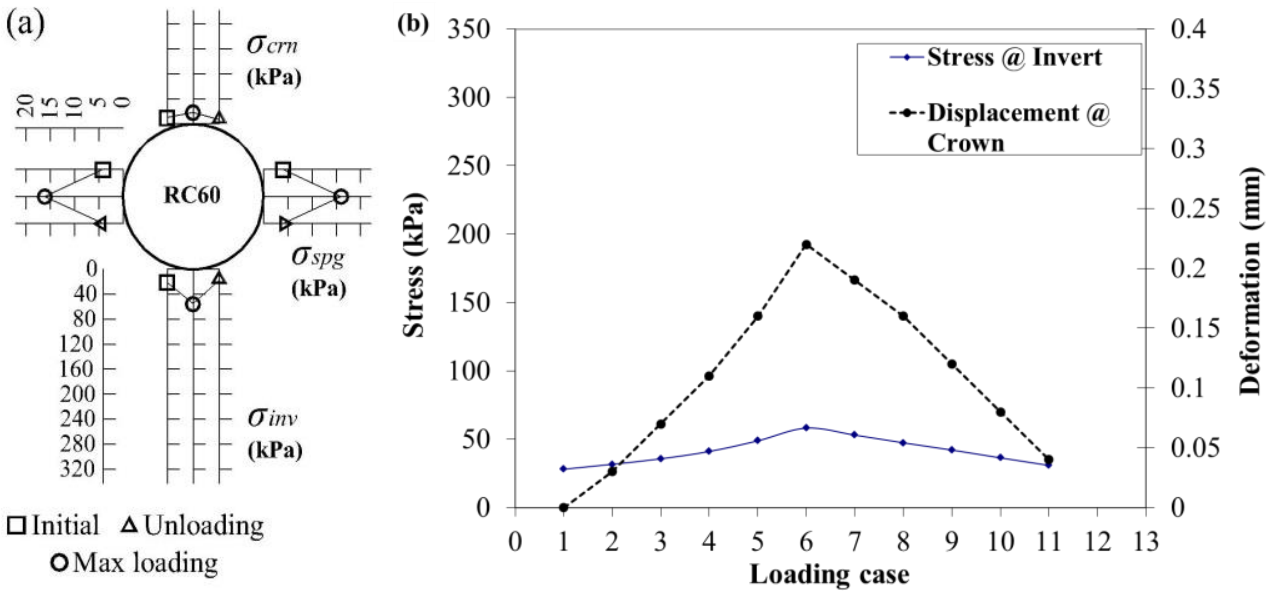

Figure 5-11 RC60 pipe (a) measured soil stresses around the pipe, and (b) Soil- pipe response during loading and unloading.

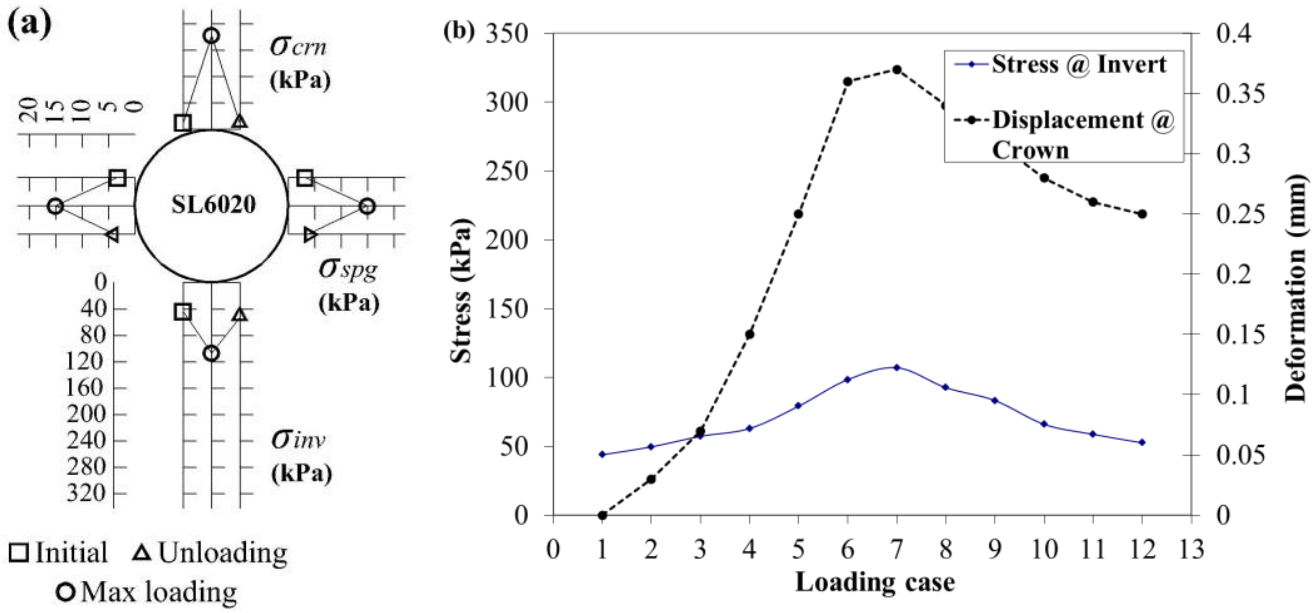

Figure 5-12 SL6020 pipe (a) measured soil stresses around the pipe, and (b) Soil- pipe response during loading and unloading.

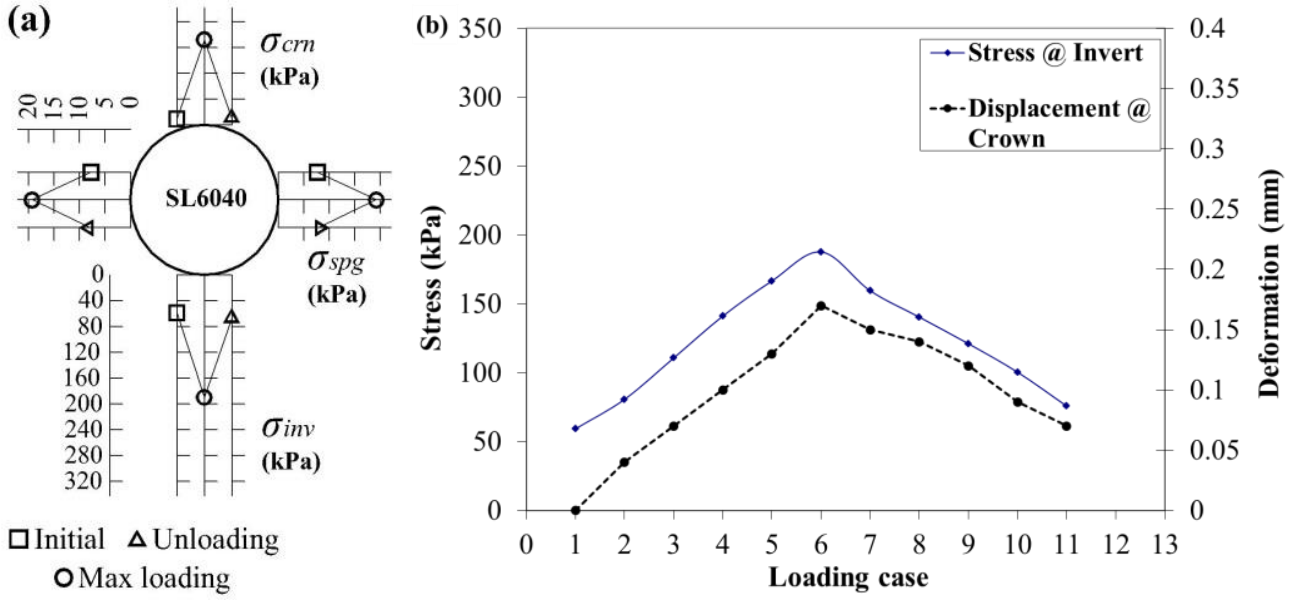

Figure 5-13 SL6040 pipe (a) measured soil stresses around the pipe, and (b) Soil- pipe response during loading and unloading.

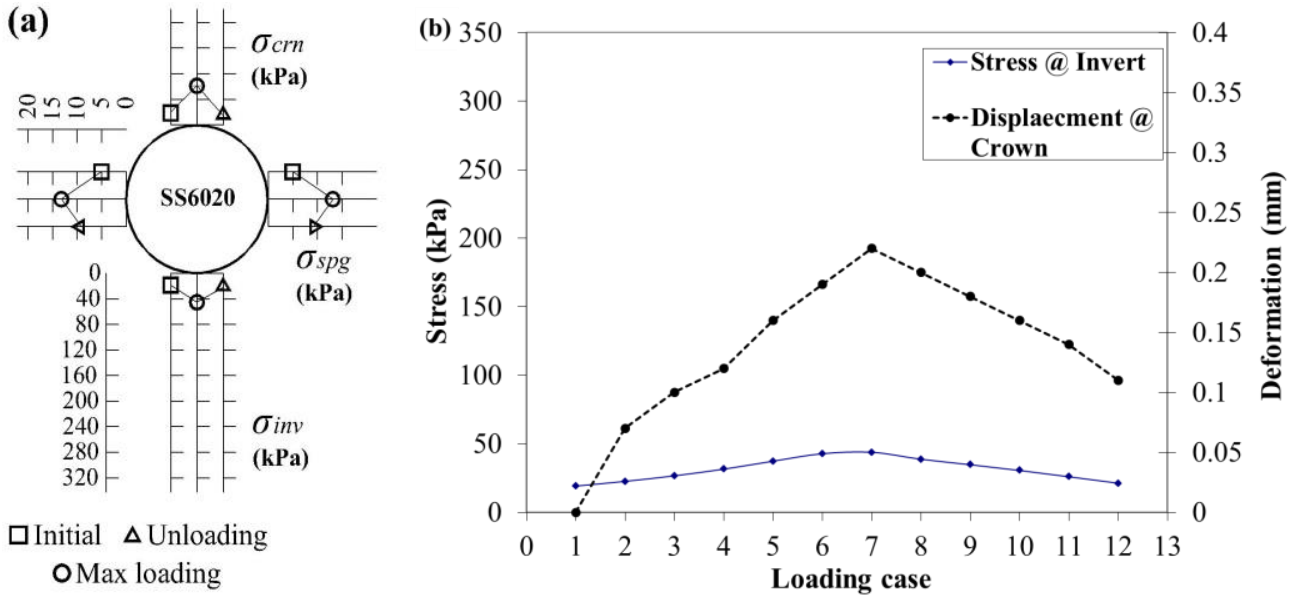

Figure 5-14 SS6020 pipe (a) measured soil stresses around the pipe, and (b) Soil- pipe response during loading and unloading.

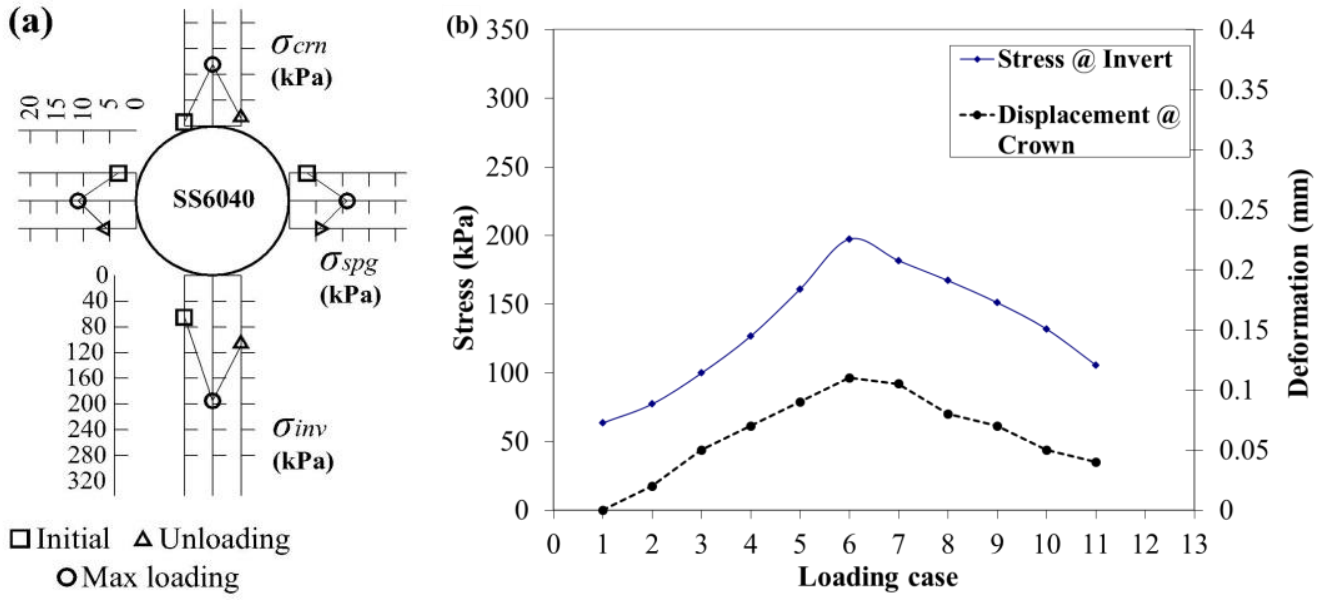

Figure 5-15 SS6040 pipe (a) measured soil stresses around the pipe, and (b) Soil- pipe response during loading and unloading.

5.3.2.3.1 Effect of pipe condition

The RC60 pipe exhibited significant reduction in the measured σ_{inv} (-80%) accompanied by an increase in the ΔD_v (83%) (**Fig. 5-11**) compared to that of the PC60 pipe (**Fig. 5-10**). This can be attributed to the reduction in rigidity of the RC60 pipe due to the pre-test cracking, allowing the dissipation of stresses in the pipe ring deformation and crack width increase, rather than being stored in the form of higher stresses in the soil around the pipe. This led to a higher horizontal support from the surrounding soil in the case of the RC60 pipe. This was evident in the 74% increase of σ_{spg} for the RC60 pipe at the maximum load was (from 4 to 15.5 kPa), while this increase was only 46% for the PC60 pipe (from 7.1 to 13 kPa) at maximum loading. It is worth mentioning that visual inspection of the PC60 pipe after extraction did not indicate any presence of cracks at critical sections.

5.3.2.3.2 Effect of reinforcement type

The advantage of SFRC pipes over RC pipes can be illustrated by comparing **Fig. 5-11** (RC60 pipe) and **Fig. 5-13** (SL6040 pipe). Lower pipe deformations accompanied by higher

stresses at the invert were reported for the SL6040 pipe compared to that of the RC60 pipe. For instance, the measured σ_{inv} and ΔD_v for the RC60 and SL6040 pipes at maximum load were 58.13 kPa and 0.22 mm, and 187 kPa and 0.17 mm, respectively. This can be attributed to the presence of steel fibres in the concrete matrix. Steel fibres restrained the opening and growth of pre-made cracks as the load increased since they are mobilized once cracks are initiated. On the other hand, regular reinforcement would be mobilized only when cracks reach to the reinforcement level. Therefore, lower deformations were measured in the case of the SL6040 pipe compared to that of the RC60 pipe.

5.3.2.3.3 Effect of fibre dosage

Figures 5-12 and **5-13** show the effect of increasing the fibre dosage on the soil-pipe response of SFRC pipes. The measured σ_{inv} and ΔD_v for the SL6020 and SL6040 pipes at the maximum load were 107.11 kPa and 0.37 mm, and 187 kPa and 0.17 mm, respectively. Higher fibre dosage led to a lower pipe deformation. Consequently, the measured stresses at the invert increased as the fibre dosage increased. A similar trend can be observed by comparing **Figs. 5-14** and **5-15**. The measured σ_{inv} and ΔD_v for the SS6020 and SS6040 pipes at maximum load were 43.85 kPa and 0.22 mm, and 197.5 kPa and 0.11 mm, respectively. This observation suggests that, for pipes of this size (D_i = 600 mm), a fibre dosage of 20 kg/m^3 may be insufficient to achieve a desirable post-cracking behaviour.

5.3.2.3.4 Effect of installation type

Pipes installed in Type III installation (pipes SS6020 and SS6040) were fabricated using a different type of steel fibres than those installed in Type IV installation (pipes SL6020 and SL6040) (see **Table 5-2**). Hence, it is difficult to directly investigate the effect of the installation type on the soil-pipe interaction. Thus, the improvement in the pipe stiffness (i.e. applied load/ pipe deformation) offered by the bedding installation, over the pipe stiffness obtained from the TEBT was compared instead. **Figure 5-16** shows the pipe stiffness obtained from the second cycle of the TEBT performed on replicates of SL6040 (**Fig. 5-16a**) and SS6040 (**Fig. 5-16b**) pipes as well as the pipe stiffness obtained from field loading.

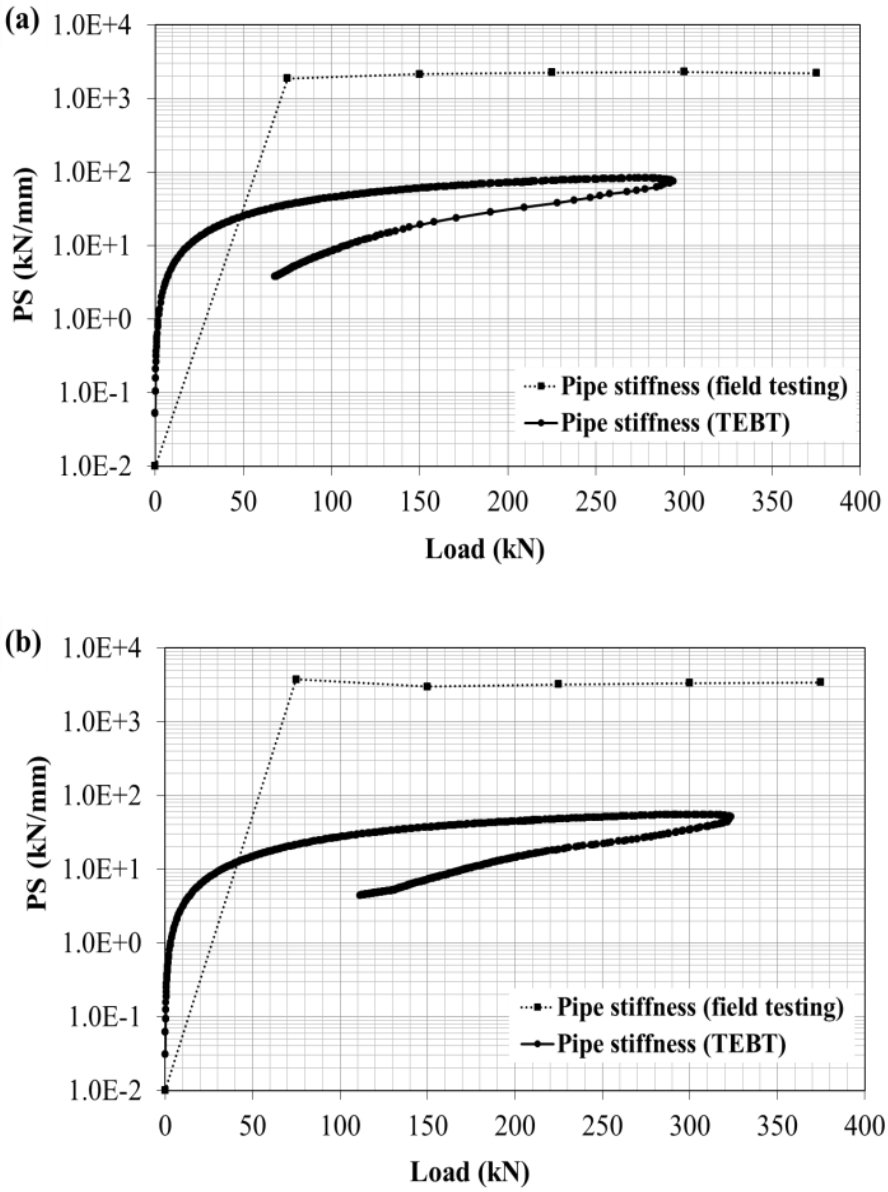

Figure 5-16 Pipe stiffness (PS) obtained from the second cycle of the TEBT and from field testing for (a) SL6040 pipe and (b) SS6040 pipe.

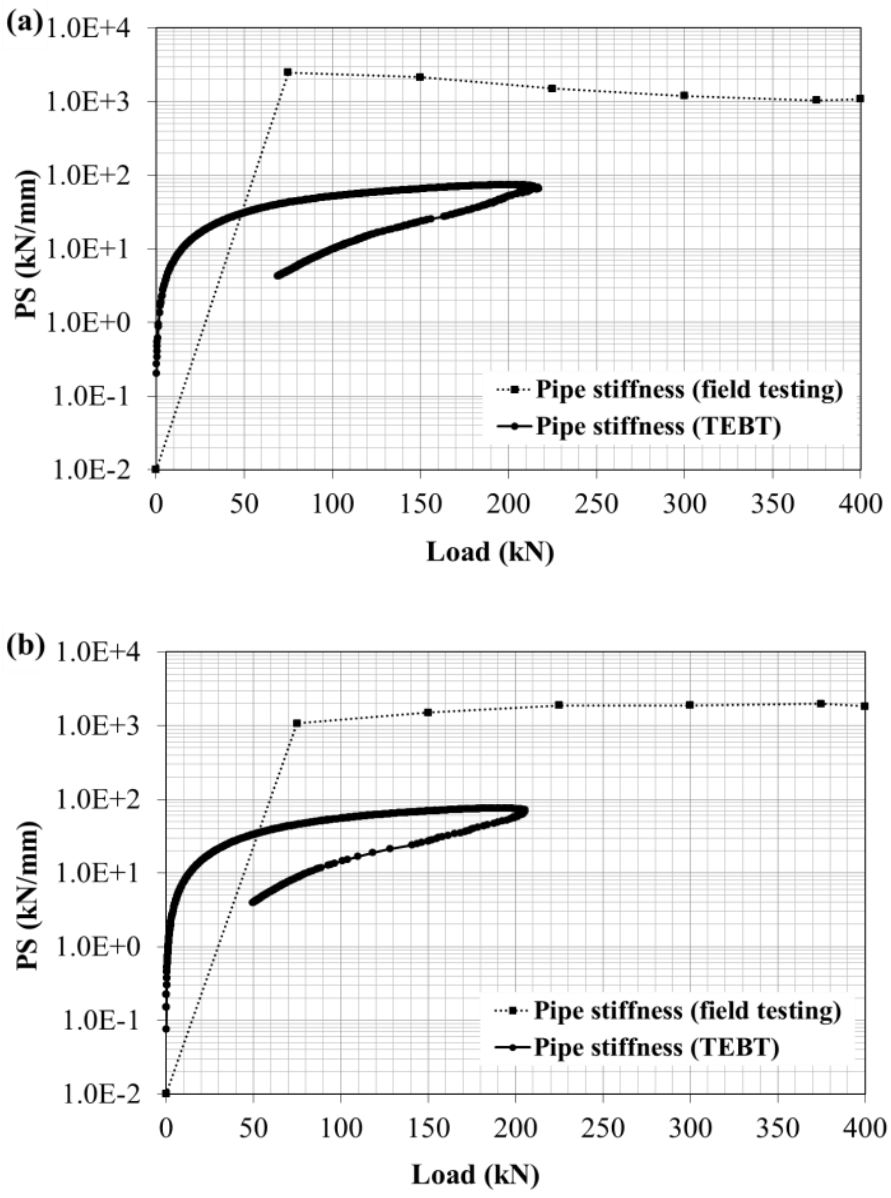

Figure 5-17 Pipe stiffness (PS) obtained from the second cycle of the TEBT and from field testing for (a) SL6020 pipe and (b) SS6020 pipe.

For the SL6040 pipe, the stiffness increased from 0.09 x 10^3 to 2.0 x 10^3 kN/mm due to the support offered by Type IV installation. For the SS6040 pipe, stiffness increased from 0.05 x 10^3 to 3.0 x 10^3 kN/mm due to the support offered by Type III installation. The SS6040 pipe exhibited higher stiffness than that of the SL6020 pipe, despite having lower stiffness in the TEBT. This can be attributed to the better support provided by Type III installation over that

of Type IV installation, since it employs a better quality bedding material. This was implied since the increase in σ_{spg} for the SS6040 pipe at the maximum load was 72% (from 2.96 to 10.57 kPa), while it was 64% for the SL6040 pipe (from 6.63 to 18.57 kPa). Similarly, Type III installation offered greater support to the SS6020 pipe (stiffness increase by 1.925 x 10^3 kN/mm), than did Type IV installation for the SL6020 pipe (stiffness increase by 0.925 x 10^3 kN/mm) (**Fig. 5-17**). From **Figs. 5-16** and **5-17**, it seems that most SFRC pipes exhibited a constant stiffness regardless of the load increase, with the exception of the SL6020 pipe, whose stiffness decreased as the loading increased. This is due to the lower fibre dosage used in this pipe as well as the lack of support from the installation (Type IV).

5.4 SUMMARY AND CONCLUSIONS

This chapter explored the behaviour of full-scale SFRC pipes when buried in soil and subjected to live loads. The main interest was the earth pressure around the pipe and the pipe diametrical deformations. Two experimental phases were conducted. A revised strategy was used in the second phase by employing heavier live loads and installing SFRC pipes that were intentionally pre-cracked in the laboratory. From this full-scale pipe field-testing program, the following conclusions can be drawn:

1. The current design recommendations for the pipe wall thickness in ASTM C76 (Type C wall) are overly conservative, since no sign of cracks or reduced stiffness was detected in the plain concrete pipe (or the SFRC pipe) installed in a shallow Type IV installation (the least quality installation Type) and subjected to a fully loaded CL 625 Ontario standard truck.
2. The SIDD method provides reasonable estimation of the vertical stresses at the pipe invert. However, it overestimates the vertical stress at the pipe crown and underestimates the lateral support provided by the haunch and lower side represented by the horizontal stress at the pipe spring-line level.
3. Vertical stresses at the pipe invert were reduced significantly when the pipe ring is allowed to deform (due to pre-induced cracks in this study).
4. SFRC pipes fabricated with 40 kg/m^3 of Dramix 80/60 fibres exhibited lower deformations than that of the conventional control RC pipe.

5. The response of pre-cracked SFRC pipes is more sensitive to the installation type than to the fibre type. SFRC pipes fabricated with short steel fibres exhibited lower deformations and higher stiffness than that of SFRC pipes fabricated with long steel fibres when installed in a better installation type (Type III instead of Type IV).

5.5 REFERENCES

American Concrete Pipe Association (ACPA), *Concrete pipe technology handbook: a presentation of historical and current state-of-the-art design and installation methodology*, 3rd printing, American Concrete Pipe Association, Irving, Texas, 1993, 330 p.

American Concrete Pipe Association (ACPA), *Concrete pipe design manual*, 19th printing, American Concrete Pipe Association, Irving, Texas, 2007, 540 p.

ASCE 15-98, American Society of Civil Engineers, "Standard practice for direct design of buried precast concrete pipe using standard installations SIDD," American Society of Civil Engineers, Reston, Virginia, 2000, 50 p.

ASTM C76-13, "Standard specification for reinforced concrete culvert, storm drain, and sewer pipe," American Society for Testing and Materials, ASTM International, West Conshohocken, PA, 2013, 11 p.

ASTM C1765-13, "Standard specification for steel fibre reinforced concrete culvert, storm drain, and sewer pipe," American Society for Testing and Materials, ASTM International, West Conshohocken, PA, 2013, 6 p.

ASTM D698-12e1, "Standard test methods for laboratory compaction characteristics of soil using standard effort (12400 ft-lbf/ft^3 (600 kN-m/m^3))," American Society for Testing and Materials, ASTM International, West Conshohocken, PA, 2012, 13 p.

Canadian Standards Association (CSA), "Canadian highway bridge design code." CSA Standard CAN/CSA-S6-06. Canadian Standards Association, Mississauga, Ontario, 2006.

European Standards, EN 1916, "Concrete pipes and fittings, unreinforced, steel fibre and reinforced." European Committee for Standardization, 2002, 89 p.

Erdogmus, E., and Tadros, M., "Behavior and design of buried concrete pipes phase II- final report" Nebraska Department of Roads, Lincoln, Nebraska, 2009, 124 p.

Erdogmus, E., Skourup, B.N., and Tadros, M., "Recommendations for design of reinforced concrete pipe," Journal of Pipeline Systems Engineering and Practice, 1(1), 2010, pp. 25-32.

Gopalaratnam, V.S., and Shah, S.P., "Softening response of plain concrete in direct tension." *ACI Journal Proceedings*, 82(3), 1985, pp. 310-323.

Hill, J.J., Kurdziel, J.M., Nelson, C.R., Nystrom, J.A., and Sondag, M.S. "Minnesota department of transportation overload field tests of standard and standard installation direct design reinforced concrete pipe installations." *Transportation Research Record: Journal of the Transportation Research Board*, 1656(1), 1999, pp. 64-72.

Kaklauskas, G., and Ghaboussi, J., "Stress-strain relations for cracked tensile concrete from RC beam tests." *Journal of Structural Engineering*, 127(1), 2001, pp. 64-73.

Lay, G.R., and Brachman, R.W.I., "Full-scale physical testing of a buried reinforced concrete pipe under axle load." *Canadian Geotechnical Journal*, NRC Research Press, 51(1), 2014, pp. 394-408.

Maximos, H., Erdogmus, E., and Tadros, M., "Full scale test installation for reinforced concrete pipe," *Proceedings of Pipelines 2008: Pipeline Asset Management: Maximizing Performance of our Pipeline Infrastructure*, sponsored by ASCE, Atlanta, Georgia, 2008, pp. 1-10.

McGrath, T. J., Selig, E.T., and Webb, M.C., "Field test of concrete pipe performance during backfilling." *Concrete Pipe for the New Millennium, Kaspar, I., and Enyart, I. (ed.)*, American Society for Testing Materials, Special Technical Publications, ASTM SPT-1368, 2000, pp. 73-88.

Munro, S.M., Moore, I.D., and Brachman, R.W.I., "Laboratory testing to examine deformations and moments in fiber-reinforced cement pipe." *Journal of Geotechnical and Geoenvironmental Engineering*, 135(11), 2009, pp. 1722-1731.

Sargand, S.M., Hazen, G.A., Vaithianathan, E., and Hurd, J.O., "Performance verification of a concrete pipe." *Concrete International*, 17(7), 1995, pp. 23-27.

Smeltzer, P., and Daigle, L., "Field performance of a concrete pipe culvert installed using standard installations," *In Proceedings of the 33rd CSCE Annual Conference*, Toronto, Ontario, Canada, 2005, pp. GC 210:10-20.

Song, P.S. and Hwang, S., "Mechanical properties of high-strength steel fibre-reinforced concrete," *Construction and Building Materials Journal*, 18(9), 2004, pp. 669-673.

Wong, S., Allouche, E., Dhar, A., Baumert, M., and Moore, I., "Long-term monitoring of SIDD type IV installations." *Canadian Geotechnical Journal*, 43(4), 2006, pp. 392-408.

Zhao, J.Q., and Daigle, L., "SIDD pipe bedding and Ontario provincial standards," *In Proceedings of the International Conference on Underground Infrastructure Research*, Kitchener, Ontario, Canada: NRC Canada, 2001, pp. 143-152.

CHAPTER SIX

6 RATIONAL FINITE ELEMENT ASSISTED DESIGN OF PRECAST STEEL FIBRE REINFORCED CONCRETE PIPES[4]

6.1 INTRODUCTION

Recently, there has been growing interest in using steel fibres in precast concrete pipes as a replacement for regular steel rebar reinforcement. Over the last decade, several experimental studies (e.g. MacDonald and Trangsrud, 2004; Haktanir *et al.*, 2007; de la Fuente and de Figueiredo, 2011; de Figueiredo *et al.*, 2012- a, Abolmaali *et al.*, 2012; and Mohamed *et al.*, 2014) investigated the mechanical performance of precast SFRC pipes. Several parameters were explored, including the pipe internal diameter (D_i), wall thickness (h), fibre content (W_f), fibre type, and the targeted pipe ultimate strength. The main goal was to find the optimal fibre content for a specific pipe configuration (diameter/wall thickness) to achieve a certain strength class. This procedure is generally uneconomical and inefficient due to the variety of parameters that need to be accounted for (de Figueiredo *et al.*, 2012- b).

de Figueiredo *et al.* (2012-b) and de la Fuente *et al.* (2012) reported the development of a numerical model (MAP or Mechanical Analysis of Pipes) for the analysis and design of SFRC pipes. The MAP model is presumed to simulate the three-edge-bearing test that is

[4] A version of this chapter was submitted for publication to the *Engineering Structures Journal*.

widely used by the industry as a basis for the design check of concrete pipes. The main model hypotheses and basic governing equations were given in (de Figueiredo *et al*., 2012-b, and de la Fuente *et al*., 2012). However, final design equations were not provided in the related literature. Moreover, the model was validated using experimental data generated only by the same authors and did not include data from other sources.

This chapter aims at developing a 3D finite element model simulating the three-edge-bearing test (TEBT) of SFRC pipes. The model was validated using experimental data generated by the author, as well as other experimental results available in the open literature. Consequently, the validated model was used to conduct a parametric study capturing the following parameters: pipe diameter, pipe wall thickness, and fibre type and content. Finally, the findings of the parametric study were presented in a tabular form in order to facilitate the rational design process of SFRC pipes. The TEBT was described earlier in **Section 2.1.3.**. **Table 2-4** shows the pipe strength requirements for SFRC pipes according to ASTM C1765 (D_{test} and $D_{service}$).

6.2 FINITE ELEMENT MODELLING OF TEBT

A finite element analysis (FEA) using the commercially available software ABAQUS (Version 6.9) was performed in order to conduct the parametric study. A 3D model was constructed to simulate the TEBT. The model consists of the upper loading strip, lower supporting strips, and the concrete pipe. The upper and lower strips had dimensions of 50 x 50 mm. The lower bearing strips were 50 mm apart. The model's length was maintained at 1000 mm, while the pipe diameter and wall thickness varied depending on the case under investigation. The pipe was modeled using hexahedral (8-node) isoparametric linear solid elements with reduced integration and hourglass control. Three different element sizes were considered (50, 20, and 10 mm) for meshing the pipe. The predicted results were similar when the element size was 20 and 10 mm. However, the execution time of the 20 mm element size model was about 15% of that of the 10 mm element size model. Therefore the element size was maintained at 20 mm.

Figure 6-1 shows the 3D modelling of the TEBT. The upper and lower bearing strips were modeled as rigid elastic bodies. The two lower bearing strips served as supports to the system and were fixed at the bottom to prevent rotational or translational degrees of freedom. Displacement controlled loading was accomplished by applying a 20 mm downward displacement at the upper bearing strip. The interaction between the pipe barrel and the upper and lower strips was modeled using a simple tie constraint.

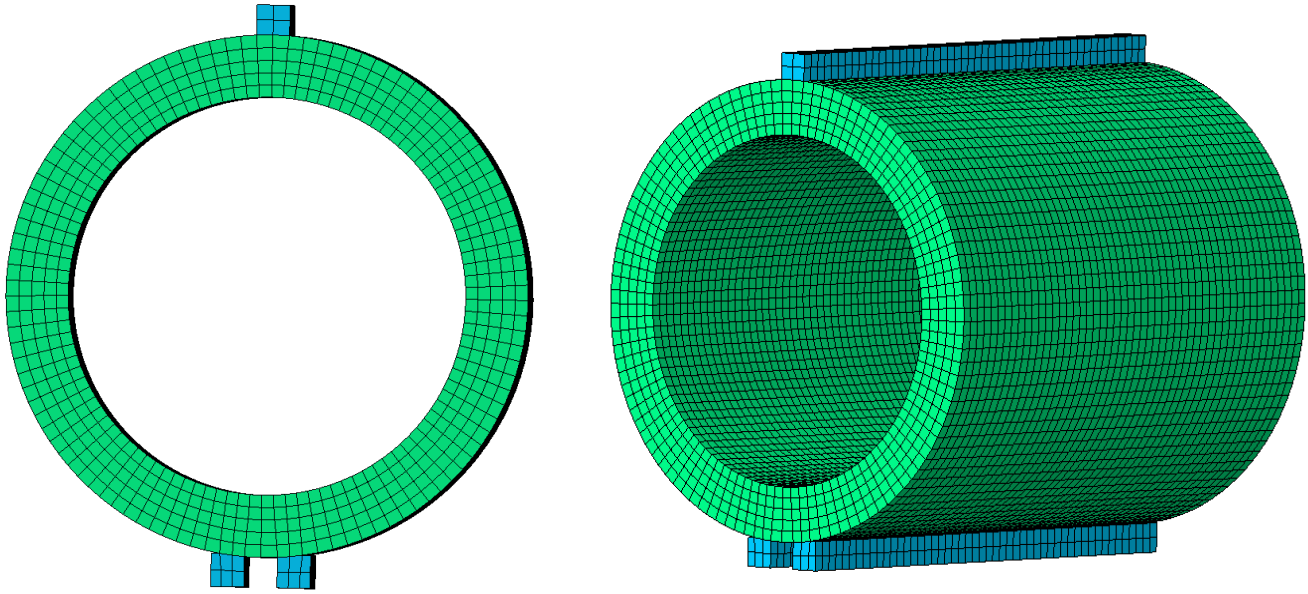

Figure 6-1 Finite element modelling of the three edge bearing test.

6.3 SFRC MODELLING: CONCRETE DAMAGED PLASTICITY MODEL

The constitutive behaviour of SFRC differs significantly from that of plain concrete, especially for tension stiffening. Steel fibres (SFs) enhance the post-cracking behaviour of hardened concrete through maintaining some of its load-carrying capacity after crack formation. Moreover, during fracture, energy is consumed in the de-bonding, pulling-out, and rupture of fibres, leading to higher concrete toughness (Bentur and Mindess, 2007). The

overall improvement in the engineering properties of concrete owing to SFs addition is a function of several variables, including the fibre shape, length, aspect ratio, volume fraction with respect to the total concrete volume, and the quality of the hosting matrix (Brandt, 2008). Thus, an accurate constitutive modelling of SFRC behaviour is essential for achieving a reliable FE model of SFRC pipes. Two concrete constitutive models are available in ABAQUS. These are the concrete smeared cracking (CSC) model and the concrete damaged plasticity (CDP) model.

The CSC model is used for modelling the concrete behaviour under monotonic loading and low confining pressure (less than four to five times the magnitude of the largest stress that can be carried by the concrete in uniaxial compression) and can be used to model plain and reinforced concrete (ABAQUS Analysis User's Manual, 2006). The model employs an isotropically hardening yield surface that is active when the stress is dominantly compressive and an independent "crack detection surface" that determines if a point fails by cracking. After failure, the behaviour across cracks is modeled using strain softening for cracked concrete (ABAQUS Analysis User's Manual, 2006). However, the CSC model is known to have difficulty converging after steel yielding (Ahn, 2011, and Chen and Graybeal, 2012). Since the main contribution of SF's lies in the post-cracking regime, it was decided to rather employ the CDP model.

The CDP model is generally used for modelling monotonic, cyclic, and/or dynamic loading under low confining pressure and can also be used to model plain and reinforced concrete (ABAQUS Analysis User's Manual, 2006). It assumes that the main two failure mechanisms are tensile cracking and compressive crushing of concrete. The evolution of the failure surface is controlled by the compressive plastic strain (ε_c^{pl}) and the tensile plastic strain (ε_t^{pl}). **Figure 6-2** shows the assumed uniaxial tension and compression stress-strain behaviour. The model follows a linear elastic relationship until the failure stress (σ_{to}) in the case of tension or the yielding stress (σ_{co}) in the case of compression. The tensile failure stress (σ_{to}) corresponds to the onset of micro-cracking in the concrete material, after which, progressive cracking is represented by a softening stress-strain response (**Fig. 6-2a**). In compression, the response in the plastic regime is characterized by stress hardening, followed by strain softening beyond the ultimate stress (σ_{cu}) (**Fig. 6-2b**).

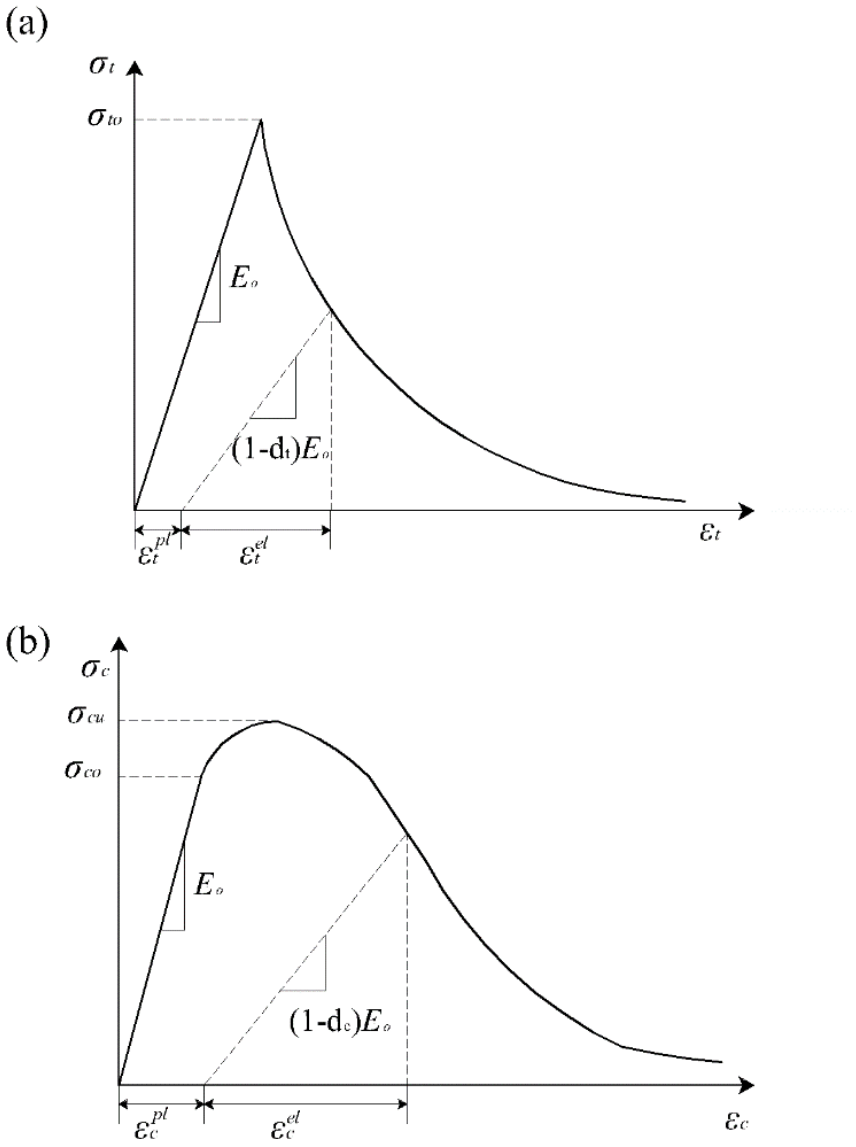

Figure 6-2 Response of concrete to uniaxial loading in (a) tension and (b) compression (ABAQUS Analysis User's Manual, 2006).

6.3.1 Defining Tensile and Compressive Behaviours

Tension stiffening can be defined by means of a post-cracking stress-strain relation. In this case, the post-cracking stress is given as a function of the cracking strain (ε_t^{ck}), where: $\varepsilon_t^{ck} = \varepsilon_t - \varepsilon_{to}^{el}$ and $\varepsilon_{to}^{el} = \sigma_t / E_o$ and E_o is the modulus of elasticity. Moreover, the tension stiffening can be defined by applying a fracture energy cracking criterion. In this case, the behaviour is

characterized by a stress-displacement response rather than a stress-strain response. Under tension, a concrete specimen will crack across its critical section. When the specimen has been pulled apart (sufficiently for most of the stress to be removed and the undamaged elastic strain becomes relatively small), its length will be determined primarily by the opening at the crack (ABAQUS Analysis User's Manual, 2006). The opening does not depend on the specimen's length. The fracture energy cracking criterion can be characterized by specifying the post-cracking stress as a function of cracking displacement (u_t^{ck}) (**Fig. 6-3**), where: $u_t^{ck} = 2G_f/\sigma_{to}$ and G_f is the fracture energy. Typical values of G_f range between 40-120 N/m for concrete with compressive strength between 20-40 MPa. This method was introduced by Hillerborg (1976), and since then it has been preferred for many practical purposes over the post-cracking stress-strain approach. This is because the latter will introduce unreasonable mesh sensitivity into the results in areas where reinforcement does not exist (i.e. SFRC member without steel reinforcement). Compressive behaviour in the plastic regime is specified as a stress-inelastic strain (ε_c^{in}) relation, where: $\varepsilon_c^{in} = \varepsilon_c - \varepsilon_{co}^{el}$ and $\varepsilon_{co}^{el} = \sigma_c / E_o$.

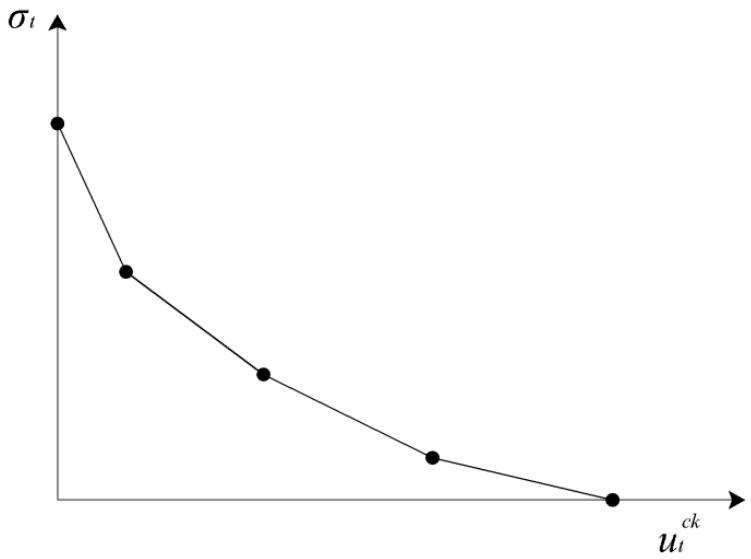

Figure 6-3 Post-cracking stress-displacement curve (ABAQUS Analysis User's Manual, 2006).

6.3.2 Defining Concrete Plasticity

In the CDP model, concrete plasticity is defined by assuming a non-associated potential plastic flow and a bi-linear yield surface as shown in **Fig. 6-4**. The CDP model employs the yield function of Lubliner *et al.* (1989), with some modifications introduced by Lee and Fenves (1998) to account for different evolution of strength under tension and compression (ABAQUS Analysis User's Manual, 2006). **Table 6-1** shows the parameters used in this study to define concrete plasticity in the CDP model. The dilatation angle (ψ) and eccentricity (m) control the plastic straining response of the material. The ratio σ_{co}/σ_{bo} and K_c determine the shape and size of the bi-linear yield surface (Blazejowski, 2012). Since the response of the structure (SFRC pipe) will be predominately uniaxial, it is not anticipated that there will be significant changes to the analyses by varying these parameters. Viscosity has been set to zero and this assumes that there are no strain rate effects. Values of parameters in **Table 6-2** were set similar to previous studies on SFRC (Ahn, 2011; Blazejowski, 2012; Chen and Graybeal, 2012; and Abbas, 2014). Definition of each of these parameters and further information regarding the plastic flow function (G) and yield surface function can be found in (ABAQUS User's Manual, 2006).

6.3.3 Modelling Compression Behaviour

Several analytical models that describe the compressive behaviour of SFRC concrete can be found in the literature (e.g. Soroushian and Lee, 1989; Ezeldin and Balaguru, 1992; Nataraja *et al.*, 1999; and Barros and Figueiras, 1999). Most of these models are based on equations similar to those of plain concrete. However, the compressive strength and the strain corresponding to the peak stress are evaluated empirically by adding a dimensionless factor to the peak stress and the corresponding strain of plain concrete. Bencardino *et al.* (2008) conducted a critical evaluation of these models using a large database of experimental results available in the literature. They found that these models agree well with the experimental data from which the model equations were derived. However, they do not show the same degree of agreement when applied to other published data (Bencardino *et al.*, 2008). Nevertheless, they reported that, in general, the stress- strain behaviour of SFRC could be

"reasonably" predicted by the model proposed by Barros and Figueiras (1999) (Bencardino *et al.*, 2008).

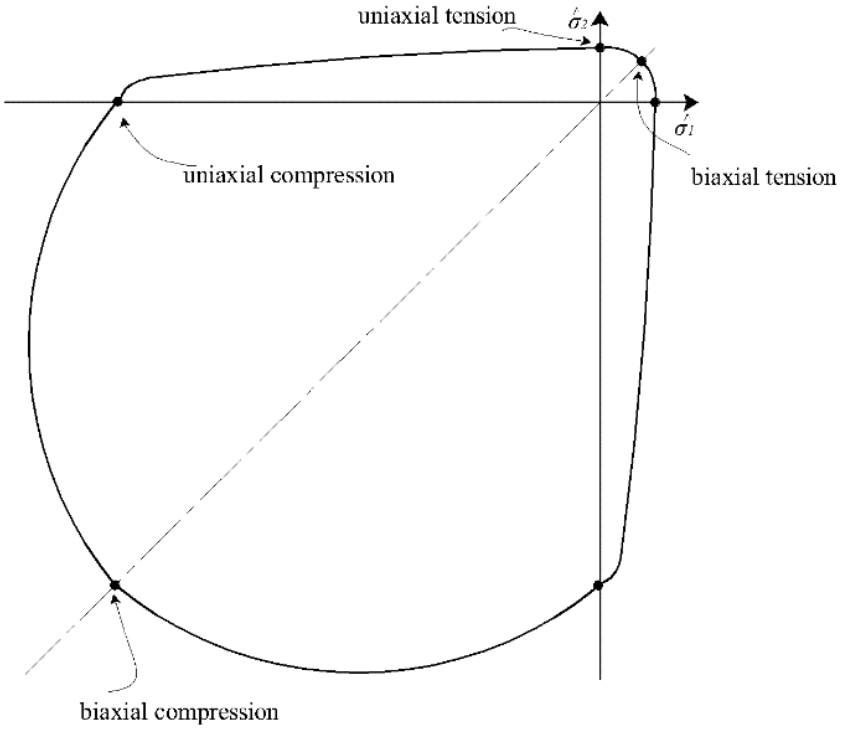

Figure 6-4 Plane stress yield surface of concrete in CDP model (ABAQUS Analysis User's Manual, 2006).

Table 6-1 CDP model plasticity parameters

CDP Parameter	Value
Dilation angle (ψ)	36.31°
Viscosity parameter (μ)	0
Eccentricity (m)	0.1
σ_{co}/σ_{bo}	1.16
K_c	0.67

Therefore, the model proposed by Barros and Figueiras (1999) was used herein to model the compression stress-strain behaviour of SFRC in this study. The model can be described using the following relationships:

$$\sigma = f_{cf} \frac{\frac{\varepsilon}{\varepsilon_{pf}}}{(1-p-q)+q\left(\frac{\varepsilon}{\varepsilon_{pf}}\right)+p\left(\frac{\varepsilon}{\varepsilon_{pf}}\right)^{\frac{(1-q)}{p}}} \quad \textbf{Eq. 6-1}$$

$$\text{with: } q = 1 - p - \frac{E_{pf}}{E_c},\ p + q \in]0,1[\text{ , and } \frac{1-q}{p} > 0 \quad \textbf{Eq. 6-2}$$

$$E_{pf} = \frac{f_{cf}}{\varepsilon_{pf}} \text{, and } E_c = 21.500 \sqrt[3]{\frac{f_{cf}}{10}} \quad \textbf{Eq. 6-3}$$

where: f_{cf} is the compression strength. For hooked-end fibres (l_f = 30 mm, d_f = 0.5 mm, l_f/d_f = 60):

$$\varepsilon_{pf} = \varepsilon_{co} + 0.0002\, W_f \quad \textbf{Eq. 6-4}$$

$$p = 1 - 0.919 e^{-0.394 W_f} \quad \textbf{Eq. 6-5}$$

For hooked-end fibres (l_f = 60 mm, d_f = 0.8 mm, l_f/d_f = 75):

$$\varepsilon_{pf} = \varepsilon_{co} + 0.00026\, W_f \quad \textbf{Eq. 6-6}$$

$$p = 1 - 0.722 e^{-0.144 W_f} \quad \textbf{Eq. 6-7}$$

where ε_{co} is the strain at peak stress for plain concrete (ε_{co} = 2.2 x 10^{-3} according to CEB-FIP Model Code 1990 (CEB-FIP, 1993)), ε_{pf} is the strain at peak stress, and W_f is the fibre weight percentage in the mixture. The model is valid for concrete with f_{cf} values ranging from 30 to 60 MPa and for W_f up to 3.33% (fibre content = 80 kg/ m³ or 1% by concrete volume). Steel fibres used in this study (l_f = 35 mm, d_f = 0.55 mm, l_f/d_f = 65 and l_f = 60 mm, d_f = 0.75 mm, l_f/d_f = 80) are very similar to those employed by Barros and Figueiras (1999). Thus, **Eqs. 6-4** to **6-7** used to determine ε_{pf} and p can be used to describe the compression stress-strain behaviour of SFRC incorporating various fibre contents. **Figure 6-5** shows the compression stress-strain curves used in the FEM in this study.

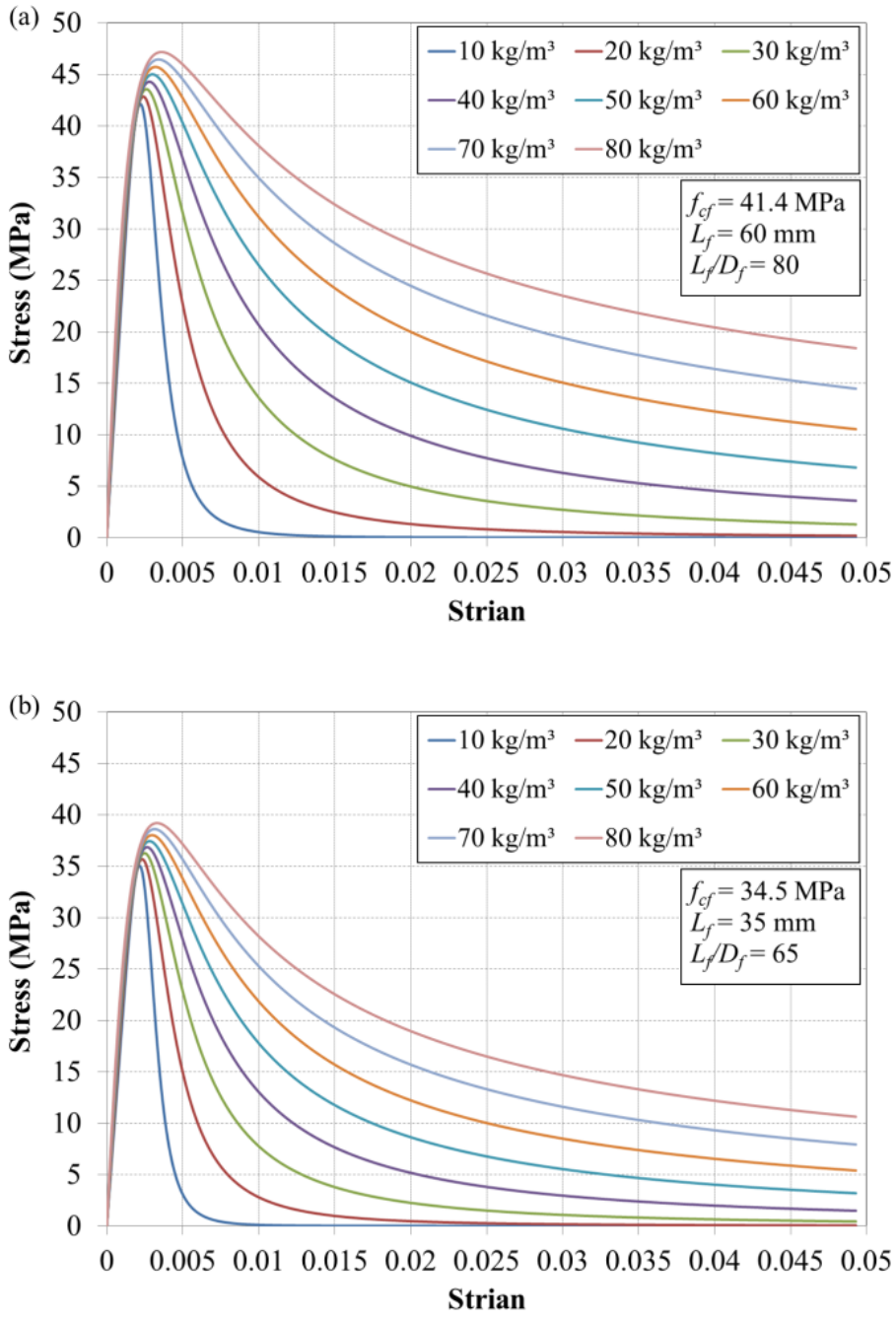

Figure 6-5 Compression stress-strain curves for SFRC used in the FEM.

6.3.4 Modelling Tensile Behaviour

In this study, the tensile behaviour of SFRC in the post-cracking regime was defined using the fracture energy-cracking criterion by providing the software with tensile stress-crack width displacement relations. The Variable Engagement Model (VEM) proposed by Voo and Foster (2003) was used to quantify the contribution of SF's to the tensile strength of SFRC as described below:

The strength of the composite (σ (w)) for a given crack opening displacement (COD) (w) is the summation of stress carried by the concrete at a given COD (σ_c(w)) including any beneficial coupling effect from the fibres on the matrix, and the stress carried by fibres (σ_f(w)) (**Eq. 6-8**). The contribution of the matrix is significant prior to cracking and fades in the post-cracking regime. **Figure 6-6** shows a scheme of this combined response. The tensile softening of plain concrete σ_c (w) can be taken as indicated in **Eq. 6-9** (Amin *et al.*, 2014):

$$\sigma(w) = \sigma_c(w) + \sigma_f(w) \qquad \textbf{Eq. 6-8}$$

$$\sigma_c(w) = c_1 f_{ct} e^{-c_2 w} \qquad \textbf{Eq. 6-9}$$

where f_{ct} is the tensile strength of concrete without fibres, c_1 is a coefficient for any beneficial effect of the fibres on the peak strength, and c_2 is a coefficient that controls the steepness of the descending branch, and is influenced by the volume of fibres and the cementitious matrix composition (Amin *et al.*, 2014). According to Voo and Foster (2004), Lee and Foster (2008), and Voo and Foster (2009) c_1 can be taken as unity for mode I fracture, while c_2 can be calculated using the formula proposed by Ng *et al.* (2012) for concretes with maximum size aggregate > 10 mm (cited in Amin *et al.*, 2014) (**Eq. 6-10**):

$$c_2 = \frac{20}{(1+100V_f)} \qquad \textbf{Eq. 6-10}$$

where V_f is the fibre content by volume. Tensile strength (f_{ct}) can be taken as 0.6 $\sqrt{f_{cf}}$ (Voo and Foster, 2003). The fibres' component σ_f(w) is calculated using **Eq. 6-11**:

$$\sigma_f(w) = \frac{1}{\pi} tan^{-1}(\frac{\alpha_e.w}{d_f})(1 - \frac{2.w}{l_f})^2.\frac{l_f}{d_f}.V_f.\tau_b \qquad \textbf{Eq. 6-11}$$

where α_e is the fibre engagement parameter, with a recommend value of 3.5 for hooked end fibres (Voo and Foster, 2003), τ_b is the mean shear stress between the fibre and the matrix measured. τ_b can be taken as $0.8\sqrt{f_{cf}}$ for normal-strength concrete (Gouveia *et al.*, 2014). **Figure 6-7** shows the tension stress- crack opening curves used in the FEM in this study.

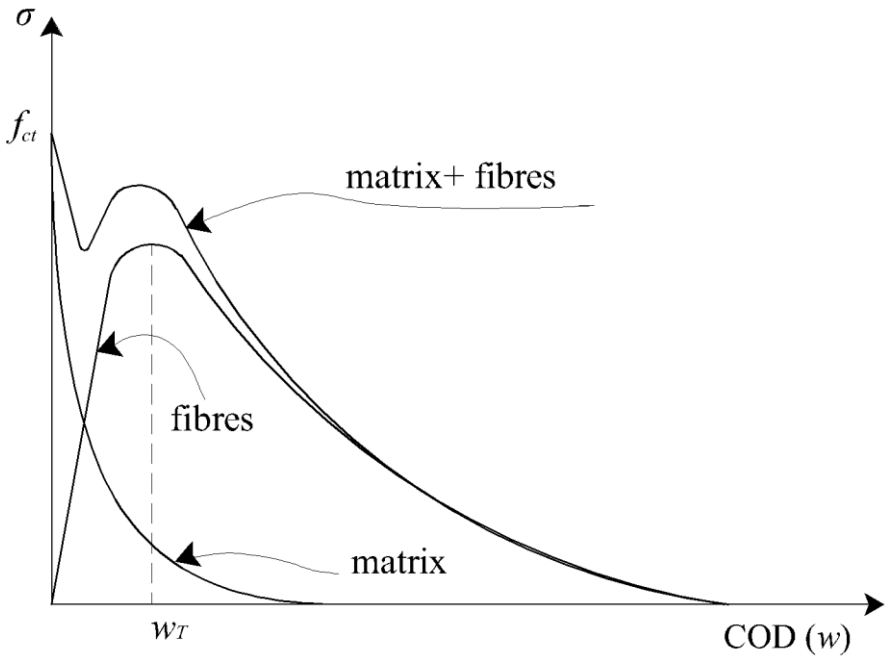

Figure 6-6 Tensile stress versus the COD for SFRC.

6.3.5 Elastic Properties

As mentioned earlier, the concrete modulus of elasticity (E_c) was defined using **Eq. 6-3**. The concrete's Poisson's ratio (υ) and density (ρ) were taken as 0.20 and 2400 kg/m³,

respectively. Both loading and supporting strips were modeled to exhibit a rigid behaviour using an enlarged modulus of elasticity. Their Poisson's ratio was set to 0.3.

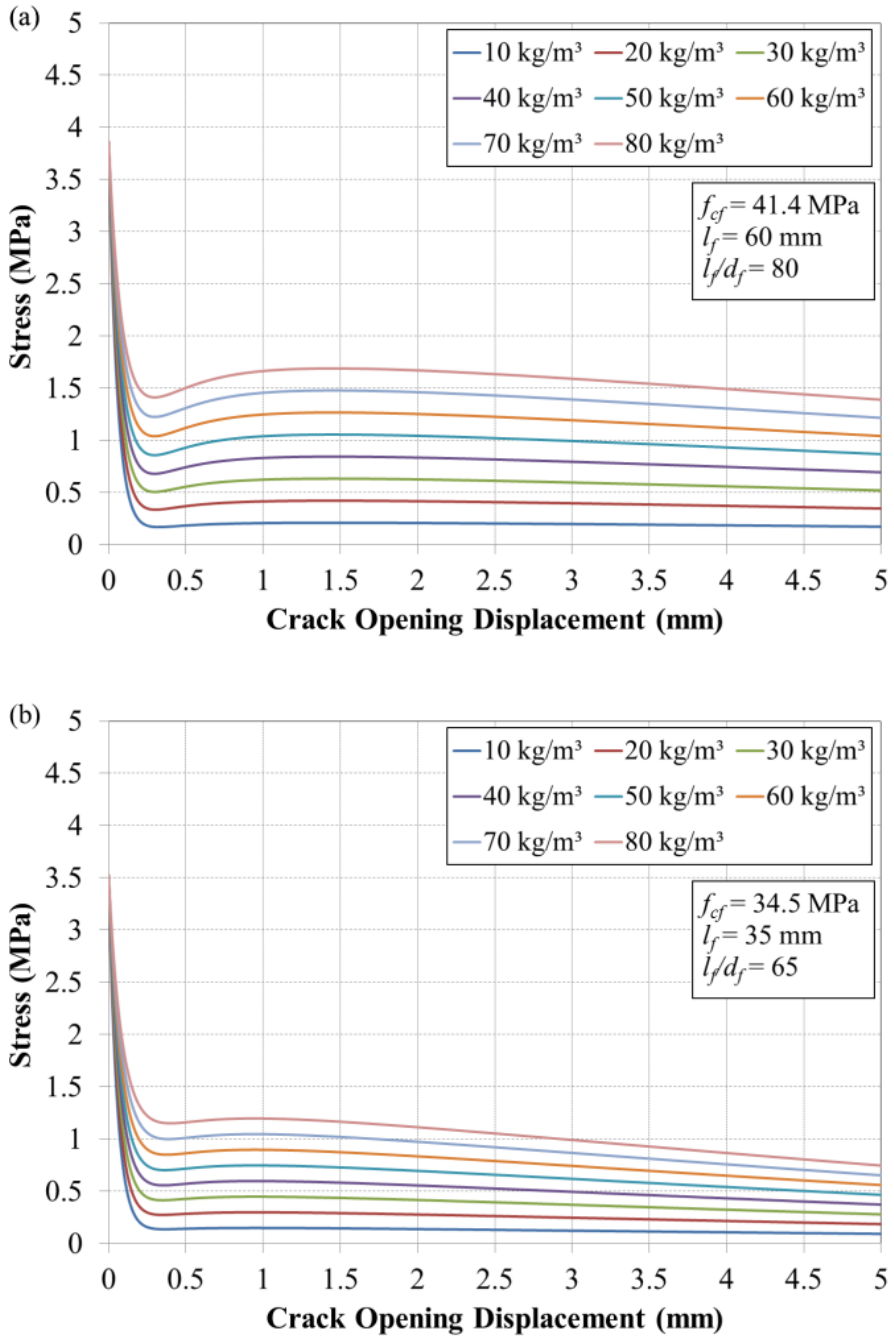

Figure 6-7 Tension stress-crack opening curves for SFRC used in the FEM

6.4 EXPERIMENTAL PROGRAM AND RESULTS

To calibrate and verify the FE model, a group of full-scale SFRC pipes were fabricated and tested under the TEBT. Two pipe diameters were manufactured; namely, 450 mm and 600 mm. All pipes had a Type C wall. Details regarding pipe production, mixture proportions and curing regime were given earlier in **Section** 3.2.3. Dramix RC-65/35-CN and Dramix RC-80/60-CN fibres were added manually at rates of 30 and 40 kg/m³. The physical and mechanical properties of these steel fibres are shown in **Table 3-2**. Simultaneously, 100 x 200 mm cylinder specimens were cast for measuring the compressive strength of the mixtures. **Table 6-2** lists the fabricated 450 and 600 mm diameter pipes, their fibre type and content, and the compressive strength of the corresponding concrete mixtures. Three pipe replicates were cast for each mixture composition for a total of 12 full-scale pipes. The cyclic TEBT procedure described in the European standard EN 1916 was used to evaluate the mechanical performance of SFRC pipes. Test setup and pipe instrumentation were similar to pipes tested in chapter 4 (**Section** 4.2.2). The achieved average ultimate (D_{ult}) D-loads are summarized in **Table 6-2.**

Table 6-2 Results of SFRC pipes tested under TEBT for model verification

Pipe Designation	D_i (mm)	Fibre type	W_f (kg/m³)	h (mm)	f_c' (MPa)	D_{ult} (N/m/mm)		% diff.
						Exp.	FEM	
SS4530	450	Short fibres	30	82	42.5	256.7	236.8	-7.7
SL4530	450	Long fibres	30	82	35.8	273.9	253.7	-7.3
SS6040	600	Short fibres	40	94	73.0	224.5	210.1	-6.5
SL6040	600	Long fibres	40	94	65.0	239.5	228.6	-4.6

Note: Short fibres: Dramix RC-65/35-CN, and Long fibres: RC-80/60-CN.

6.5 MODEL CALIBRATION

The load-deflection response of SFRC is mainly controlled by the tensile capacity. Therefore, material parameters for other aspects, such as compression response and shear, are less

relevant (Mobasher, 2011). When modelling the load-deflection response of SFRC round panels, Mobasher (2011) reported that Young's modulus and the tensile stress-crack width model are the two most critical parameters for concrete. Furthermore, a study on FE modelling of SFRC precast tunnel linings (Blazejowski, 2012) performed a sensitivity analysis to quantify the effects of varying material parameters of the numerical model on the model outputs. Material parameters included: compressive stress-strain, tensile stress- strain, Young's modulus (E_c), Poisson's ratio (υ), and concrete density (ρ). Similarly, Blazejowski (2012) reported that the elastic modulus and the stress-strain tension stiffening parameters had the most significant effect on the model outputs. Therefore, model calibration in this study was limited to these parameters. In addition, in order to facilitate the calibration process and reduce the program running time, tensile stress-strain relations shown in **Fig. 6-7** were approximated into bi-linear relations as shown in **Fig. 6-8**.

The FE model was first calibrated using results of the TEBT of the SL6040 pipe. **Figure 6-9** shows a comparison between the experimental and numerical load-deflection curves at the pipe's crown. The experimental curve shows an unloading/reloading cycle, which is not matched in the FE model. Nevertheless, it has already been established that this extra loading cycle does not alter or modify the overall pipe behaviour (de Figueiredo and Gettu, 2008; de la Fauente *et al.*, 2012; and de la Fuente *et al.*, 2013). The experimental and numerical behaviours had comparable shape. However, the FE model overestimated the ultimate D-load by 35%. In addition, the experimental curve exhibited a deflection-hardening plateau followed by a descending branch, while the FE model exhibited a steep decrease in load carrying capacity followed by an ascending branch. It can be observed that a good agreement existed until a deflection of 0.3 mm (D-load = 140 N/m/mm). Hence it can be deduced that the assumption for the Young's modulus was valid. Therefore the model calibration focused on adjusting the tension stiffening parameters only.

Several trials were made in order to fit the numerical curve with the experimental one by altering the tension stiffening parameters one at a time. The best fit was found when the schematic shown in **Fig. 6-10** was adopted. However, constant fracture energy (G_f) was maintained before and after modification.

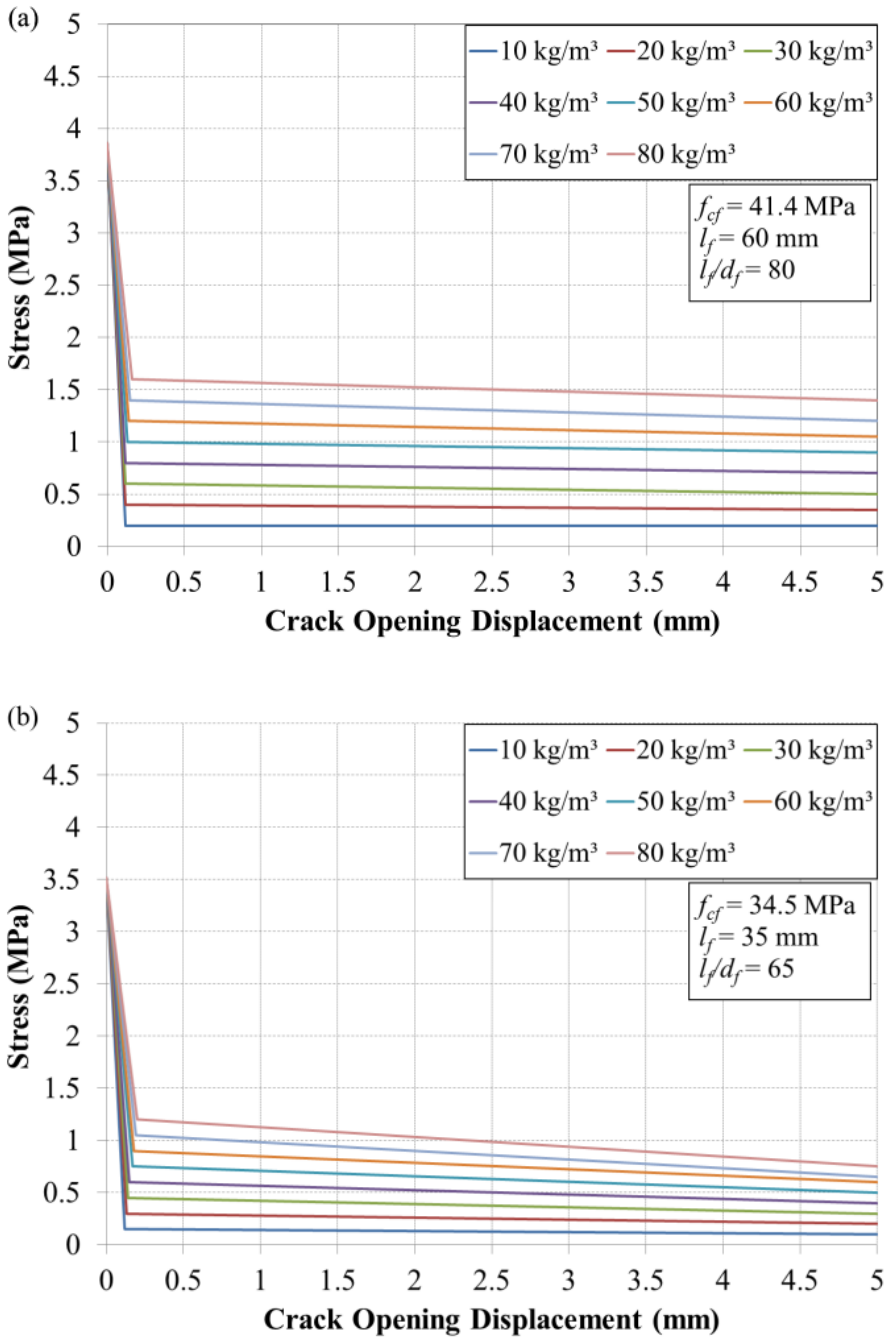

Figure 6-8 Bi-linear approximations for tension stress-strain curves for SFRC used in the FEM.

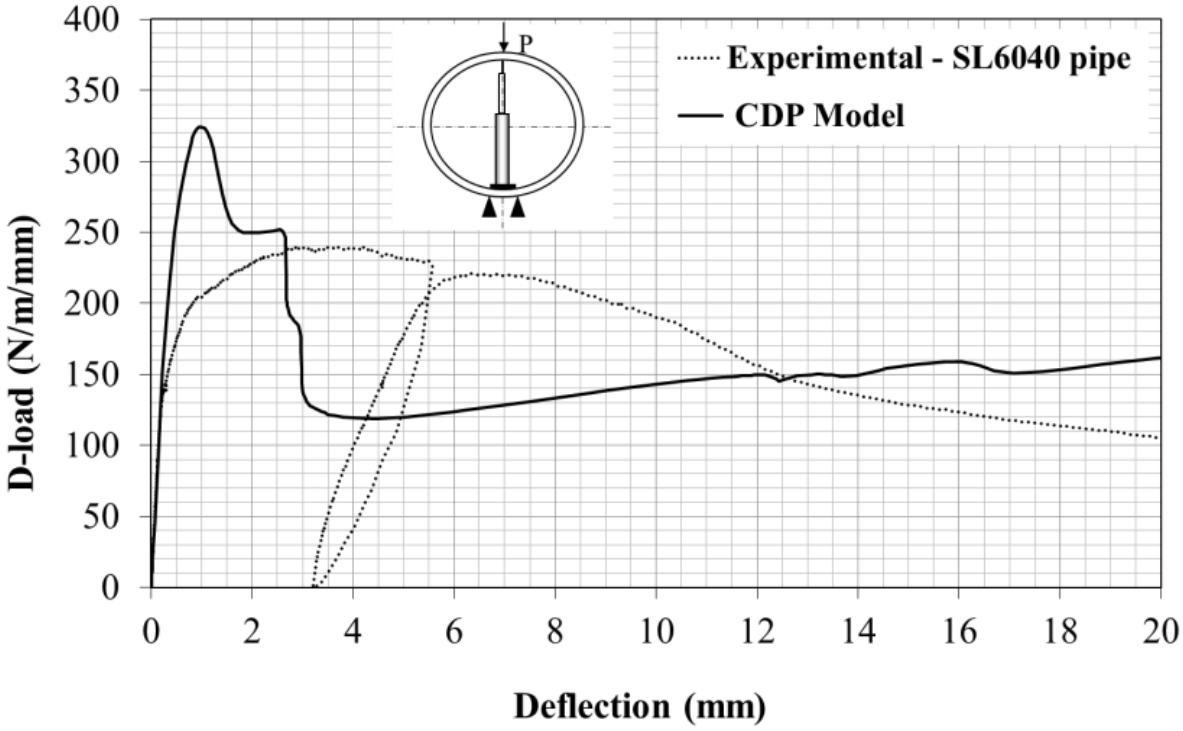

Figure 6-9 Load-deflection curve of SL6040 pipe obtained experimentally and numerically.

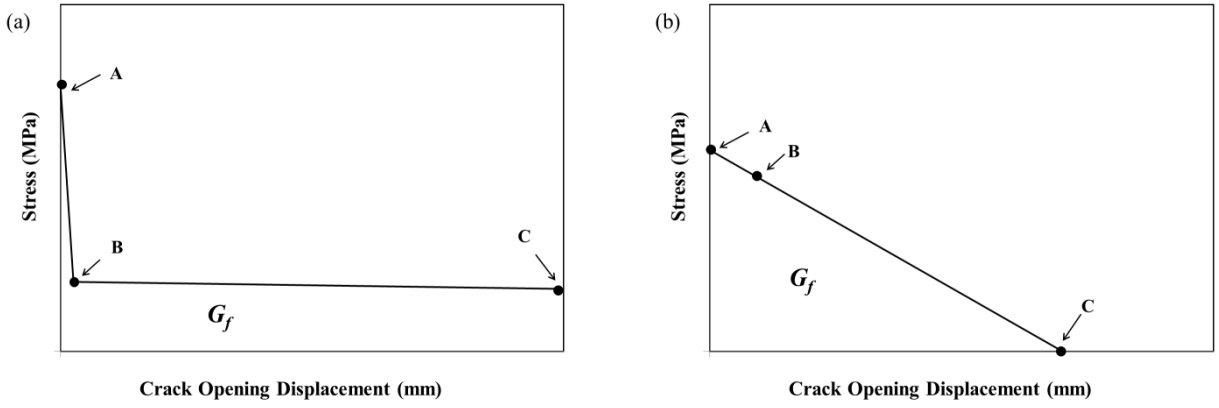

Figure 6-10 Schematic showing tension stiffening (a) before, and (b) after modification.

6.6 MODEL VERIFICATION

Figure 6-11 shows the FE load-deflection curves using the modified tension stiffening parameters for SFRC pipes. Overall good agreement between experimental and modelling results can be observed in **Fig. 6-11**, especially up to a displacement of 10 mm. The predicted ultimate D-loads were, on average, 6.50 % lower (i.e. on the conservative side) than the experimental D-loads (**Table 6-2**).

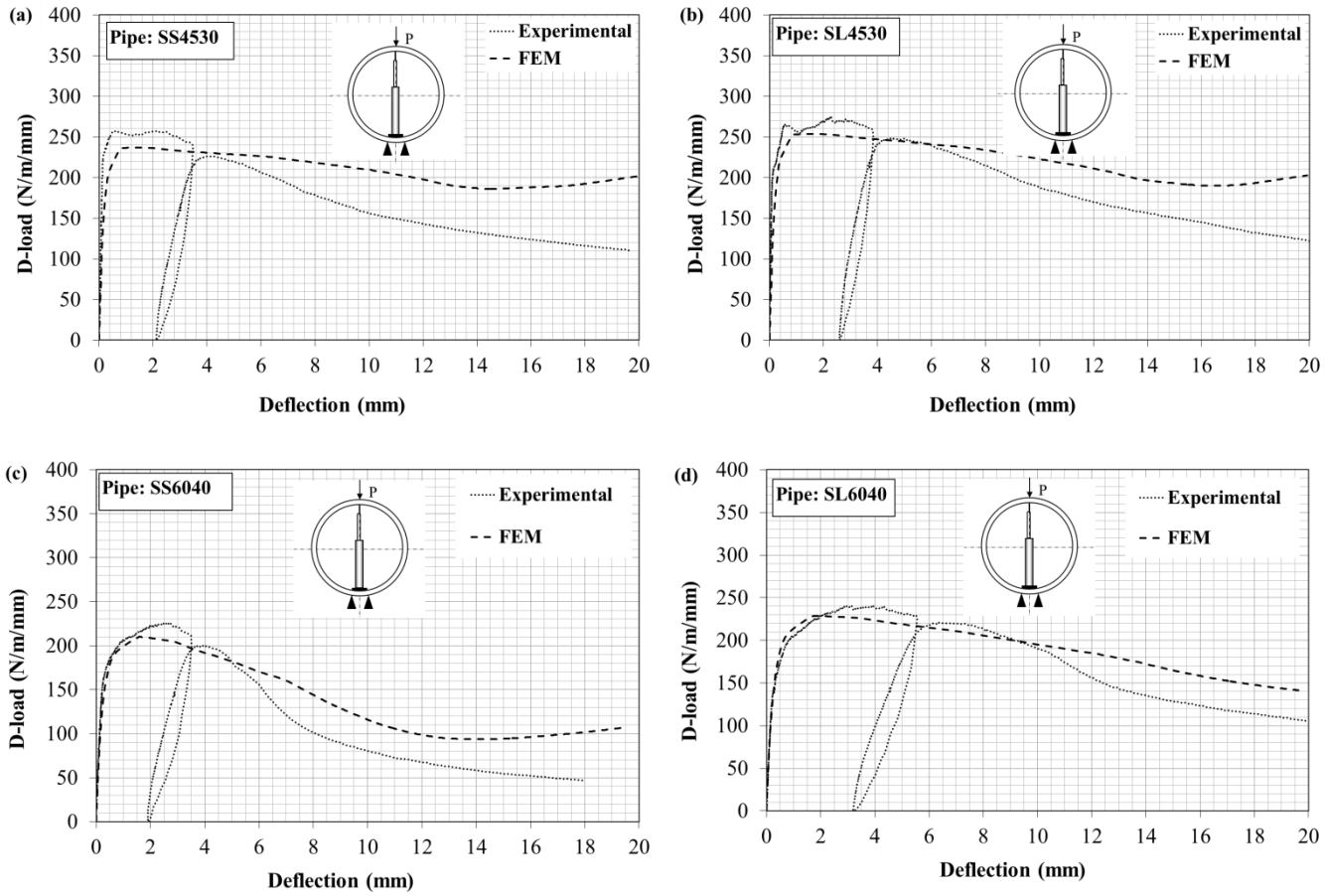

Figure 6-11 Comparison between experimental and numerical load-deflection curves of (a) SS4530, (b) SL4530, (c) SS6040, and (d) SL6040 pipes.

For further verification, experimental and numerical results reported by de Figueiredo *et al.* (2012-b), and de la Fuente *et al.* (2012) were compared to the predictions of the finite element model developed in this study. **Figures 6-12a and 6-12b** show the achieved ultimate D-loads for 600 and 800 mm diameter SFRC pipes, respectively. Details of SFRC pipes' design and the MAP model development are mentioned elsewhere (de Figueiredo *et al.*, 2012-b and de la Fuente *et al.*, 2012). For the MAP model, the reported average error was -10.63 % for 600 mm diameter pipes (de Figueiredo *et al.*, 2012-b), and -1.45 % for 800 mm diameter pipes (de la Fuente *et al.*, 2012). For the FE model in this study, the average error was -6.40 %, and -4.35 for 600 mm and 800 diameter pipes, respectively.

It can be concluded that the finite element model predictions agree reasonably with the experimental data obtained by the present authors and reported by others. Furthermore, the observed error, in most cases, fell on the conservative side of the experimental results.

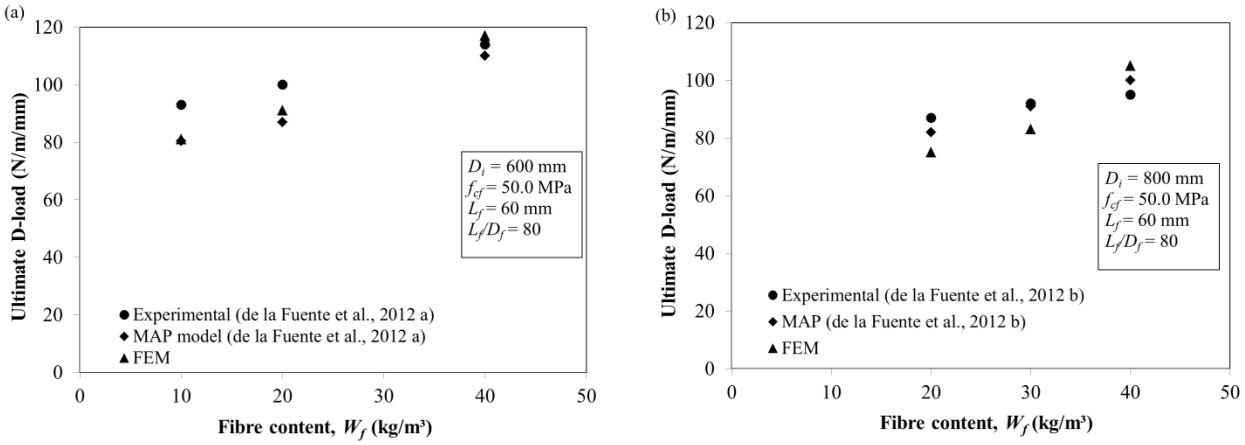

Figure 6-12Comparison between experimental and numerical results reported by de la Fuente *et al.* (2012 b, and 2012 c) and the developed finite element model for (a) 600 mm and (b) 800 mm diameter SFRC pipes.

6.7 PARAMETRIC STUDY

Following model verification, a parametric study was conducted. The main goal was to provide the concrete pipe industry with a rational design tool that can be used to fabricate SFRC pipes that can satisfy strength requirements of a certain pipe class as specified in ASTM C1765. The outcome of this parametric study is presented in a tabular form to specify the optimal fibre type and content for a specific pipe diameter/wall thickness configuration sufficient to achieve a certain pipe class. This form is intended to be similar to design tables presented in ASTM C76 (Standard Specification for Reinforced Concrete Culvert, Storm Drain, and Sewer Pipe) for RC pipes. Therefore, the following parameters were considered when conducting the parametric study and the rationale behind their limitations is described:

- Internal pipe diameter (D_i): the pipe diameter ranged from 300 mm to 1200 mm as specified in ASTM C1765. The pipe diameter was increased by a 75 mm increment until D_i = 900 mm, then the increment became 150 mm until D_i = 1200 mm.
- Pipe wall thickness (h): for each pipe diameter, three wall thicknesses were considered. Similar to RC pipes wall thicknesses specified in ASTM C76, these included Type A wall, Type B wall, and Type C wall. These thicknesses correspond to D_i /12, D_i /12 + 25.4 (mm), and D_i /12 + 44.5 (mm) for Type A, B, and C walls, respectively.
- Fibre type: two types of steel fibres were considered in this study: short and long Dramix fibres. Physical and mechanical properties of these fibres are provided in **Table 3-2**. These fibres were recommended for SFRC pipes fabrication based on previous experimental work carried out by the author (Mohamed *et al.*, 2014, and Mohamed *et al., 2015*).
- Fibre dosage (W_f): the fibre content ranged between 25 and 80 kg/m³ (i.e. 0.31 % to 1.0 % by concrete volume). The lower limit coincides with the critical fibre volume (V_f) below which no significant enhancement to the concrete post-cracking behaviour could be observed (Bentur and Mindess, 2007). The upper limit was set at 80 kg/m³ since higher fibre contents would be uneconomical and hard to mix. Fibre content was increased by a 10 kg/m³ increment (0.125 % by volume) (only the first increment was 5.0 kg/m³).
- Concrete compressive strength (f_{cf}): for RC pipes, ASTM C76 specifies, depending on the pipe diameter/wall thickness/targeted strength configuration, three minimum

strengths, namely 27.6, 34.5, and 41.4 MPa (4000, 5000, and 6000 psi). In this study, f_{cf} was taken as f_{cf1} = 34.5 and f_{cf2} = 41.4 MPa. f_{cf1} and f_{cf2} were matched with short and long Dramix fibres, respectively. The first configuration was assigned to small pipe diameters (D_i = 300 to 600 mm), while the second configuration was assigned to intermediate pipe diameters (D_i = 675 to 1200 mm). This is because SFRC pipes are known to have a problem of steel fibres "sticking out" of the matrix. Using shorter fibres with small diameter pipes, hence small wall thicknesses, would reduce the possibility of such a problem.

- Target pipe strength: all the five strength classes specified in ASTM C1765 were considered (**Table 2-4**).

As an example**, Fig. 6-13** shows load-deflection curves obtained for a certain pipe configuration (D_i = 1050 mm, h = 132 mm (C Wall), f_{cf} = 41.4 MPa, and long Dramix fibres). Load-deflection curves were contrasted against D_{test} (**Fig. 6-13a**), and $D_{service}$ (**Fig. 6-13b**) for the aforementioned strength classes. As mentioned earlier, the extra loading cycle is not expected to alter the pipe behaviour; therefore the generated curves can be used to determine the optimal fibre content for a certain pipe class. From **Fig. 6-13**, it can be deduced that, for this configuration, a fibre dosage of 80, 60, 40, 30, and 25 kg/m³ would be sufficient to achieve strength requirements of Class V, IV, III, II, and I, respectively.

Tables 6-3 to **6-7** show the outcome of the parametric study. Examining these tables reveals that, with the current design limitations, D_i = 1050 mm is the maximum pipe size that can be produced and is able to fulfil strength requirements of Class V pipes. In addition, regardless of the fibre type and content, Type B-Wall pipes cannot fulfil strength requirements of Class V pipes (with the exception of 300 mm and 375 mm diameter pipes). Finally, regardless of the fibre type and content, Type A-Wall pipes cannot fulfil strength requirements of Class V and Class IV pipes. **Tables 6-3** to **6-7**, similar to tables available in ASTM C76 for RC pipes, can serve as a complimentary design tool to ASTM C1765 for SFRC pipes.

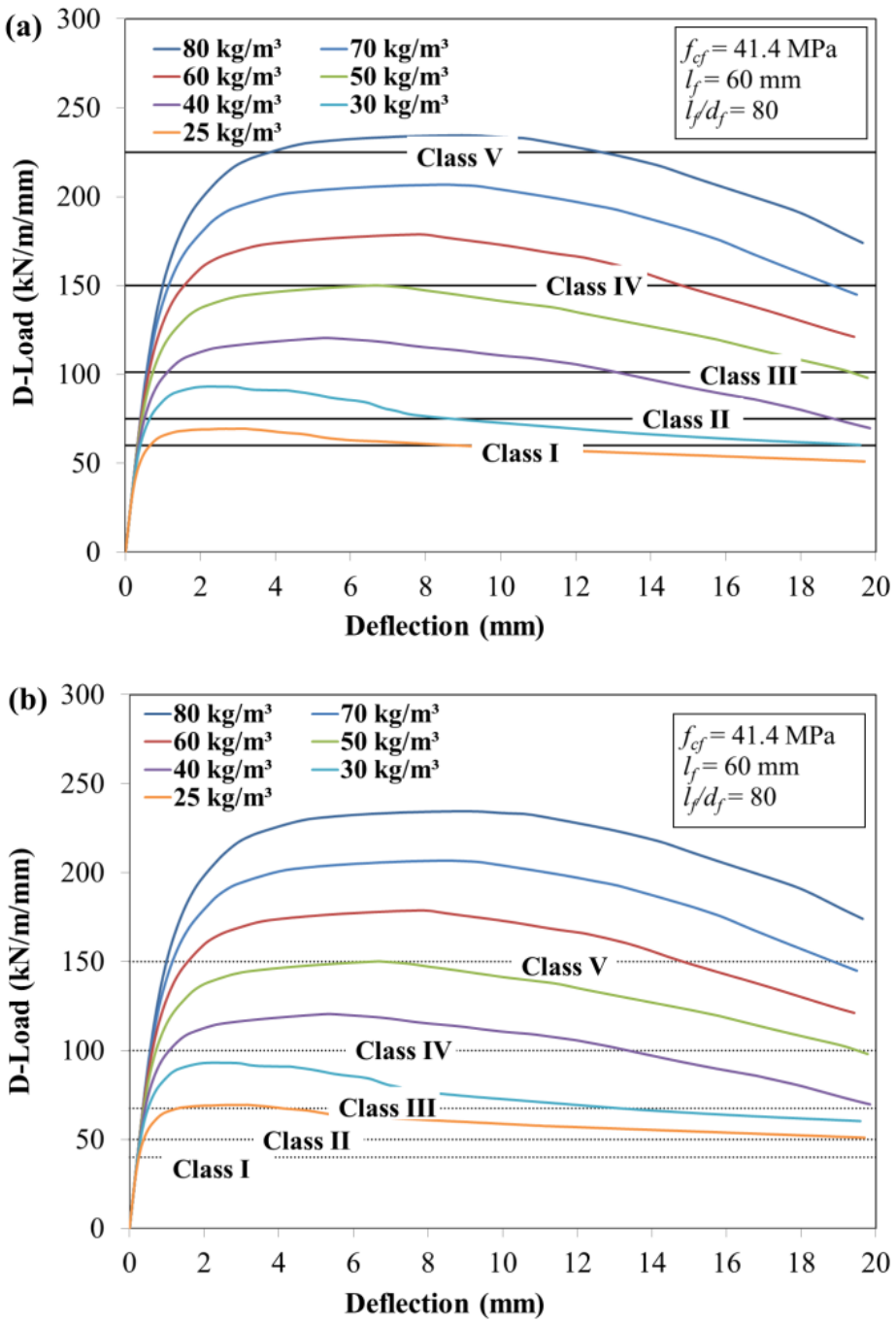

Figure 6-13 Load-deflection curves for a C-wall 1050 mm diameter pipe reinforced with various steel fibres contents imposed on (a) Dtest, and (b) Dservice loads specified in ASTM C1765 for pipe strength classes.

Table 6-3 Fibre content requirements for Class I SFRC pipes

D_i (mm)	Wall A		Wall B		Wall C	
	h (mm)	W_f (kg/m³)	h (mm)	W_f (kg/m³)	h (mm)	W_f (kg/m³)
300[1]	44	25	50	25	69	25
375[1]	47	30	57	25	75	25
450[1]	50	30	63	25	82	25
525[1]	57	30	69	25	88	25
600[1]	63	40	75	30	94	25
675[2]	66	30	82	25	100	25
750[2]	69	40	88	30	107	25
825[2]	72	40	94	30	113	25
900[2]	75	50	100	30	119	25
1050[2]	88	50	113	30	132	25
1200[2]	100	60	125	40	144	30

Notes:

- For Class I SFRC pipes: $D_{Service}$ = 40 N/m/mm, D_{Test} =60 N/m/mm
- [1] Steel fibres type: Dramix RC-65/35-CN- f_c' = 34.5 MPa
- [2] Steel fibres type: Dramix RC-80/60-CN- f_c' = 41.4 MPa

Table 6-4 Fibre content requirements for Class II SFRC pipes

D_i (mm)	Wall A		Wall B		Wall C	
	h (mm)	W_f (kg/m³)	h (mm)	W_f (kg/m³)	h (mm)	W_f (kg/m³)
300[1]	44	30	50	25	69	25
375[1]	47	40	57	25	75	25
450[1]	50	40	63	25	82	25
525[1]	57	40	69	25	88	25
600[1]	63	50	75	30	94	25
675[2]	66	50	82	30	100	25
750[2]	69	60	88	40	107	25
825[2]	72	60	94	40	113	25
900[2]	75	70	100	40	119	25
1050[2]	88	70	113	40	132	30
1200[2]	100	80	125	50	144	40

Notes:

- For Class II SFRC pipes: $D_{Service}$ = 50 N/m/mm, D_{Test} =75 N/m/mm
- [1] Steel fibres type: Dramix RC-65/35-CN- f_c' = 34.5 MPa
- [2] Steel fibres type: Dramix RC-80/60-CN- f_c' = 41.4 MPa

Table 6-5 Fibre content requirements for Class III SFRC pipes

D_i (mm)	Wall A		Wall B		Wall C	
	h (mm)	W_f (kg/m³)	h (mm)	W_f (kg/m³)	h (mm)	W_f (kg/m³)
300[1]	44	40	50	25	69	25
375[1]	47	50	57	25	75	25
450[1]	50	60	63	40	82	25
525[1]	57	60	69	40	88	25
600[1]	63	70	75	50	94	25
675[2]	66	70	82	40	100	25
750[2]	69	80	88	50	107	30
825[2]	72	80	94	50	113	30
900[2]	75	80	100	50	119	30
1050[2]	88	80	113	50	132	40
1200[2]	100	> 80	125	60	144	50

Notes:

- For Class III SFRC pipes: $D_{Service}$ = 67.5 N/m/mm, D_{Test} =101.25 N/m/mm
- [1] Steel fibres type: Dramix RC-65/35-CN- f_c' = 34.5 MPa
- [2] Steel fibres type: Dramix RC-80/60-CN- f_c' = 41.4 MPa

Table 6-6 Fibre content requirements for Class IV SFRC pipes

D_i (mm)	Wall A		Wall B		Wall C	
	h (mm)	W_f (kg/m³)	h (mm)	W_f (kg/m³)	h (mm)	W_f (kg/m³)
300[1]	44	> 80	50	30	69	25
375[1]	47	> 80	57	40	75	25
450[1]	50	> 80	63	60	82	30
525[1]	57	> 80	69	70	88	30
600[1]	63	> 80	75	70	94	30
675[2]	66	> 80	82	60	100	40
750[2]	69	> 80	88	70	107	40
825[2]	72	> 80	94	70	113	50
900[2]	75	> 80	100	70	119	50
1050[2]	88	> 80	113	80	132	50
1200[2]	100	> 80	125	> 80	144	60

Notes:

- For Class IV SFRC pipes: $D_{Service}$ = 100 N/m/mm, D_{Test} =150 N/m/mm
- [1] Steel fibres type: Dramix RC-65/35-CN- f_c' = 34.5 MPa
- [2] Steel fibres type: Dramix RC-80/60-CN- f_c' = 41.4 MPa

Table 6-7 Fibre content requirements for Class V SFRC pipes

D_i (mm)	Wall A		Wall B		Wall C	
	h (mm)	W_f (kg/m³)	h (mm)	W_f (kg/m³)	h (mm)	W_f (kg/m³)
300[1]	44	> 80	50	70	69	25
375[1]	47	> 80	57	80	75	25
450[1]	50	> 80	63	> 80	82	30
525[1]	57	> 80	69	> 80	88	30
600[1]	63	> 80	75	> 80	94	40
675[2]	66	> 80	82	> 80	100	50
750[2]	69	> 80	88	> 80	107	60
825[2]	72	> 80	94	> 80	113	70
900[2]	75	> 80	100	> 80	119	80
1050[2]	88	> 80	113	> 80	132	80
1200[2]	100	> 80	125	> 80	144	> 80

Notes:

- For Class V SFRC pipes: $D_{Service}$ = 150 N/m/mm, D_{Test} =225 N/m/mm
- [1] Steel fibres type: Dramix RC-65/35-CN- f_c' = 34.5 MPa
- [2] Steel fibres type: Dramix RC-80/60-CN- f_c' = 41.4 MPa

6.8 SUMMARY AND CONCLUSIONS

In this chapter, a non-linear 3D finite element model was developed in order to simulate the three-edge-bearing test of precast SFRC pipes. The model employs the Concrete Damaged Model offered by the finite element simulation program, ABAQUS. An experimental campaign on full-scale SFRC pipes was also conducted in order to calibrate and validate the developed FE model. The average error in the predicted ultimate D-loads was 6.50% on the conservative side. Interestingly, the average error was found to be 6.4% and 4.35% on the conservative side when contrasted against experimental data available in the literature. Subsequently, a parametric study was conducted. Six independent parameters were investigated with limitations adjusted to the specifications of ASTM C1765 and ASTM C76 standards. Finally, a rational design tool was developed in order to recommend an optimal steel fibre type and dosage to satisfy a certain pipe strength class. The developed design tables can be used as a supplementary aid to the ASTM C1765 standard.

6.9 REFERENCES

Abaqus, F. E. A. "ABAQUS Analysis user's manual." Dassault Systemes,Vélizy-Villacoublay, France, 2006.

Abbas, S., "Structural and durability performance of precast segmental tunnel linings," Ph.D. dissertation, The University of Western Ontario, London, Ontario, 2014.

Abolmaali, A., Mikhaylova, A., Wilson, A. and Lundy, J., "Performance of steel fibre-reinforced concrete pipes." *Journal of the Transportation Research Board*, 2313(1), 2012, pp. 168-177.

Ahn, T., "Thermal and mechanical studies of thin spray-on liner (TSL) for concrete tunnel linings," Ph.D. dissertation, The University of Western Ontario, London, Ontario, 2011.

Amin, A., Foster, S.J., and Muttoni, A., "Derivation of the σ-w relationship for SFRC from prism bending tests." *Structural Concrete*, 2014, article in press.

ASTM C76-13, "Standard Specification for Reinforced Concrete Culvert, Storm Drain, and Sewer Pipe," American Society for Testing and Materials, ASTM International, West Conshohocken, PA, 2013, 11 p.

ASTM C497-13, "Standard test methods for concrete pipe, manhole sections or tile." American Society for Testing and Materials, ASTM International, West Conshohocken, PA, 2013, 14 p.

ASTM C1765-13, "Standard specification for steel fibre reinforced concrete culvert, storm drain, and sewer pipe." American Society for Testing and Materials, ASTM International, West Conshohocken, PA, 2013, 6 p.

Barros, J.A.O., and Figueiras, J.A., "Flexural behavior of SFRC: testing and modeling," *Journal of materials in civil engineering*, 11 (4), 1999, pp. 331-339.

Bencardino, F., Rizzuti, L., Spadea, G., and Swamy, R. N., "Stress-strain behavior of steel fiber-reinforced concrete in compression," Journal *of Materials in Civil Engineering*, 20 (3), 2008, pp. 255-263.

Bentur, A., and Mindess, S., "*Fibre-Reinforced Cementitious Composites.*" 2nd edition; New York: Taylor & Francis, 2007, 660 p.

Blazejowski, M., "Flexural behaviour of steel fibre reinforced concrete tunnel linings," MSc. dissertation, The University of Western Ontario, London, Ontario, 2012.

Brandt, A.M., "Fibre-reinforced cement-based (FRC) composites after over 40 years of development in building and civil engineering." *Composite Structures,* 86(1–3), 2008, pp. 3-9.

Chen, L., and Graybeal, B.A., "Modeling structural performance of ultrahigh performance concrete I-girders." *Journal of Bridge Engineering*, 17(5), 2011, pp. 754-764.

Comité euro-international du béton, "*CEB-FIP Model Code 1990: Design Code*," No. 213-214. FIB- Fédération International du Béton, 1993.

de la Fuente, A., and De Figueiredo, D., "Experimentation and numerical simulation of steel fibre reinforced concrete pipes." *Materiales de Construcción*, 61(302), 2011, pp. 275-288.

de Figueiredo, A. and Gettu, R., "Evaluation of the test method for crushing strength of steel fibre reinforced concrete pipes." *Seventh RILEM International Symposium on Fibre Reinforced Concrete*, RILEM Publications SARL, 2008, pp. 989-1000.

de Figueiredo, D., de la Fuente, A., De Cea, A., Borrell, C., and Chama Neto, P., "Steel fiber reinforced concrete pipes. Part 1: technological analysis of the mechanical behaviour." *IBRACON Structures and Materials Journal*, 5 (1), 2012-a, pp. 1-11.

de Figueiredo, D., de la Fuente, A., De Cea, A., Borrell, C., and Chama Neto, P., "Steel fiber reinforced concrete pipes. Part 2: numerical model to simulate the crushing test." *IBRACON Structures and Materials Journal*, 5 (1), 2012-b, pp. 12-25.

de la Fuente, A., Escariz, R.C., De Figueiredo, A.D., Molins, C., and Aguado, A., "A new design method for steel fibre reinforced concrete pipes," *Construction and Building Materials*, 30, 2012, pp. 547-555.

de la Fuente, A., Escariz, R.C., De Figueiredo, A.D., Molins, C., and Aguado, A., "Design of Macro-synthetic Fibre Reinforced Concrete Pipes," *Construction and Building Materials*, 43, 2013, pp.523-532.

Ezeldin, A. S., and Balaguru, P.N., "Normal-and high-strength fiber-reinforced concrete under compression," *Journal of materials in civil engineering*, 4 (4), 1992, pp. 415-429.

Gouveia, N.D., Fernandes, N. A.G., Faria, D., Ramos, A.M.P., and Lúcio, V.J.G., "SFRC flat slabs punching behaviour–Experimental research," *Composites Part B: Engineering*, 63, 2014, pp. 161-171.

Haktanir, T., Ari, K., Altun, F., and Karahan, O., "A Comparative experimental investigation of concrete, reinforced-concrete and steel-fibre concrete pipes under three-edge-bearing test," *Construction and Building Materials*, 21(8), 2007, pp. 1702-1708.

Hillerborg, A., Modéer, M., and Petersson, P.E., "Analysis of crack formation and crack growth in concrete by means of fracture mechanics and finite elements," *Cement and concrete research*, 6(6), 1976, pp. 773-781.

Lee, J., and Fenves, G.L., "Plastic-damage model for cyclic loading of concrete structures," *Journal of engineering mechanics*, 124(8), 1998, pp. 892-900.

Lee, G.G., and Foster, S.J., "Modelling of shear-fracture of fibre-reinforced concrete," in *Tailor made concrete structures, fib symposium*, Amsterdam, The Netherlands, 2008, pp. 19-22.

Lubliner, J., Oliver, J., Oller, S., and Onate, E., "A plastic-damage model for concrete," *International Journal of solids and structures*, 25(3), 1989, pp. 299-326.

MacDonald, C. and Trangsrud, J., "Steel fiber product introduction through pre-cast reinforced concrete pipe." *ACI Special Publication*, 222, 2004, pp. 185-199.

Mobasher, B. "*Mechanics of fiber and textile reinforced cement composites*." CRC Press, 2011, 450 p.

Mohamed, N., Soliman, A.M., and Nehdi, M.L., "Full-scale pipes using dry-cast steel fibre-reinforced concrete," *Construction and Building Materials,* 72, 2014, pp. 411-422.

Mohamed, N., Soliman, A.M., and Nehdi, M.L., "Mechanical performance of full-scale precast steel fibre-reinforced concrete pipes," Engineering *Structures,* 84, 2015, pp. 287-299.

Nataraja, M.C., Dhang, N., and Gupta, A.P., "Stress–strain curves for steel-fiber reinforced concrete under compression," *Cement and concrete composites*, 21 (5), 1999, pp. 383-390.

Ng, T.S., Htut, T.N.S., and Foster, S.J., "Fracture of steel fibre reinforced concrete—the unified variable engagement model," *UNICIV Report R-460,* School of Civil and Environmental Engineering, The University of New South Wales, Sydney, 2012, 114 p.

Soroushian, P., and Lee, C.D., "Constitutive modeling of steel fiber reinforced concrete under direct tension and compression." *International Conference on Recent Developments in Fibre Reinforced*-Conference Proceedings, Elsevier Applied Science, 1989, pp. 363-377.

Voo, J.Y.L., and Foster, S.J., "Tensile-fracture of fibre-reinforced concrete: variable engagement model," In *6th International RILEM Symposium on Fibre Reinforced Concretes*, edited by di Prisco, M., Felicetti, R., and Plizzari, G.A., RILEM Publications SARL, 2004, pp. 875-884.

Voo, J.Y.L., and Foster, S.J., "Variable engagement model for the design of fibre reinforced concrete structures," *Advanced materials for construction of bridges, buildings, and other structures III, Conference Proceedings*, 2003,

Voo, Y. L., and Foster, S.J., "*Reactive powder concrete: analysis and design of RPC girders*," Lambert Academic Publishing, 2009, 364 p.

CHAPTER SEVEN

7 SUMMARY, CONCLUSIONS AND RECOMMENDATIONS

7.1 SUMMARY AND CONCLUSIONS

This study aimed at providing the precast concrete pipe industry with technical information and recommendations regarding the production, testing, structural performance, and design of SFRC pipes, as well as providing a confidence level to infrastructure owners and the general public in such pipe option.

In Chapter 3, the mechanical properties of dry-cast steel fibre-reinforced concrete (DCSFRC) were investigated. Four commercially available steel fibres were added at rates of 0, 20, 40 and 60 kg/m³. Results showed that the mechanical properties of DCSFRC were enhanced as the fibre dosage increased. Generally, hooked-end fibres with the highest aspect ratio led to highest tensile and flexural strengths. Consequently, full-scale 300 mm diameter precast pipes were fabricated using the tested DCSFRC mixtures to examine its potential for such an application. In addition, plain (PC) and conventionally reinforced concrete (RC) precast pipes were fabricated and tested for comparison. The continuous three-edge-bearing test was used to characterize the structural performance of precast pipes. SFRC pipes achieved ultimate loads greater than the required strength for Class V pipes according to the ASTM C76 standard. In addition, the post-peak behaviour of SFRC pipes was comparable or superior to that of conventional RC pipes. In general, using discrete steel fibres was shown to be a viable alternative to the labour intensive and time-consuming steel cages normally used for reinforcing precast concrete pipes.

Chapter 4 expanded on the findings of Chapter 3. Full-scale 450 and 600 mm diameter SFRC pipes were cast. Two types of steel fibres having round cross-sections and hooked ends were used. Steel fibres had lengths and aspect ratios of 35 and 60 mm, and 65 and 80, respectively. The steel fibres content ranged from zero to 40 kg/m^3. Pipe specimens were instrumented with strain gauges mounted on critical sections of each pipe. In addition, vertical and horizontal deformations of the pipe's cross-section were monitored using LVDTs. Precast pipes were tested using both the continuous and cyclic loading procedures as per the ASTM C497 and EN 1916 guidelines, respectively. PC and RC pipes of 450 and 600 mm diameter were cast and tested for comparison. Results showed that a fibre dosage of 30 kg/m^3 satisfied the strength requirements of ASTM C76 Class V pipe for 450 and 600 mm diameter pipes. In addition, the post-peak behaviour of SFRC pipes was comparable or superior to that of conventional RC pipes at small deformations. It was also found that using a hybrid system of long and short steel fibres did not result in synergetic effects. Improvements due to the usage of a hybrid fibre system over short fibres were due to the inclusion of long fibres. Finally, it was demonstrated that the behaviour of SFRC pipes could be fully explored using the continuous three-edge-bearing test without need of the extra loading cycle specified in the EN 1916 standard.

Chapter 5 presented novel data on the behaviour of buried full-scale 600 mm diameter SFRC pipes under actual and simulated live loads. The first phase of this experimental campaign monitored the behaviour of SFRC pipes under standard CL 625 truckloads (standard Ontario truck). Results showed that SFRC pipes could sustain the regular standard truckloads without exhibiting significant deformations or cracks. Therefore, it is believed that the current design recommendations for the pipe wall thickness in ASTM C76 (Type C wall) are overly conservative. In the second phase, the post-cracking behaviour of SFRC pipes under artificial live loads was examined. Cracked SFRC pipes incorporating a relatively high fibre dosage of 40 kg/m^3 exhibited less deformation than that of cracked regularly reinforced concrete pipes. The post-cracking behaviour of SFRC pipes depended primarily on the steel fibre dosage and type of bedding installation.

Chapter 6 presented the development, calibration, and further verification of a non-linear three-dimensional finite element model of SFRC pipes under the three-edge-bearing test. The concrete damaged plasticity (CDP) model, integrated in the ABAQUS software,

was used to model SFRC. Constitutive models describing the compressive and tensile behaviour of SFRC were adapted from the literature. Variability in the steel fibres' type and dosage and its effect on the behaviour of SFRC could be captured by the employed constitutive models. The model was verified using experimental data generated in the present study, as well as other data available in the open literature. The model was capable of reasonably simulating the load-deformation curves of SFRC pipes tested using the three-edge-bearing method. The average error in model-predicted ultimate D-loads was about 6.5% on the conservative side. Subsequently, a parametric study was conducted. The pipe diameter, pipe wall thickness, fibre type and content, concrete compressive strength, and targeted pipe strength were the parameters under investigation. The generated load-deformation curves were contrasted against service and ultimate loads specified in the ASTM C1765 standard for SFRC pipes and used to determine the optimal fibre content for a certain pipe class. The findings of the parametric study were presented in a tabular form that can be used as a design aid supplementary to the ASTM C1765 standard.

7.2 RECOMMENDATIONS FOR FUTURE RESEARCH

The current research revealed that some further studies on SFRC pipes maybe needed as follows:

1) In the present thesis, full-scale tests were conducted on RC and SFRC pipes in order to evaluate their mechanical behaviour. Therefore, it is recommended to investigate the use of conventional steel reinforcement and steel fibre reinforcement at various dosages in full-scale pipes with hybrid reinforcement.
2) In the present thesis, due to time and budgetary constraints, soil-structure interaction of buried SFRC pipes was investigated under a short-term loading condition. It is recommended to explore the soil-pipe interaction under long-term loading conditions where the pipe is instrumented and installed in a high traffic area and the data collection spans over a period of several months or years. The effects of repeated loading/unloading cycles need to be addressed.
3) In the present thesis, numerical modelling was limited to the three-edge-bearing test. This approach is consistent with the indirect design method. For SFRC pipes to be

implemented in the direct design method, numerical modelling of the entire soil-pipe system is needed. Soil parameters associated with the four standard installations, as well as parameters associated with steel fibre reinforcement need to be investigated in a parametric study.

4) Susceptibility to body and joint leakage, as well as the joints' ability to withstand differential loading need to be investigated for SFRC pipes.
5) The durability performance of SFRC pipes remains largely unexplored. Therefore, durability issues need to be investigated experimentally. Specifically, the chloride ions penetration and corrosion potential of full-scale SFRC pipes as well as sulfate attack resistance need to be studied. Consequently, a detailed numerical analysis and service life estimation, accounting for mechanical degradation of SFRC pipes in harsh environments, may be developed.
6) The application of hybrid micro-macro fibres, synthetic fibres and hybrid metallic-synthetic fibres in precast concrete pipes should be investigated.
7) The application of ultra-high performance concrete (UHPC) and ultra-high performance fibre-reinforced concrete (UHPFRC) in precast pipes should be considered in future investigations.

Appendices

Appendix A

Calculations of theoretical bending moments M_{SIDD} (SIDD method)

$$M_{SIDD} = \frac{D_m}{2} (C_{mp}\ W_p + C_{ml}\ W_l) \qquad \textbf{Eq. 5-2}$$

D_m = 600 mm + (2x 94 mm)/2 = 694 mm

C_{mp} = 0.235, C_{ml} = 0.211 @ invert

C_{mp} = 0.101, C_{ml} = 0.145 @ spring-line

W_p = pipe volume x concrete density

= 0.5 m³ x 2400 kg/m³ = 1200 kg = 11.77 kN

W_p = 11.77 kN/ pipe length (2.44 m) = 4.82 kN/m

$$w_l = \frac{P x\ I_f}{AL_1 x\ AL_2}$$

AL_1 = L + 1.75 H = 0.2 m + 1.75 (0.6 m) = 1.25 m

AL_2 = W + 1.75 (H + 0.75 D_o) = 0.5 m + 1.75 (0.6 + 0.75x 0.8m) = 2.6 m

Loading case #1 = P_1 = 68.5 kN

Loading Case #2 = P_2 = 34.25 kN

Loading Case #3 = P_2 = 68.5 kN

Loading Case #4 = P_2 = 68.5 kN

W_{l1} = (68.5 kN x 1.2)/ (1.25 m x 2.6 m) x 0.8 m = 20.23 kN/m

W_{l2} = (34.25 kN x 1.2)/ (1.25 m x 2.6 m) x 0.8 m = 10.12 kN/m

W_{l3} = (68.5 kN x 1.2)/ (1.25 m x 2.6 m) x 0.8 m = 20.23 kN/m

W_{l4} = (137 kN x 1.2)/ (1.25 m x 2.6 m) x 0.8 m = 20.23 kN/m

@ Invert

$M_{SIDD\,(1)}$ = 0.694 m /2 x (0.235 x 4.82 kN/m + 0.211 x 20.23 kN/m) = 1.87 kN.m

$M_{SIDD\,(2)}$ = 0.694 m /2 x (0.235 x 4.82 kN/m + 0.211 x 10.12 kN/m) = 1.13 kN.m

$M_{SIDD\,(3)}$ = 0.694 m /2 x (0.235 x 4.82 kN/m + 0.211 x 20.23 kN/m) = 1.87 kN.m

$M_{SIDD\,(4)}$ = 0.694 m /2 x (0.235 x 4.82 kN/m + 0.211 x 20.23 kN/m) = 1.87 kN.m

@ Spring-line

$M_{SIDD\,(1)}$ = 0.694 m /2 x (0.101 x 4.82 kN/m + 0.145 x 20.23 kN/m) = 1.18 kN.m

$M_{SIDD\,(2)}$ = 0.694 m /2 x (0.101 x 4.82 kN/m + 0.145 x 20.23 kN/m) = 0.68 kN.m

$M_{SIDD\,(3)}$ = 0.694 m /2 x (0.101 x 4.82 kN/m + 0.145 x 20.23 kN/m) = 1.18 kN.m

$M_{SIDD\,(4)}$ = 0.694 m /2 x (0.101 x 4.82 kN/m + 0.145 x 20.23 kN/m) = 1.18 kN.m

Appendix B

Example on calculations of Heger earth pressures

D_o = 800 mm = 0.8 m, H = 1.1 m, γ = 22.0 kN/m³

$PL = (\gamma D_o)\,[H + 0.107\,D_o]$ **Eq. 5-3**

PL = (22.0 kN/m³ x 0.8m) (1.1 m + 0.107 x 0.8m) = 20.87 kN/m

From **Fig. 2-4:**

VAF = 1.4, HAF = 0.37

A_1 = 1.05

c = 0.2, u = 0.85,

a = 1.45, b = 0.36

$h_1 = 1.5 \times A_1 / (c \times (1+u)) = (1.5 \times 1.05) / (0.2 \times (1+0.85)) = 4.26$

Calculation of stresses

σ_{inv} = (PL x VAF x h_1) /D_o = (20.87 kN/m x 1.4 x 4.26)/ 0.8 m = 155.59 kPa

σ_{inv} = (PL x VAF x a) /D_o = (20.87 kN/m x 1.4 x 1.45)/ 0.8 m = 52.96 kPa

σ_{inv} = (PL x HAF x b) /D_o = (20.87 kN/m x 0.37 x 0.36)/ 0.8 m = 3.47 kPa

CURRICULUM VITAE

Nedal Mohamed, P. Eng.

Education

Ph.D. in Structural Engineering (2010- 2015)
Western University, London, ON

Master of Structural Engineering (2007-2009)
University of Saskatchewan, Saskatoon, SK

B. Sc. in Civil Engineering (1999-2004)
Assiut University, Assiut, Egypt

Relevant Work Experience

Research & Teaching Assistant (2010- 2015)
Western University, London, ON

Structural Engineer-in-Training (2009-2010)
Amec Americas Ltd., Saskatoon, SK

Research & Teaching Assistant (2007- 2009)
University of Saskatchewan, Saskatoon, SK

Structural Engineer (2004-2006)
Center of Engineering Designs and Consults, Assiut, Egypt

Publications

N. Mohamed, A. Soliman, and M. Nehdi, (2015) *"*Mechanical Performance of Full-Scale Precast Steel Fibre-Reinforced Concrete Pipes*" Engineering Structures*, Elsevier, 84, pp. 287- 299.

N. Mohamed, A. Soliman, and M. Nehdi, (2014) *"*Full-Scale Pipes Using Dry-Cast Steel Fibre-Reinforced Concrete*" Journal of Construction and Building Materials*, Elsevier, 72, pp. 411- 422.

N. Mohamed, A. Soliman, and M. Nehdi, (2014) **"**Optimum Fibre Content for Precast Steel Fibre-Reinforced Concrete Pipes*" Conference Proceedings, 2nd FRC International Workshop (1st ACI–fib Joint Workshop) Fibre Reinforced Concrete: from Design to Structural Applications*, Polytechnique Montreal, 24-25 July 2014, Montreal, QC, Canada, pp. 500-510.

N. Mohamed, M. Boulfiza, and R. Evitts, (2013) "Corrosion of Carbon Steel and Corrosion-Resistant Rebars in Concrete Structures under Chloride Ion Attack*." Journal of Materials Engineering and Performance*, 22(3), pp. 787-795.

N. Mohamed, A. Soliman, and M. Nehdi, (2012) *"*Utilization of Steel Fibres in Precast Concrete Pipes*" Conference Proceedings, Tunnels and Underground Spaces: Sustainability and Innovations. Tunneling Association of Canada*, 17-20 Oct 2012, Montreal, QC, Canada, 8p.

N. Mohamed, M. Boulfiza , and R. Evitts (2010) "Corrosion Behaviour of Carbon Steel and Corrosion Resistant Rebars in Fresh and Carbonated Concrete Pore Solutions under Chloride Ion Attack" *Conference Proceedings, CSCE 2010 Annual Meeting*, 9-12 June, Winnipeg, Manitoba, Canada.